Actin and Microtubule Cross-talk during Cytokinesis

By

Jennifer Landino

Dissertation
Submitted to the Faculty of the
Graduate School of Vanderbilt University
in partial fulfillment of the requirements
for the degree of

DOCTOR OF PHILOSOPHY
in
Cell and Developmental Biology
May, 2017
Nashville, Tennessee

Approved:

Ryoma Ohi, Ph.D.

Irina Kaverina, Ph.D.

Kathleen L. Gould, Ph.D.

Matthew J. Lang, Ph.D.

David M. Bader, Ph.D.

To my parents and my husband, for their endless love and support

ACKNOWLEDGEMENTS

I would like to start by thanking my thesis advisor Dr. Ryoma "Puck" Ohi for entrusting me with this project. I am so grateful to have had the opportunity to pursue work that allows me to constantly re-imagine how I think about biology. His commitment to the "big picture" has served as the foundation of my scientific development. Additionally, I would like to thank the members of the Ohi lab for creating an environment that produced excellent research and friendship. Emma Sturgill and Sophia Gayek and Yaqing Du, were instrumental during my early training and, along with Megan Dumas and Stephen Norris, have kindly shared their time, insight, and laughter over the years. I would also like to thank my thesis committee, Drs. Irina Kaverina, Kathy Gould, Matthew Lang, and David Bader, for supporting my education and professional development as well as the M. Ohi and Zanic labs for their continued camaraderie. The Vanderbilt Center for Teaching and Dr. Brian Nelms have provided me with exceptional training in teaching, an opportunity for which I am enormously grateful.

My achievements would not be possible without the expanding community of love and support that surrounds me every day. My parents, Susan and Don, have always encouraged my excitement to learn, and Katie continues to inspire my curiosity and creativity. I am forever grateful to David, Collin, and Maris for celebrating life's milestones by my side, and to Mary, Doug, and Steve for warmly welcoming me into their family. I cannot overemphasize my appreciation for my husband, Kevin, who has endured the day-to-day highs and lows of graduate school, and has always lifted me up when I needed it most. Finally a big "thank you" to my friends, both near and far, who have kept me grounded, helped me grow, and brought me joy throughout this adventure.

TABLE OF CONTENTS

LIST OF TABLES

LIST OF FIGURES

LIST OF ABRREVIATIONS

ABK	Aurora B kinase
A.U.	Arbitrary units
C phase	Contractile phase
Cas-9	CRISPR-associated protein-9 nuclease
CPC	Chromosomal Passenger Complex
CR	Charge reversal
CRIPSR	Clustered regularly interspaced short palindromic repeats
DIC	Differential interference contrast
DMEM	Dulbecco's Modified Eagle Medium
DMSO	Dimethyl sulfoxide
DPBS	Dulbecco's phosphate-buffered saline
DNA	Deoxyribonucleic acid
FBS	Fetal Bovine Serum
FRAP	Fluorescence recovery after photo-bleaching
FRET	Förster resonance energy transfer
G block	Gene block
gRNA	Guide RNA
GST	Glutathione-S-transferase
iMT	Interpolar MTs
Kif	Kinesin family member
MAP	Microtubule associated protein
MCAK	Mitotic centromere-associated kinesin
MCS	Multiple cloning site
Mklp1	Mitotic kinesin-like protein 1
Mklp2	Mitotic kinesin-like protein 2

MSD	Mean-squared displacement
MT	Microtubule
NA	Numerical aperture
NE	Nuclear envelope
PBS	Phosphate-buffered saline
PBST	Phosphate-buffered saline with TWEEN
PCR	Polymerase chain reaction
Plk1	Polo-like kinase 1
ORF	Open reading frame
RMCE	Recombination-mediated cassette exchange
RNA	Ribonucleic acid
RNAi	RNA-interference
RPE-1	Retinal pigment epithelial cells
SAC	Spindle assembly checkpoint
SDS-PAGE	Sodium dodecyl sulfate polyacrylamide gel electrophoresis
SE	Standard error of the mean
SD	Standard deviation
siRNA	Small interfering RNA
STLC	S-trityl-L-cystein
TBS	Tris-buffered saline
TBST	Tris-buffered saline with Triton-X-100

CHAPTER 1

INTRODUCTION

Cell cycle and genome maintenance

The cell represents the simplest unit that is able to satisfy all of the characteristics of life, including the ability to use energy, maintain homeostasis, respond to the environment, grow and reproduce (Campbell et al., 2004). Cells function as the building blocks for all known lifeforms; they can proliferate as single cells or construct tissues and multicellular organisms (Campbell et al., 2004). The capacity of the cell to pass on hereditary information through reproduction differentiates life from other natural processes and makes the cell the smallest self-sustaining vehicle for the genome (Alberts et al., 2008). The "cell cycle" refers to the events of growth and reproduction that allow cells to transfer genomic information to their progeny. The eukaryotic cell cycle is comprised of four phases: two growth phases, an intervening DNA synthesis phase, and M phase, which is comprised of nuclear division (mitosis) and cytoplasmic division (cytokinesis) (Alberts et al., 2008). Mitosis itself is also divided into phases. These are based on the cytological changes that occur as the genome is segregated (Flemming, 1965). Chromosome condensation, nuclear envelope breakdown, and formation of the mitotic spindle occur during prophase and prometaphase (Alberts et al., 2008). The mitotic spindle aligns duplicated chromosomes at the cell equator during metaphase in preparation for segregation (Kapoor, 2017) and the genome is physically separated during anaphase when sister chromosomes are pulled apart (Asbury, 2017). The final step of mitosis is telophase; the chromosomes de-condense and the nuclear envelope re-forms around each copy of the genome (Alberts et al., 2008). Anaphase and telophase are closely coupled to cytokinesis, which cleaves the cell to create two distinct daughters (Green et al., 2012).

The cell cycle is a carefully orchestrated sequence of events that is controlled temporally by a series of biochemical switches (Nurse, 2000). These regulatory "checkpoints" ensure each phase of the cycle is complete before continuing, and that the cell cycle only progresses in one direction (Nurse, 2000; Reed, 2003). Cell cycle checkpoints function to maintain the integrity of the genome and promote accurate chromosome segregation (Hoeijmakers, 2009). Erroneous cell cycle regulation can have potentially disastrous effects on cell viability and health of an organism. If cells attempt to enter mitosis before completing DNA synthesis, daughter cells inherit an incomplete genome, resulting in cell death (Tyson and Novak, 2008). Alternatively, genome duplication in the absence of mitosis causes polyploidy, or too many copies of the genome (Porter, 2008). Progeny can also inherit an abnormal number of chromosomes, termed aneuploidy, if sister chromosomes are missegregated during anaphase (Heald and Khodjakov, 2015) due to faulty connections between duplicated chromosomes and the mitotic spindle (Holland and Cleveland, 2012; Rode et al., 2016). Notably, aneuploidy is a hallmark of cancer cells indicating that accurate transmission of the genome is essential for the homeostasis of multicellular organisms (Holland and Cleveland, 2012; Nojima, 1997; Rode et al., 2016). Even if dividing cells successfully pass each cell cycle checkpoint, daughters can still become polypoid if cytokinesis fails (Steigemann et al., 2009). Failure to cleave the cytoplasm results in a doubling of the genome, making cells susceptible to chromosome missegregation in future cell cycles (Green et al., 2012; Holland and Cleveland, 2012). In this way cytokinesis can be regarded as the culmination of the preceding cell cycle events and also as the linchpin for genomic maintenance and heredity. If the final step of cell division fails, the careful orchestration of the cell cycle is for naught.

The cytoskeleton

If the cell is the smallest self-sustaining vehicle for the genome, then the cell's cytoskeleton is the undercarriage or chassis that supports that vehicle. The cytoskeleton creates a frame that determines cell shape, provides a scaffold to organize cellular contents, and harnesses energy to generate mechanical force (Alberts et al., 2008). Unlike a chassis, the cytoskeleton is not a static structure, and a number of cellular processes require dynamic rearrangements of cytoskeletal networks (Goode et al., 2000). Cell division is one such process, as chromosome segregation and cell cleavage require the force-generating activities of the microtubule and actin cytoskeletons, respectively (Eggert et al., 2006). In eukaryotes, actin and microtubules, along with their associated regulatory proteins, are the most thoroughly studied cytoskeletal networks, and are the primary focus of this study.

Actin

Actin filaments (F-actin) are polymeric structures assembled through the head-to-tail assembly of actin monomers (globular or G-actin) (Mitchison, 1992). Actin is an inherently polar filament with a barbed (plus) end, which is the preferred site of monomer addition, and a pointed (minus) end, the site of disassembly (Alberts et al., 2008). G-actin is an enzyme that hydrolyzes ATP as it polymerizes and at steady state, plus end growth is matched to minus end disassembly, a phenomenon termed treadmilling (Wang, 1985). A single actin filament is thin and flexible as it is made of only two protofilaments wound around each other (Mitchison, 1992), however, actin can contribute to large-scale force generation by assembling into more complex arrays (Kasza and Zallen, 2011). The organization of actin in the cell is regulated by nucleation factors which promote the assembly of branched or linear actin arrays (Skau and Waterman, 2015). Formin-

mediated nucleation creates arrays of linear actin, which can exist as polarized bundles, with all barbed ends pointing in the same direction, or as non-polar arrays, with barbed ends pointing in opposite directions (Alberts et al., 2008). The cell's ability to modulate and remodel F-actin is essential for a wide variety of cellular functions and these functions can be probed using small molecules that induce F-actin disassembly, such as cytochalasin B (Cimini et al., 1998; MacLean-Fletcher and Pollard, 1980).

While actin filaments can generate force on their own, by treadmilling (Ridley et al., 2003), actin can also work with molecular motors to produce forces that alter cell shape (Cooper, 2000). The myosin superfamily of proteins is an important component of the actin cytoskeletal network and myosin proteins carry out a number of diverse, actin-based cellular processes including muscle contraction, cell migration and cleavage furrow ingression (Alberts et al., 2008). To facilitate such processes, myosin hydrolyzes ATP to generate force on the F-actin network (Houdusse and Sweeney, 2016). The role of acto-myosin force generation in cells can be observed using blebbistatin, a small molecule inhibitor of non-muscle myosin (Straight et al., 2003). Force generation by myosin motors is intrinsically linked to the geometry of the F-actin network. For example, polarized actin bundles in sarcomeres are optimized for long-range contraction (Alberts et al., 2008) while branched actin structures in the lamellipodia are tailored to cell migration (Skau and Waterman, 2015). The cytokinetic contractile array is one example where the relationship between F-actin geometry and myosin force generation is not well understood. Formins promote assembly of linear actin filaments, of mixed polarity, within the contractile ring (Green et al., 2012) and how myosin generates forces on these filaments to promote cleavage is a subject of intense debate (Murthy and Wadsworth, 2005). Models for acto-myosin contraction during furrow ingression are discussed below.

Microtubules

Microtubules (MTs) are cylindrical, miniature tubes assembled from heterodimers of α and β-tubulin (Alberts et al., 2008). Similar to actin, MTs are polar polymers with a fast growing, dynamic plus end, and a slow growing minus end (Mitchison, 1992). MTs switch between states of growth and shrinkage, a phenomenon termed "dynamic instability" (Brouhard, 2015; Mitchison and Kirschner, 1984) and this property distinguishes MTs from actin. At steady state individual MTs within a population can exist in a state of growth or shrinkage (Kristofferson et al., 1986) and these parameters of dynamic instability are modulated by MT regulatory proteins (Brouhard, 2015). Compared to actin, MTs are sturdier filaments that can withstand greater force (Mitchison, 1992), due in part to their hollow structure and the fact that a MT is built from thirteen protofilaments held together through lateral non-covalent bonds (Alushin et al., 2014). Cellular organization of MTs is generally controlled by MT-organizing centers (MTOCs) such as the centrosome (McIntosh and Hays, 2016) which anchors MT minus ends. If MTs are anchored at both ends, filaments can undergo a process termed flux, whereby plus end growth is coordinated with minus end disassembly (Mitchison et al., 1986). Flux is distinct from treadmilling in that the individual tubulin subunits move within the MT towards the minus end (Shirasu et al., 1999).

MTs can generate force in two ways: polymerization produces pushing forces, and depolymerization creates pulling forces (Inoue and Salmon, 1995). Both force generation mechanisms occur during nuclear division, as depolymerizing MTs segregate sister chromosomes and plus end polymerization in the cell center pushes chromosomes further apart (Asbury, 2017; Scholey et al., 2017). Polymerizing MTs can produce force as they grow against a barrier through "thermal ratcheting" (Joglekar et al., 2010), and energy released during disassembly allows depolymerizing MTs to do work (Caplow et al., 1994). Similar to actin, tubulin dimers also

hydrolyze nucleotide upon incorporation into the filament. GTP-hydrolysis by the β-subunit is coupled to a "bent" conformational change (Alushin et al., 2014) which produces strain and makes MT depolymerization energetically favorable. The growing plus end is protected against depolymerization by a cap of "straight" GTP-bound tubulin (Alberts et al., 2008; Nogales et al., 1999) and the loss of this stabilizing cap is rapidly followed by disassembly (Brouhard, 2015; Desai et al., 1999; Howard and Hyman, 2003). To study the role of MT dynamics in cells, MT stability can be modified pharmacologically. Taxol, for example, stabilizes MTs by binding the lattice (Kellogg et al., 2017), and nocodazole destabilizes MTs by sequestering tubulin dimers leading to the loss of the stabilizing cap (Hu et al., 2011). Exposure to cold temperature also induces disassembly, by slowing monomer addition at the growing end, and has been classically used to assay the stability of discrete MT populations in cells (Brinkley and Cartwright, 1975).

Proteins that associate with MTs can also modulate dynamics and the majority of those alter growth and disassembly at the plus end (Alberts et al., 2008). These same factors also control the organization and stability of the cellular MT network. Proteins that interact with the MT cytoskeleton can be divided into two major classes: non-enzymatic MT-associated proteins (MAPs), and ATP-hydrolyzing molecular motors, including plus-end directed kinesin, and minus-end directed dynein (Wittmann et al., 2001). MAPs organize the MT cytoskeleton in cells by regulating dynamics, cross-linking MT bundles, and mediating interactions with other cellular proteins (Andersen, 2000). During anaphase, protein regulator of cytokinesis (PRC1) stably cross-links anti-parallel MTs to build the spindle midzone (Kellogg et al., 2016). This MAP is proposed to function by switching from a flexible to rigid state upon interaction with two MTs (Kellogg et al., 2016; Subramanian et al., 2010). The kinesin superfamily of proteins constitute a class of MT-based molecular motors that couple ATP hydrolysis to mechanical force, and these forces organize

and remodel the MT cytoskeleton. For example, the homo-tetrameric kinesin Eg5 (Avunie-Masala et al., 2011; Zhu et al., 2005b) promotes mitotic spindle assembly by sliding anti-parallel MTs (Kapoor, 2017). Non-motile kinesins can also use ATP to alter MT dynamics. The kinesin-13 family of proteins, including MCAK and Kif2a, destabilize MTs by inducing curvature at the protofilament end (Hirokawa and Takemura, 2004; Manning et al., 2007; Walczak, 2003; Walczak et al., 2013). Finally, MTs can serve as tracks for kinesin motors to transport cargo. As cells exit mitosis, mitotic kinesin-like protein 1 (Mklp1) and mitotic kinesin-like protein 2 (Mklp2) transport factors needed for division plane specification and cleavage furrow ingression to MT plus ends (Neef et al., 2006). The relationship between MTs and their associated proteins is essential to build, maintain, and remodel cytoskeletal arrays.

A number of cellular structures are built from MT arrays, and one of the most iconic is the MT-based mitotic spindle. The spindle is a cellular machine which aligns and segregates sister chromatids (McIntosh and Hays, 2016) made of highly dynamic MTs (Mitchison and Kirschner, 1984). The mitotic spindle is a bipolar structure comprised of three major classes of MTs, all of which have minus ends embedded in the centrosomes (McIntosh and Hays, 2016). The first class of MTs interacts with centromeric chromatin *via* the kinetochore (K-MTs) and function to align chromosomes at the cell equator and segregate sister chromatids during anaphase (Asbury, 2017). The bulk of the bipolar spindle is comprised of interpolar MTs (iMTs) which invade the spindle but do not interact with the kinetochore (Mastronarde et al., 1993). Finally, astral MTs extend to the cell cortex and are necessary to maintain spindle orientation during chromosome alignment (Grill and Hyman, 2005). These spindle MT subsets all have essential roles during mitotic exit as well, and those functions are discussed below.

Cytoskeletal coordination underlies cellular functions

The actin and MT cytoskeletal networks have long been studied independently and the function of proteins that regulate dynamics and organization are well-understood within a single filament system. The cell, however, uses both actin and MTs to facilitate processes that are essential for life, and many of these events rely on the coordinated activity of actin and MTs (Goode et al., 2000). For example, "dual-transport" of vesicles (Langford, 1995) occurs through cooperative activity of molecular motors on both cytoskeletal filaments (Benashski et al., 1997; Huang et al., 1999). Actin and MTs are also both required to drive cell migration; disrupting either filament system impairs cell motility (Ballestrem et al., 2000; Ridley et al., 2003). Cytoskeletal cooperation is also central to chromosome alignment and segregation during mitosis. During metaphase, myosin-10 tethers astral MTs to the cortical actin "cloud" and this tethering functions to position the centrosomes and orient the mitotic spindle (Kwon et al., 2015). While this type of cooperation is mediated by a physical interaction between actin and MTs, the cytoskeleton can also functionally coordinate the activities of actin and MTs through signaling or cytoskeletal cross-talk (Goode et al., 2000). One example of this occurs when cells specify the cleavage plane as they exit mitosis. As cells enter anaphase, Mklp1 uses MT tracks to deliver signaling factors to the cortex that promote assembly of the contractile array (Mishima, 2016). Cytoskeletal cross-talk has also been proposed to promote the formation of the spindle midzone (Giansanti et al., 1998; Hu et al., 2008) although the molecular factors that mediate this signaling have not been identified. Investigating how actin and microtubules work together to carry out cellular functions is fundamental to understanding how the cell accurately divides the genome.

Mitotic exit

Together, the stages of anaphase and telophase make up the cell's exit from mitosis. These phases are linked in space and time to cytokinesis, which divides the cytoplasm (Green et al., 2012). Mitotic exit is triggered by a biochemical switch that degrades the cell cycle regulator cyclin B (Tyson and Novak, 2008) and represents a distinct mitotic state. Importantly, mitotic exit can be uncoupled from cytokinesis, using perturbations that block cleavage furrow ingression (Straight et al., 2003). Cells have a limited window in which the furrow is competent to contract, referred to as C phase (Canman et al., 2000), and should cells pass this window without cleaving they will re-enter interphase as a binucleate cell. While the steps of mitotic exit can be broken down into the classically-recognized stages of anaphase, telophase and cytokinesis, cells can also be classified with respect to the state of cleavage furrow ingression during C phase (pre- or post-cleavage furrow ingression), or with respect to the time spent exiting mitosis (early or late mitotic exit).

Anaphase A

Satisfaction of the spindle assembly checkpoint during metaphase triggers the physical segregation of sister chromosomes. The first step of this process, anaphase A, is marked by chromosomes moving towards each end of the spindle (Asbury, 2017). In animal cells, poleward directed movement is largely due to K-MT depolymerization, and chromosomes are observed to move with the centromere leading and arms trailing (Mazia, 1961). As evidence that kinetochores link chromosomes to segregation forces during anaphase, laser ablation of the kinetochore results in chromosome "drift" and abolishes poleward directed movement (McNeill and Berns, 1981). After loss of sister chromosome cohesion at anaphase onset, kinetochores remain stably coupled

to depolymerizing MTs which powers chromosome segregation (Powers et al., 2009). While K-MTs are known to undergo flux within the mitotic spindle, it remains unclear whether this contributes to anaphase chromosome segregation in animal cells (Desai et al., 1998; Ganem et al., 2005; Manning et al., 2007; Waters et al., 1996).

As sister chromosomes segregate, the mitotic spindle is dramatically re-organized to form the spindle midzone (also known as the central spindle). K-MTs depolymerize, pulling chromosomes apart, and iMTs template the formation of the midzone, an array of anti-parallel MTs with overlapping plus ends (Mastronarde et al., 1993) that acts as barrier between segregated chromatids (Straight et al., 2003). While the midzone is templated by iMTs, its formation is regulated by factors that are distinct from those required to build the spindle (Glotzer, 2009). For example, the midzone MT plus end overlap is cross-linked by PRC1. The localization of PRC1 to midzone MTs is regulated by Polo-like kinase 1 (Plk1), which prevents PRC1 from binding iMTs in the mitotic spindle, and ensures that midzone formation does not occur until mitotic exit (Hu et al., 2012). PRC1 also regulates midzone length in concert with the kinesin Kif4A (Nunes Bastos et al., 2013; Subramanian et al., 2013).

In addition to the midzone, the C phase MT array includes astral MTs that emanate from the centrosomes and project towards the presumptive cleavage furrow, hereafter referred to as furrow-associated astral MTs (Bringmann and Hyman, 2005; Dechant and Glotzer, 2003). The geometry of furrow-associated astral MTs is cell-type dependent. For example, in Ptk1 cells, astral MTs straight and angled towards the division plane relative to the spindle axis (Canman et al., 2003). In HeLa and RPE-1 cells, furrow-associated astral MTs are less pronounced, and resemble the geometry of the midzone MT array as they curve and then run parallel to the spindle axis and the cortex (Mishima, 2016; Rankin and Wordeman, 2010). Classically, these MTs are thought to

position the division site (Pollard, 2003), although more recent studies suggest that midzone MTs and astral MTs work together to specify placement of the cleavage furrow (Eggert et al., 2006). The redundancy for division plane specification can potentially be explained by factors that localize to the plus ends of both MT subsets.

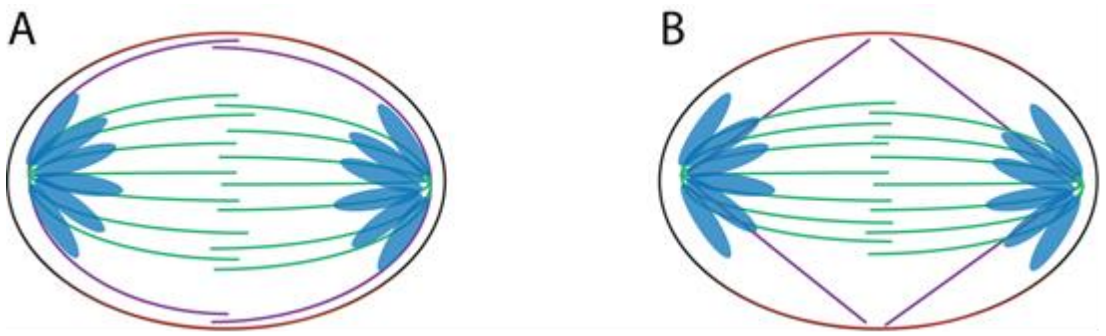

Figure 1.1 Models for furrow-associated astral MT arrangements A, B) Diagram of midzone MTs (green), astral MTs (purple), chromatids (blue), and cortical actin (red) in a C phase cell. In A) astral MTs emanate from the centrosomes and run parallel to the midzone and the cortex with overlapping plus ends. In B) Astral MTs are angled relative to the midzone and the plus ends terminate at the cell cortex.

One such factor that localizes to the plus ends of midzone and furrow-associated astral MTs is centralspindlin, which is required for both midzone organization and cytokinesis (Mishima et al., 2002; Raich et al., 1998). Centralspindlin is a complex of the plus end directed, kinesin-6 motor, Mklp1 (Kif23), and the Rho GTPase activating protein (GAP), MgcRacGAP (CYK4) (Pavicic-Kaltenbrunner et al., 2007). Mklp1 bundles anti-parallel MTs *in vitro* (Davies et al., 2015; Zhu et al., 2005a), which may explain role of centralspindlin in midzone organization. The anaphase localization of these proteins is interdependent; depletion of either in cells abolishes midzone targeting of its partner (Pavicic-Kaltenbrunner et al., 2007; Tao et al., 2016). Centralspindlin targeting to furrow-associated astral MT plus ends is required to recruit the Rho guanine nucleotide exchange factor (GEF), ECT2, to the cell equator (Mishima, 2016; Su et al.,

2011). Recruitment of ECT2 locally activates RhoA, triggering downstream signaling that leads to assembly of the contractile array and cleavage furrow ingression (Prokopenko et al., 1999).

A second essential anaphase transporter is the plus end directed kinesin Mklp2 (Kif20A) which targets the Chromosomal Passenger Complex (CPC) to C phase MT plus ends (Gruneberg et al., 2004; Neef et al., 2006). Cells depleted of Mklp2 fail to complete cleavage furrow ingression, suggesting that Mklp2-dependent transport of the CPC is essential for cytokinesis (Kitagawa et al., 2013). The CPC regulates a number of processes during mitotic exit (Carmena et al., 2012) and its localization to the cell middle is critical for carrying out these functions (Afonso et al., 2014; Fuller et al., 2008). Like centralspindlin, recruitment of the Mklp2-CPC complex is interdependent (Gruneberg et al., 2004; van der Horst et al., 2015) and cell cycle regulated. Cdk1 phosphorylation prevents Mklp2 from associating with the spindle until after cyclin B degradation ensuring that motor transport and CPC off-loading from the centromere are coordinated (Kitagawa et al., 2014; Malumbres and Barbacid, 2009). Mklp2 is also known to bundle MTs *in vitro* (Neef et al., 2003), suggesting it may also be involved in organizing the midzone MT array.

Anaphase B

After midzone formation and division site specification, the central spindle elongates, further segregating sister chromosomes (Scholey et al., 2017). While sister chromatid segregation during anaphase A occurs *via* K-MTs pulling forces, chromosome segregation during anaphase B relies on pushing forces generated by midzone MT polymerization (Saxton and McIntosh, 1987). Microinjection of fluorescent tubulin in Ptk1 cells demonstrates that the bulk of microtubule growth during C phase occurs at the plus end overlap (Saxton and McIntosh, 1987). This plus end

growth is thought to be coupled to motor-dependent MT sliding (Cole et al., 1994; Hogan et al., 1993), however, the molecular motors that drive spindle elongation in mammalian cells have not been characterized. The most likely candidate to slide anti-parallel MTs is Eg5 (Avunie-Masala et al., 2011; Zhu et al., 2005b), although, in animal cells Eg5 has been shown to function as a brake that slows midzone elongation (Collins et al., 2014). Small molecule inhibition of Eg5 also does not disrupt elongation (Kapoor et al., 2000), making the role of Eg5 during anaphase B unclear. It is possible that multiple motors work to drive spindle elongation in mammalian cells, as has been observed for mitotic spindle assembly (Sturgill and Ohi, 2013). Midzone MTs are also known to undergo flux during anaphase B, but the role that flux plays in pushing sister chromosomes apart is not well understood (Brust-Mascher et al., 2004). Cortical pulling forces, generated through dynein acting on polar astral MTs (Palmer et al., 1992), could serve as a third mechanism to elongate the central spindle (Aist et al., 1991; Fink et al., 2006), however, this is largely unexplored in tissue culture cells.

As the cleavage furrow ingresses the midzone MTs become bundled and eventually coalesce to form the midbody (Hornick et al., 2010). The mechanism of bundling during ingression is not well defined, although it has been shown that midzone MTs become resistant to nocodazole and pressure-induced disassembly after furrowing (Hu et al., 2011; Salmon et al., 1976), indicating they are highly stable. The midbody is a highly conserved structure made of densely packed MTs that creates an intracellular bridge between the two daughter cells (Eggert et al., 2006; Otegui et al., 2005; Straight and Field, 2000). Proteins localized to the midzone plus end overlap become incorporated into the midbody after coalescence (Glotzer, 2009). Midbody formation is followed by abscission, the final step in cell division, which severs the intracellular bridge between the newly formed daughter cells (Nashe et al., 2017). Abscission is regulated by

CPC-dependent recruitment of ESCRT proteins (Capalbo et al., 2016; Fung et al., 2017), and thus represents the final checkpoint of the cell cycle (Nahse et al., 2017). Midbody MTs are thought to be required for the localization of abscission factors (Eggert et al., 2006) and for transport of new membrane vesicles to the cut site (Finger and White, 2002), however, other functions of midbody MTs are still under investigation.

Cytokinesis

Once the duplicated genome has been segregated to opposite spindle poles, cellular division produces two daughter cells. Cytokinesis requires cortical remodeling to facilitate the changes in cell shape that underlie cleavage furrow ingression (Green et al., 2012). Positioning the division plane is an essential part of completing the cell cycle. Cleavage always occurs perpendicular to chromosome segregation, and generally at the cell equator, although asymmetric cell division occurs in some cell types (Eggert et al., 2006). Three major models account for cleavage plane specification, and all of these models theorize that MT-dependent signaling positions the furrow. The *polar relaxation model* hypothesizes that astral MTs extending toward the polar cortices negatively regulate contractility, thereby indirectly stimulating ingression in the cell center (Canman et al., 2003). The *equatorial stimulation model* also implicates a role for astral MTs, although it suggests that astral MTs at the cell equator promote contraction (Mishima, 2016; Rappaport, 1961). The *midzone stimulation model* postulates that midzone MTs define the division site by propagating signaling to the cortex along the plus end overlap (Nguyen et al., 2014; Wheatley, 1999). Currently, it is thought that all three models contribute to cleavage plane specification, although only the molecular players for equatorial and midzone stimulation have been defined (Eggert et al., 2006; Green et al., 2012).

Assembly of the contractile array at the division plane is largely mediated through the GTPase RhoA (Bement et al., 2005). In fact, local activation of RhoA can induce transient furrowing regardless of cell cycle state (Wagner and Glotzer, 2016). Like other GTPases, RhoA activity is controlled by regulatory proteins: MgcRacGAP, part of the centralspindlin complex, and the Rho-GEF, Ect2 (Fededa and Gerlich, 2012). Recent studies suggest that cycling RhoA activation and actin polymerization indicate that the cortex of a dividing cell is an excitable medium (Goryachev et al., 2016). RhoA stimulates formin-dependent nucleation of actin at the division site, and initiates a signaling cascade that leads to myosin II-dependent furrowing (Fededa and Gerlich, 2012). Rho-associated protein kinase (ROCK) activates myosin contractility by simultaneously phosphorylating myosin light chain and inhibiting myosin phosphatase (Matsumura, 2005).

The mechanical forces that drive cleavage furrow ingression are generated by myosin II cross-linked to actin at the equatorial cortex. When myosin II activity is blocked, using blebbistatin, cleavage furrow ingression halts (Straight et al., 2003). The mechanism of force generation is still not well understood, due in part to competing models for how actin and myosin are oriented in the ring (Eggert et al., 2006). Current models include the *purse string model*, where parallel actin filaments are proposed to slide past one another as the furrow closes (Miller, 2011; Schroeder, 1972) and the *gelation contraction model* which hypothesizes that randomly oriented actin filaments form a "gel" that myosin II acts on to generate force (Fededa and Gerlich, 2012). It is known that the concentration of actin in the ring remains the same as the cleavage furrow ingresses, as opposed to muscle sarcomeres which get thicker (becoming more concentrated) as they shorten (Pollard, 1976; Schroeder, 1972). This implies that contraction of the furrow is coupled to regulated F-actin disassembly (Green et al., 2012), although, high dose treatment with

an actin-depolymerizing drug arrests furrow ingression similar to myosin II inhibition (Schroeder, 1972). Cytokinesis ends in midbody formation, and is follow by abscission as described above.

The CPC regulates cell division

The Chromosomal Passenger Complex (CPC) is a key regulator of a number of mitotic processes including chromosome segregation, midzone formation, cytokinesis and abscission (Carmena et al., 2012). The CPC is tetrameric complex comprised of the scaffolding protein INCENP (Inner Centromeric Protein), two regulatory proteins – Survivin (BIRC5) and Borealin (Darsa/CDCA8), and the enzymatic component ABK (aurora B kinase). INCENP forms a triple helix bundle with Survivin and Borealin at a 1:1:1 ratio at its N-terminus (Jeyaprakash et al., 2007) and binds ABK through the highly conserved IN-box at its C-terminus (Adams et al., 2000). During mitosis, all members of the CPC participate in complex formation (Carmena et al., 2012). Whether the CPC oligomerizes to form higher-order structures is the subject of current investigations (van der Horst et al., 2015). The CPC is *trans*-activated by ABK-dependent phosphorylation of a conserved Thr-Ser-Ser motif in INCENP (Bishop and Schumacher, 2002), and the T-loop (Thr232, kinase domain) of ABK (Sessa et al., 2005). Therefore, increasing the local concentration of CPC through clustering stimulates ABK activity, and this mechanism of CPC activation is observed throughout the cell cycle (Noujaim et al., 2014; Rosasco-Nitcher et al., 2008; Wang et al., 2011).

The sub-cellular localization of the CPC is tightly coupled to its function during cell division. For example, when cells enter mitosis the CPC associates with the centromere where it corrects erroneous MT attachments to the kinetochore (Carmena et al., 2012). This localization is so important for cell cycle progression that multiple pathways function to ensure the CPC is

correctly targeted. ABK feedback signaling (Emanuele et al., 2008) and phospho-regulation of Borealin (Tsukahara et al., 2010) work together to promote centromere localization, and both ABK inhibition and Borealin depletion result in an increased frequency of incorrect MT attachments (Carmena et al., 2012). When cells exit mitosis, Mklp2-dependent transport of the CPC to midzone MT plus ends and the equatorial cortex is required for midzone organization and cleavage furrow

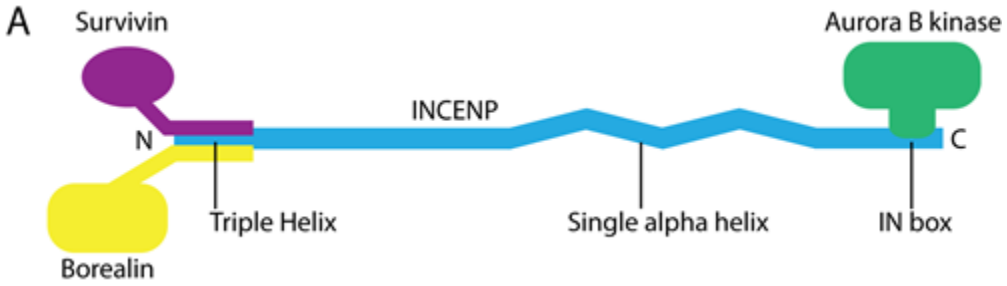

Figure 1.2 Model of the Chromosomal Passenger Complex A) Diagram of the proteins that make up the CPC and relevant domains of INCENP. The triple helix is made of the N-terminal region of INCENP complexed with Survivin and Borealin. The C-terminal half of INCENP contains the SAH domain and the IN box, which is where INCENP and ABK interact.

ingression (Douglas et al., 2010; Gruneberg et al., 2004; Kitagawa et al., 2013). The CPC is required to recruit centralspindlin (Basant et al., 2015; Douglas et al., 2010) which is one reason the C phase localization is key for furrowing. Similarly, midbody-localized CPC regulates the recruitment of ESCRT proteins and the timing of abscission (Fung et al., 2017; Nahse et al., 2017). One model that describes the relationship between CPC localization and function, is the *spatial gradient model* which theorizes that mitotic events are regulated by a gradient of ABK activity. Evidence for this model largely relies on the cellular expression of an FRET sensor that undergoes a conformation change after ABK phosphorylation (Wang et al., 2011). Analysis of this sensor indicates that ABK activity is high at the centromere during metaphase, and on midzone MT plus ends during C phase, and gradually decreases towards the spindle poles (Afonso et al., 2014; Fuller

et al., 2008). This gradient is thought to generate spatial cues that help promote accurate nuclear and cytoplasmic division. There are some caveats to this model, however, it is clear that the cell takes great effort to target the CPC to where its activity is needed, and that perturbing CPC localization disrupts successful cell division. This study demonstrates that the CPC functions at the cortex to mediate cytoskeletal cross-talk between acto-myosin contraction and midzone stabilization. Moreover, we find that the C phase localization of the CPC is carefully regulated by cooperation between the actin and microtubule cytoskeletons.

CHAPTER 2

MATERIALS AND METHODS

Cell culture and transfections

Cell lines were cultured in media supplemented with 10% fetal bovine serum (FBS) and penicillin/streptomycin at 37°C, with 5% CO_2. HeLa "Kyoto" cells were cultured in DMEM. HeLa cells stably expressing GFP-Tubulin and mCherry-H2B (a gift from Dr. Dan Gerlich) additionally contained 500mg/ml G418. Stable HeLa cells expressing GFP-INCENP under the control of a doxycycline-inducible promoter were cultured in DMEM containing 1 µg/ml puromycin during selection and then cultured in DMEM without antibiotic. RPE-1 cells were cultured in 50% DMEM/50% F-12 media.

Target	Sequence	Source	Reference
INCENP 3' UTR	5'AAGGCTTGGCCAGGTGTATAT	Qiagen	
Kif2a	ON-TARGET plus SMARTpool 5'GAAAUGGUUUACAGGUUA 5'CUACACAACUUGAAGCUAU 5'GAAAACGACCACUCAAUAA 5'GACCCUCCUUCAAGAGAUA	Dharmacon	
Mklp2	5'AACCACCTATGTAATCTCATG	Qiagen	(Kitagawa et al., 2013)
LoGC Duplex #3	Proprietary	Life Technologies	

Table 2.1 Sequences of siRNAs used in this study.

Transfections were performed using Lipofectamine 2000 (Invitrogen) for plasmid DNA or HiPerFect (Qiagen) for siRNAs according to manufacturer instructions. For both, cells were

cultured in Opti-MEM supplemented with 10% FBS following transfection. The siRNA sequences used in this study are shown in Table 2.1. Cells were fixed for immunofluorescence or used for live cell imaging 24 hours after transfection. For Kif2a siRNA depletion cells were transfected twice, 96 hours and 48 hours before they were fixed for immunofluorescence. For doxycycline-inducible stable cell lines 2 µg/ml doxycycline was added to Opti-MEM supplemented with with 10% FBS at the time of transfection.

Stable cell lines

The CRISPR-Cas9 system was used to generate stable cell lines depleted of Kif2a (Kif2a KO) (Mali et al., 2013). HeLa cells were transfected using guide RNAs (gRNA), outlined in Table 2.2, targeting the *Kif2a* ORF. These gRNA sequences were selected to reduce the possibility of off-target effects, as each sequence is only represented once within the genome. A gBlock (IDT) containing the U6 promoter, *Kif2a* targeting sequence, gRNA scaffold, and termination signal was synthesized and cloned into pCR-Blunt II-TOPO (Invitrogen). This was co-transfected with pcDNA3.3-Cas9 (Addgene) into HeLa cells using Lipofectamine LTX according to the manufacturer's instructions. Single clones were isolated and analyzed for Kif2a protein levels by immunostaining. Clones that displayed a reduction in Kif2a by immunostaining were transfected

Name	Target (*Kif2a* ORF)	Sequence
Kif2a gRNA 1	Nucleotides 24-46	5'GATCCAGATCGGGATTTACGTGG
Kif2a gRNA 2	Nucleotides 27-49	5'TCTCCACGTAAATCCCGATCTGG
Kif2a gRNA 3	Nucleotides 43-65	5'GTGGAGATCAAGCGCAGCGATGG

Table 2.2 Guide RNAs used in this study for CRISPR-Cas9 mediated knockout

and isolated a second time to improve the efficiency of the knock down.

To generate HeLa cells that stably express GFP-INCENP in a doxycycline-inducible manner we used the high efficiency, low background RCME system (Khandelia et al., 2011). Acceptor HeLa cells (Sturgill et al., 2016) were transfected with pEM791 containing GFP-INCENP (see Molecular biology). 24 hours after transfection, cells were cultured in the presence of 1 µg/ml puromycin, and were transferred to media containing 2 µg/ml puromycin 48 hours post-transfection to select for transgenic cells. Cells were pooled and cultured in DMEM containing 10% FBS, penicillin and streptomycin. GFP-INCENP expression was induced using 2 µg/ml doxycycline for 24 hours.

Cold and pharmacological perturbations

To destabilize MTs, cells were incubated in DMEM chilled to < 4°C and placed on ice for 10 min. Drug stocks in DMSO were diluted in DMEM immediately before use. All drugs were stored at -20°C and diluted in media promptly before use. Drug concentrations, sources, and treatment times for fixed cell imaging are outlined in Table 2.3. All drug treatments were performed at 37°C for the time indicated before fixation. For live cell imaging, drug concentrations, sources, and

Drug	Source	Solvent	Concentration	Duration
Blebbistatin	Tocris Bioscience	DMSO	100 µM	30 min
Cytochalasin B	Sigma	DMSO	5 µg/ml 10 µg/ml	30 min 10 min
ZM447439	Tocris Bioscience	DMSO	2 µM	10 min
Nocodazole	Sigma	DMSO	5 µM	10 min
Taxol	Sigma	DMSO	2.5 nM	30 min
BI 25436	Selleck Chemicals	DMSO	100 nM	20 min

Table 2.3 Drugs used in this study for fixed cell imaging

treatment times are outlined in Table 2.4. Live cell "nocodazole shock" experiments cells were performed by pre-incubating cells in drug for the duration indicated prior to the addition of high dose nocodazole. To destabilize MTs during live cell experiments an equivalent volume of movie medium was added during imaging containing 2X nocodazole ([Final] = 10 μM) and 1X blebbisatin or ZM 447439. For cortical imaging, cells were incubated with media containing cytochalasin B or nocodazole for the time indicated.

Drug	Source	Solvent	Concentration	Duration
Nocodazole	Sigma	DMSO	10 μM 5 μM	During imaging (shock) 5 min (cortical imaging)
Blebbistatin	Tocris Bioscience	DMSO	100 μM	30 min
ZM447439	Tocris Bioscience	DMSO	2 μM	5 min
Cytochalasin B	Sigma	DMSO	10 μg/ml	10 min

Table 2.4 Drugs used in this study for live cell imaging

Immunofluorescence and fixed-cell imaging

For most experiments, HeLa and RPE-1 cells were fixed with methanol at -20^{o}C for 3, 5 or 10 min. Primary antibodies used in this study are outlined in Table 2.5. Secondary antibodies conjugated to Alexa 488, Alexa 594, or Alexa 647 (Invitrogen) were used at 1:1000. Primary and secondary antibody incubations were performed for 1 hour each at room temperature. DNA was counterstained with 5 μg/ml Hoechst 33342. Stained cells were mounted in Prolong Gold (Invitrogen).

To quantify midzone fluorescence after cold treatment, cells were fixed in 2% glutaraldehyde in cytoskeleton buffer (CB, 10 mM MES pH 6.1, 138 mM KCl, 3 mM $MgCl_2$, 2

mM EGTA) plus 11% sucrose at room temperature for 10 minutes. To visualize actin, cells were fixed with 1% glutaraldehyde in CB plus 11% sucrose at room temperature for 10 minutes. Actin was stained with phalloidin-TRITC (Sigma) at 500 ng/µl. To visualize PRC1, cells were fixed in 4% formaldehyde and Perm-Fix (100 mM K-PIPES, 0.2% TX-100, 10 mM K-EGTA, 1 mM $MgCl_2$).

Antibody	Source	Dilution
Mouse anti-tubulin, DM1α	Vanderbilt Antibody and Protein Resource	1:500
Rat anti-tubulin, YL1/2	Accurate Chemical and Scientific Corporation	1:500
Mouse anti-AIM	BD Transduction Labs	1:500
Rabbit anti-INCENP	Abcam	1:500
Rabbit anti-Mklp2	Abnova	1:50
Rabbit anti-Mklp1	Santa Cruz Biotechnology	1:500
Mouse anti-Lamin B	Abcam	1:200
Rabbit anti-Kif2a	Abcam	1:1000
Goat anti-PRC1	Santa Cruz Biotechnology	1:50
Rabbit anti-myosin IIa	BioLegend	1:1000
Mouse anti-GFP conjugated to DyLight 488	Rockland	1:1000

Table 2.5 Primary antibodies used in this study for immunofluorescence

To visualize myosin IIA, cells were fixed with 4% paraformaldehyde (PFA) in PBS at room temperature for 10 min. To visualize Mklp2 cells were fixed in methanol at -20^{o}C for 3 min. Where indicated, cells were permeabilized with 100 mM K-PIPES (pH 6.8), 1 mM MgCl2, and 1% TX-100 for 30 seconds prior to fixation to extract free tubulin.

Cells were visualized using either a 60X 1.4 NA or 100X 1.4 NA objective (Olympus) on a DeltaVision Elite imaging system (GE Healthcare) equipped with a Cool SnapHQ2 CCD camera

(Roper). Optical sections were collected at 200 nm intervals and processed using ratio deconvolution in SoftWorx (GE Healthcare). Images were prepared (rotation, maximum projection) using Image J and NIS-Elements AR.

To quantify midzone MT fluorescence following cold treatment, cells were fixed in glutaraldehyde with or without pre-extraction as described above. Sum intensity projections were generated from 200 nm z-slices of tubulin fluorescence and a boxed region within the midzone was used to measure the integrated fluorescence intensity. To measure fluorescence from polymer only, background fluorescence was measured from an equivalently sized region outside the midzone where no detectable polymer was observed, and subtracted from midzone fluorescence. To determine the extent to which cleavage furrows had ingressed, the following formula was used: distance furrow ingressed $\div$ total cell width $\times$ 100 = % ingression. To measure ABK fluorescence after Mklp2 depletion, a boxed region at the division plane was used to determine the integrated fluorescence of a sum intensity projection. An equivalently sized region outside the division plane was used to measure background fluorescence and this was subtracted from the division plane fluorescence.

Live cell imaging

Widefield live cell imaging was performed at 37^{o}C with 5% CO_2 and a 60X 1.4 NA objective on a DeltaVision Elite imaging system equipped with a WeatherStation Environmental Chamber. For live imaging of HeLa cells stably expressing GFP-Tubulin and mCherry-H2B, cells were plated on glass bottom dishes (MatTek Corporation) 24 hours prior to imaging. Prior to imaging, cells were incubated in movie medium (L-15 medium without Phenol Red supplemented with 10% FBS, penicillin/streptomycin, and 7 mM K-HEPES, pH 7.7). One optical section was

selected and cells were imaged at 15 second intervals. For live cell imaging of transiently expressed GFP-INCENP constructs and mCherry-Utrophin, HeLa cells were plated on glass bottom dishes (MatTek Corporation) 48 hours prior to imaging. 24 hours prior to imaging cells were transfected with plasmid DNA and/or siRNA as described above. Immediately before imaging culture media was exchanged for movie medium. To image probes during C phase one optical section was selected and cells expressing GFP-INCENP were imaged at 5 second intervals. Cells expressing mCherry-Utrophin were imaged at 30 second intervals to prevent photobleaching. To image stable HeLa cell lines expressing GFP-INCENP, cells were plated on glass bottom dishes 48 hours prior to imaging. 24 hours prior to imaging siRNA was transfected as described above and 2 μg/ml doxycycline was added. Cells were imaged in movie medium and GFP-INCENP was imaged at 10 second intervals. Where indicated, differential interference contrast (DIC) imaging was used to image the cell cortex of GFP-INCENP stable cells during furrowing. For these experiments, cells were imaged at 30 second intervals.

To quantify midzone MT fluorescence in live cells after exposure to nocodazole the midzone was defined as the region between the chromosome plates in the X dimension, and the chromosome edges in Y dimension. The fluorescence intensity of GFP-tubulin within a boxed region encompassing the midzone from a single optical section was measured over time. Similar to fixed cells, a region outside the midzone lacking detectable polymer was used to measure background fluorescence for each time point, which was subtracted from the midzone fluorescence values at corresponding time points. To normalize for changes in the size of the midzone over time (due to ingression or movement of the chromosome plates), we calculated the integrated fluorescence intensity per pixel at each time point and then scored these values relative to the initial

fluorescence intensity (before nocodazole addition) to determine the percent of fluorescence decay over time.

Live cell confocal imaging was performed at at 37^{o}C with 5% CO_2 and a 60X 1.4 NA in movie medium. Cells were imaged using a Nikon spinning disk confocal microscope equipped with a stage top incubator (Tokai Hit) and an Andor DU-897 EMCCD camera. Fluorophores were excited using 488 nm and 561 nm diode laser lines. For live imaging of C phase in GFP-INCENP stable HeLa cells, cells were plated on glass bottom dishes 48 hours before imaging, and siRNA transfection and doxycycline addition occurred 24 hours before imaging. A single optical section was imaged at 15 second intervals. To image cortical movements of transiently expressed GFP-INCENP cells were plated on glass bottom dishes coated with 100 µg/ml fibronectin. Cells were transfected with plasmid DNA 24 hours prior to imaging. The optical section closest to the coverslip was imaged in pre-ingression cells at 3 second intervals. For pharmacological perturbations, cells were incubated with cytochalasin B for >10 min prior to imaging. To ensure that nocodazole treatment did not disrupt cortical delivery of GFP-INCENP, C phase cells were identified prior to drug addition, and then incubated in nocodazole for 5 min before imaging. For co-imaging of transiently expressed GFP-INCENP and Mklp2-mCherry cells were plated on glass bottom dishes coated with 100 µg/ml fibronectin and transfected with plasmid DNA 24 hours prior to imaging. Three optical sections, corresponding to the cortex, midzone, and one optical section between, were imaged at 5 second intervals using triggered acquisition to reduce temporal delay.

To quantify cortical enrichment of GFP-INCENP at the cell cortex 200 nm optical sections were collected and volume projections of the YZ dimension were generated using Image J. and Line scans across the YZ projection of the division plane were normalized for length, aligning peak intensity values or cell edges where applicable. Background fluorescence was measured

outside the cell and this value was subtracted from all intensity measurements along the line scan. Fluorescence intensity values were then normalized to cytoplasmic background, to control for variable protein expression. To determine the relative increase of fluorescence intensity at the cortex, three adjacent values from each peak of fluorescence intensity were averaged.

GFP-INCENP spot tracking was performed using the TrackMate plug-in in Image J (Tinevez et al., 2016). The TrackMate parameters used were as follows: a LoG detector, an estimated blob diameter of 1.5 µm, a threshold of 15.0, a simple LAP tracker (for non-branching tracks), a linking max distance of 1.0 µm, a gap closing max distance of 1.0 µm, and a gap closing frame of 1. Only tracks with a lifetime ≥ 9 seconds (or 3 frames) were used considered for GFP-INCENP cortical imaging. For cells co-expressing GFP-INCENP and Mklp2-mCherry, tracks were analyzed separately for each probe and optical section. The TrackMate parameters used were similar to GFP-INCENP tracking, although they were modified slightly to accommodate the dim fluorescence of mCherry. Parameters used were as follows: a LoG detector, an estimated blob diameter of 1.0 µm, a threshold of 10.0, a simple LAP tracker (for non-branching tracks), a linking max distance of 1.0 µm, a gap closing max distance of 1.0 µm, and a gap closing frame of 1. Only tracks with a lifetime of ≥ 15 seconds (or 3 frames) were considered. Diffusion coefficients were calculated using the MSDanalyzer MATLAB plugin (Tarantino et al., 2014b), where only the first 120 s were used for MSD analysis. The diffusion co-efficient was determined by dividing the slope of the best fit linear regression by 4, to account for movement in two dimensions.

To quantify the Pearson's correlation co-efficient of GFP-INCENP and Mklp2-mCherry on the midzone and the cortex, images were cropped in time to only analyze the correlation from anaphase onset to the initiation of furrowing. Only the region corresponding to the division plane on the midzone and the cortex was included so as not to analyze areas beyond the chromosomes

plates, or outside the cell. The correlation co-efficient was measured using the GDSC stack correlation analyzer with no additional thresholding or corrections. To normalize for the duration of C phase, the time cells began furrowing was normalized to 1, with anaphase onset normalized to 0.

Immunoblotting

For preparation of whole cell lysates, cells were washed three times with PBS and resuspended in 2X Laemmli buffer. For pure protein, samples were mixed with 2X Laemmli buffer. After heating to 95ºC for 5 min, proteins were resolved by SDS-PAGE and transferred to nitrocellulose (Whatman). Immunoblots were blocked with 5% w/v milk in PBST and then probed with primary

Antibody	Source	Dilution
Mouse anti-tubulin, DM1α	Vanderbilt Antibody and Protein Resource	1:1000
Mouse anti-AIM	BD Transduction Labs	1:1000
Rabbit anti-INCENP	Abcam	1:1000
Rabbit anti-Kif2a	Abcam	1:1000
Mouse anti-GFP conjugated to DyLight 488	Rockland	1:1000

Table 2.6 Primary antibodies used in this study for Western Blot

antibodies outlined in Table 2.6 for 1 hour. Blots were then probed with species-appropriate fluorescently-tagged secondary antibodies for 45 minutes. Fluorescence was measured using an Odyssey fluorescence detection system (LI-COR Biosciences) and Image J.

Molecular biology

A full-length human INCENP ORF (Source Bioscience, IOH62774:pDEST15, NCBI accession: AY714053) was used to prepare all wild type INCENP DNA constructs. Amplification of the INCENP ORF was performed using PrimeStar GXL polymerase (Takara). All constructs were prepared using isothermal assembly (Gibson et al., 2009). PCR fragments were cloned into pEGFP-C1 (Clontech) restricted with *Kpn*I and *Nde*I or into pET15 (Novagen) restricted with *Xho*I and *Nde*I.

Charge reversal mutagenesis was performed using G blocks (IDT) containing the desired mutations and a 4-part Isothermal Assembly of INCENP G blocks fragments into pEGFP-C1 restricted with *EcoRI* and *KpnI*. The following mutations were made to codons corresponding to amino acids 563-580 to change lysine and arginine to glutamic acid (mutations underlined): GGAAGAAGAACTGGAGGAGGTGGAGCTGGAGGAAGAGGAAGAACTCGAAGAG. These mutations are referred to in this study as INCENP CR. Additionally, mutations were made to codons corresponding to amino acids 622-631 to change lysine and arginine residues to glutamic acid. Mutations were also made to optimize G block synthesis which did not affect the ORF (mutations underlined): GAGGCCGAGGAAGAGGCGGCGGCCGAGGAG. In this study these mutation are referred to as INCENP MT CR. To generate stable cell lines GFP-INCENP wt, 563-580 CR, 622-631 CR, were amplified from pEGFP-C1 constructs using PrimeStar GXL and cloned into pEM791 restricted with *BsrGI* and *BglII* (a gift from E. Makeyev).

Protein expression and purification

His_6-$INCENP^{500-680}$ and His_6-$INCENP^{500-680\ CR}$ were expressed in BL21 DE3 RIPL cells with 0.4 mM IPTG for 16 hours at 16^{o}C. For purification, cells were pelleted and resuspended in

lysis buffer (PNI [50 mM sodium phosphate, 500 mM NaCl, 20 mM imidazole], 5 mM β-mercaptoethanol (β-ME), 1% NP40, and protease inhibitors [1 mM phenylmethylsufonyl fluoride, 1 mM benzamidine, and 10 μg/ml each of leupeptin, pepstatin, and chymostatin]). Cells were enzymatically lysed by incubation in 1 mg/ml lysozyme (Sigma) for 30 minutes. The lysate was sonicated, and clarified by centrifugation at 35K rpm for 1 hour in a Ti-45 rotor (Beckman). 4 ml of Ni^{++}-NTA agarose (Qiagen) was incubated with the supernatant for 1 hour at 4°C, and then washed extensively with wash buffer (PNI, 5 mM β-ME). Protein was eluted with PNI, 5 mM β-ME, and 180 mM imidazole. Peak fractions were desalted using a PD-10 column (GE Healthcare) equilibrated in 10 mM K-HEPES pH 7.7, 50 mM KCl, 1 mM DTT. Powdered sucrose was added to 20% w/v. Protein was aliquoted, frozen in liquid nitrogen and stored at -80°C.

Actin polymerization and co-sedimentation

Rabbit skeletal muscle actin (Cytoskeleton) was resuspended in 5 mM Tris-HCl pH 8.0 and 200 μM $CaCl_2$, and stored at -20°C until use. Actin was polymerized in 500 mM KCl and 20 mM MgCl2 for 10 minutes at room temperature.

Prior to use, His_6-$INCENP^{500-680}$ and His_6-$INCENP^{500-680\ CR}$ were pre-clarified by centrifugation at 90K rpm for 30 minutes at 4°C in a TLA-100 Ultracentrifuge (Beckman). For co-sedimentation with actin, His_6-$INCENP^{500-680}$ or His_6-$INCENP^{500-680\ CR}$ (5 μM) were mixed with F-actin (10 μM) in 100 μl reaction buffer (10 mM K-HEPES pH7.7, 50 mM KCl, 1 mM DTT, 1 mM $MgCl_2$-ATP). Reactions were incubated at room temperature for 15 min and centrifuged at 90K rpm for 20 minutes at 22°C. 100 μl of supernatant was collected and mixed with and equivalent volume of 2X Laemmli buffer. Pellets were resuspended in 200 μl of 2X Laemmli

buffer. Fractions were heated to 95°C for 5 min and 40 µl of each fraction was run on a 12% SDS-PAGE gel and stained using Coomassie Brilliant Blue.

Statistical analysis

Statistically relevant differences in experimental data were determined using the T.TEST function in Excel (Microsoft). In all cases, P-values report the two-tailed distribution of a two-sample Student's t-Test assuming unequal variance.

CHAPTER 3

ACTO-MYOSIN CONTRACTILITY DRIVES MIDZONE STABILIZATION

Introduction

Cytokinesis, the final step in cell division, individualizes two daughter cells through concerted actions of the actin and microtubule (MT) cytoskeletons. During anaphase, MTs positioned between segregated chromosomes are incorporated into an anti-parallel array termed the spindle midzone (midzone MTs) while F-actin and non-muscle myosin II, together with other factors, organize into the cleavage furrow (Green et al., 2012). With the exception of cleavage plane specification, little is known as to whether remodeling of the actin and MT cytoskeletons are actively coordinated throughout cytokinesis. Previous studies of the spindle midzone in somatic cells have shown that midzone MTs become highly stable after furrows have begun ingression (Hu et al., 2011), indicating that furrow-to-MT communication may occur. Consistent with this notion, midzone formation is inhibited in fly spermatocytes that fail to form a cleavage furrow (Giansanti et al., 1998) and during monopolar cytokinesis when myosin contractility is blocked by the non-muscle myosin II inhibitor blebbistatin (Hu et al., 2008). Our work shows that acto-myosin contractility underlies MT stabilization in bipolar midzones and suggests cytoskeletal coordination is fundamental to mammalian cytokinesis.

A modified version was previously published as:
Landino, J. and Ohi, R. (2016) The Timing of Midzone Stabilization during Cytokinesis Depends on Myosin II Activity and an Interaction between INCENP and Actin. *Curr Biol* 26, 698-706

Midzone MTs are differentially stable during C phase

To investigate the relationship between furrowing and midzone MT stability, we exposed asynchronous HeLa cells to cold temperature (0°C) for 10 minutes prior to fixation. This treatment indicated that midzone MTs become increasingly stable as cells progress through C phase (Canman et al., 2000; Straight et al., 2003). Cells that appeared to be in anaphase A at the time of fixation, characterized by chromosome segregation without pole separation and a non-ingressed furrow, were devoid of midzone MTs, whereas cells that apparently progressed further, *ie.*, anaphase B and telophase cells, contained cold-stable MTs (Figure 3.1 A). In agreement with previous work (Hu et al., 2011), cells with cold-stable midzone MTs had invariably initiated furrow ingression; only 5.3 ± 3.2% of non-ingressed cells (mean ± SE, n=70 cells) retained tubulin polymer following cold treatment, whereas 82.0 ± 3.5% (n=108 cells) of cells with an ingressed furrow contained polymer (Figure 3.1 B). This qualitative result was unaffected by removal of free tubulin *via* a brief permeabilization step prior to fixation (Figure 3.1 C). Quantitative analysis revealed that the sum intensities of polymeric tubulin fluorescence following cold-treatment in ingressed cells show a positive linear correlation with the degree of furrowing and this result was unaffected by the presence or absence of free tubulin (Figure 3.1 D and E). Midzone MTs behaved similarly in the non-transformed RPE-1 cell line (Figure 3.1 F and G).

To better correlate the timing of furrowing with midzone stabilization, we next used a live cell assay to monitor midzone MT stability. HeLa cells that simultaneously express GFP-tubulin and mCherry-H2B were challenged during C phase with DMSO or 10 μM nocodazole before or after furrow ingression (Hu et al., 2011). DMSO-treated cells progressed through cytokinesis normally without losing midzone MTs (Figure 3.2 A). In contrast, nocodazole caused rapid

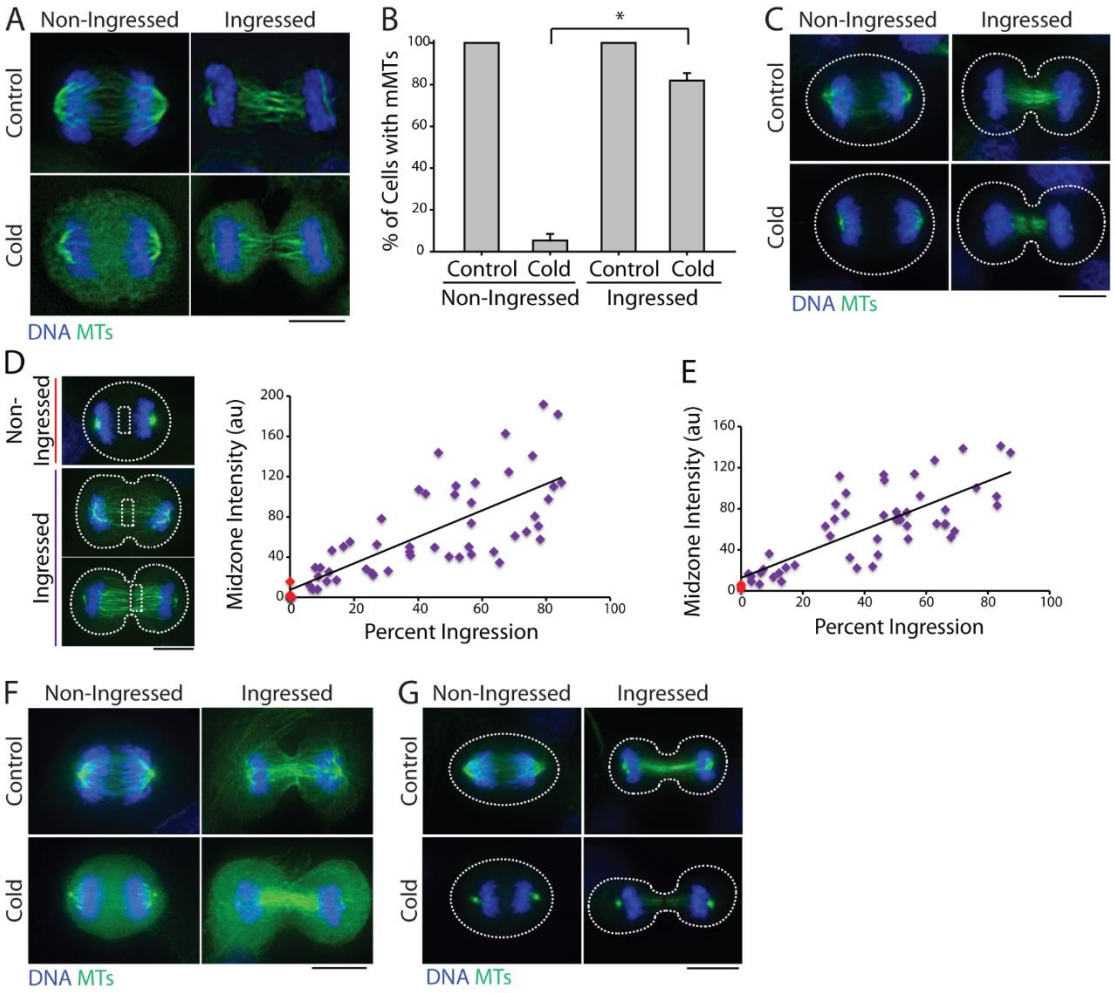

Figure 3.1 Midzone MTs are differentially stable during C phase. A) Maximum z-projections of untreated (top) or cold-treated (bottom) HeLa cells in C phase with non-ingressed or ingressed cleavage furrows. Cells were stained with antibodies against tubulin (green) and counterstained with Hoechst 33342 to visualize DNA (blue). Scale bar, 10 μm. B) Quantification of the percentage of cells with midzone MTs (mMTs) before and after cold treatment as described in A). Data represent mean ± SE. n > 150 cells from three independent experiments, * = $p < 0.005$. C) Maximum z-projections of untreated (top) and cold-treated (bottom) HeLa cells in C phase with non-ingressed or ingressed cleavage furrows. Cells were permeabilized for 30 seconds prior to fixation to extract free tubulin. Dashed lines indicate cell boundary. Cells were stained as described in A). D) Left: Maximum z-projections of cold-treated HeLa cells permeabilized prior to fixation. Cells were stained as described in A). Dashed lines indicate cell boundary. Dashed box represents regions used to quantify midzone intensity. Scale bar, 10 μm. Right: Quantification of midzone MT fluorescence intensity after cold treatment in non-ingressed (red) and ingressed (purple) cells plotted as a function of the percent furrow ingression. Cells were fixed after pre-extraction of free tubulin. (n=54). E) Quantification of midzone fluorescence intensity as described in A). Cells were fixed without extraction of free tubulin (n=52). F) Maximum z-projections of untreated (top) and cold-treated (bottom) RPE-1 cells in C phase with non-ingressed or ingressed cleavage furrows. Cells were stained as described in A). Scale bar, 10 μm. G) Maximum z-projections of RPE-1 cells permeabilized for 30 seconds prior to fixation. Cells were stained as described in A). Dashed lines indicate cell boundary. Scale bar, 10 μm.

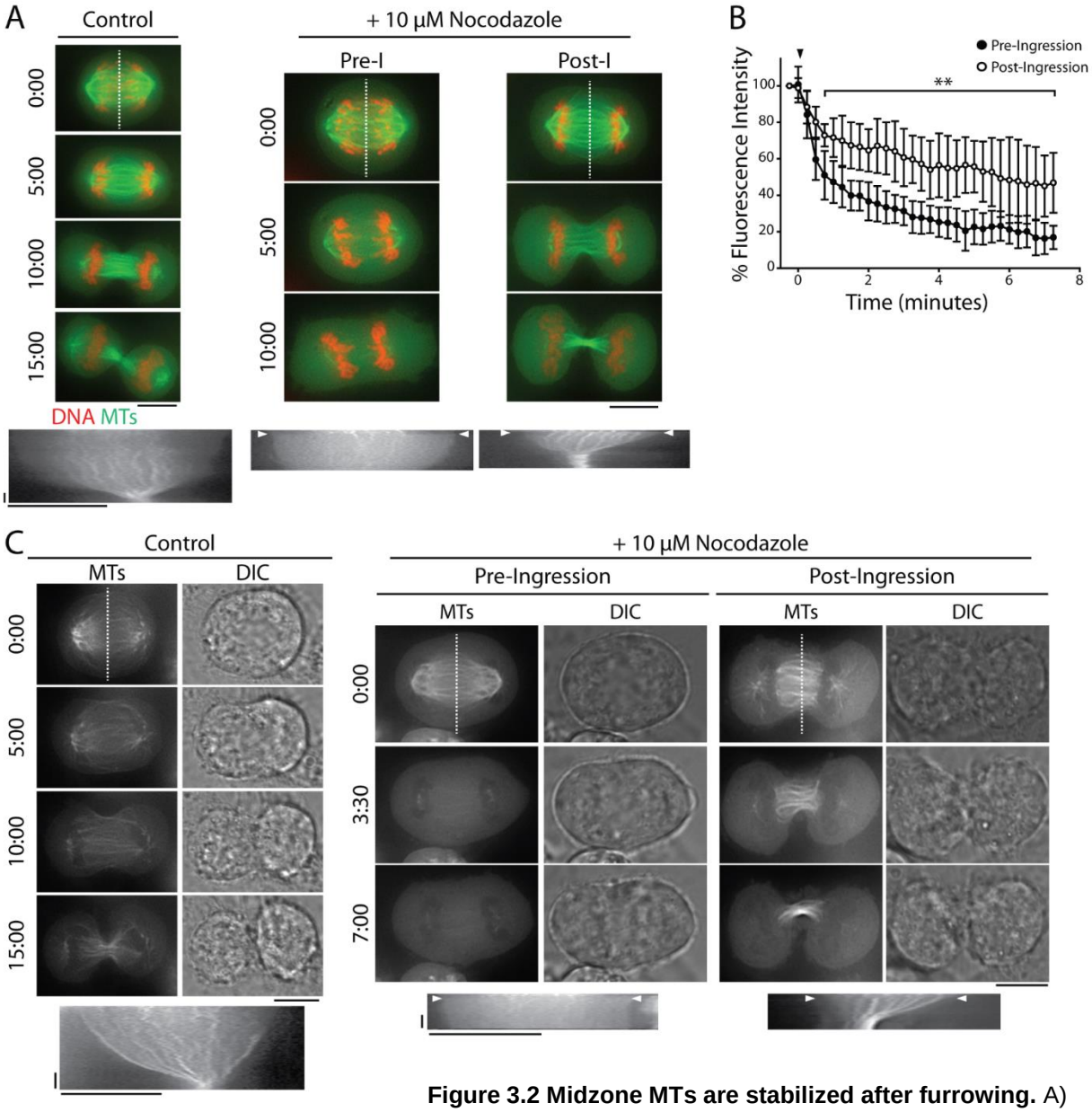

Figure 3.2 Midzone MTs are stabilized after furrowing. A) Top: Single z-plane micrographs taken from time lapse movies of HeLa cells expressing GFP-tubulin (green) and mCherry-H2B (red) exiting mitosis in the presence of DMSO (control) or 10 µM nocodazole. Time is indicated in min relative to the initial frame. Dashed lines were used to generate kymographs. Scale bars, 10 µm. Bottom: Kymographs of GFP-tubulin fluorescence across the division plane during C phase. Arrowheads (white) indicate time point of nocodazole addition. Scale bars, 2.5 min (x axis) and 10 µm (y axis). B) Quantification of midzone MT fluorescence intensity in pre- and post-ingression cells treated with 10 µM nocodazole. Arrowhead (black) indicates the time of nocodazole addition. Data represent mean ± SD. n=10 (pre-I) and 9 (post-I) from three independent experiments, ** = $p < 0.01$. Continued on next page.

Figure 3.2 continued. C) Top: Single z-plane micrographs taken from time lapse movies of C phase HeLa cells expressing mCherry-tubulin in the presence of DMSO (control) or 10 μM nocodazole. Time is indicated in min:seconds relative to the initial frame. Dashed lines were used to generate kymographs. Scale bars, 10 μm. Bottom: Kymographs of GFP-tubulin fluorescence across the division plane during C phase. Arrowheads (white) indicate time point of nocodazole addition. Scale bars, 2.5 min (x axis) and 10 μm (y axis). F) Quantification of midzone MT fluorescence intensity in pre- and post-ingression cells treated with 10 μM nocodazole. Arrowhead (black) indicates the time point of nocodazole addition. Data represent mean ± SD. n=8 (pre-I) and 9 (post-I) cells from three independent experiments, * = $p < 0.05$.

midzone MT disassembly when added to cells that had not initiated furrowing (Figure 3.2 A, Pre-I). The addition of nocodazole to cells that had begun furrowing, however, did not cause widespread midzone MT depolymerization (Figure 3.2 A, Post-I). At the terminal time point (7 min following nocodazole addition), pre-ingression cells retained an average of only 16.3 ± 8.6% (mean ± SD, n=10 cells) of the initial midzone MT fluorescence, whereas post-ingression cells retained on average 45.1 ± 16.8% (n=9 cells) of their initial midzone MT fluorescence (Figure 3.2 B). Similar results were obtained using cells expressing mCherry-tubulin (Figure 3.2 C and D). These results indicate that midzone MTs acquire nocodazole resistance after furrowing has initiated, and is consistent with observations made using our fixed cell cold-stability assay.

Stabilization of midzone MTs requires myosin II activity

Midzone MTs might acquire stability through a time-dependent process or, alternatively, become stabilized by furrowing. To discriminate between these models, we used lamin B immunofluorescence to more precisely judge how long a cell had spent in C phase. Few non-ingressed cells (9.3 ± 1.6%, n=125 cells) had detectable lamin B on chromatin, but this number increased to 95 ± 1.1% (n=123 cells) in ingressed cells (Figure 3.3 A) demonstrating that lamin B immunofluorescence is a suitable marker for late-stage C phase cells. We then treated asynchronous cells with the non-muscle myosin II inhibitor blebbistatin (100 μM) to block furrow

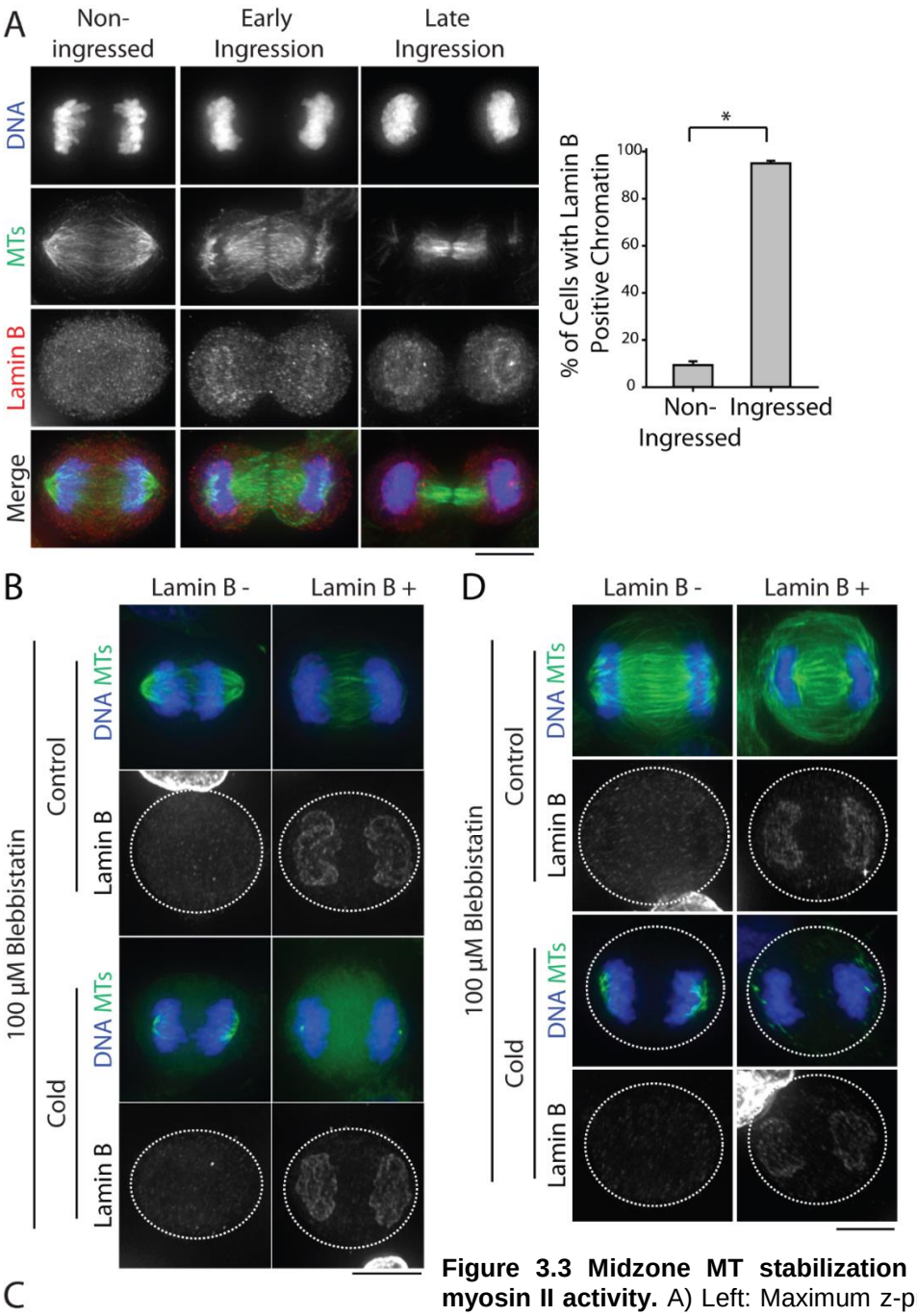

Figure 3.3 Midzone MT stabilization requires non-muscle myosin II activity. A) Left: Maximum z-projections of HeLa cells in C phase with non-ingressed or ingressed cleavage furrows showing nuclear envelope staining. Cells were stained with antibodies against tubulin (green) and lamin B (red). DNA (blue) was counterstained with Hoechst 33342. Scale bar, 10 µm. Right: Quantification of the percent of cells with lamin B staining in C phase. Data represents mean ± SE. n > 200 cells from three independent experiments, * = p < 0.005. B) Maximum z-projections of cells treated with 100 µM blebbistatin prior to fixation (top) or cold treatment (bottom). Cells were stained with antibodies to lamin B (single channels) to mark the nuclear envelope and tubulin (green). DNA was counterstained with Hoechst 33342 (blue). Scale bar, 10 µm. Continued on next page.

ingression without perturbing assembly of the contractile array (Straight et al., 2003). Although midzones were present in blebbistatin-treated cells at 37°C (Straight et al., 2003), they were cold-

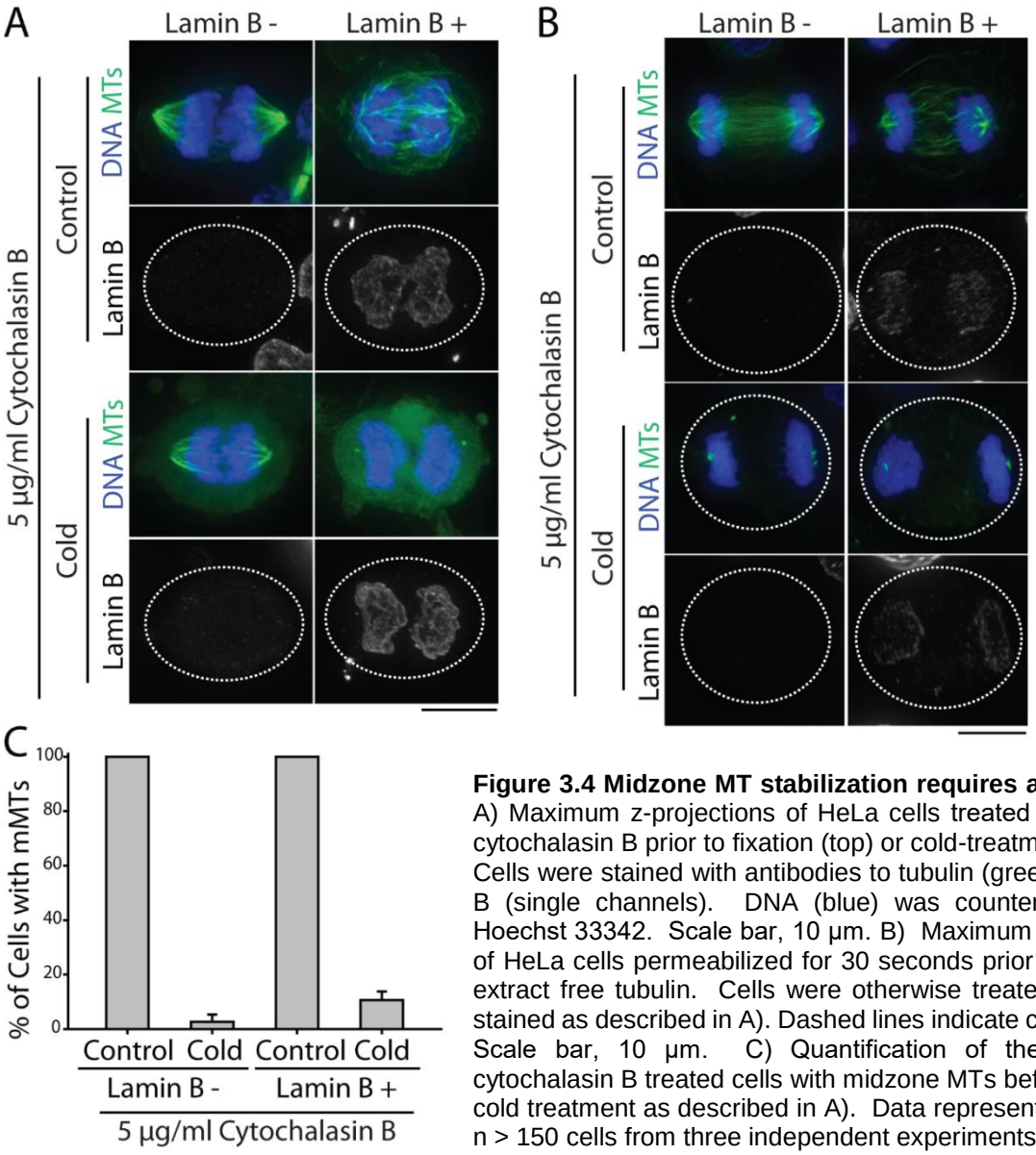

Figure 3.4 Midzone MT stabilization requires acto-myosin. A) Maximum z-projections of HeLa cells treated with 5 µg/ml cytochalasin B prior to fixation (top) or cold-treatment (bottom). Cells were stained with antibodies to tubulin (green) and lamin B (single channels). DNA (blue) was counterstained with Hoechst 33342. Scale bar, 10 µm. B) Maximum z-projections of HeLa cells permeabilized for 30 seconds prior to fixation to extract free tubulin. Cells were otherwise treated, fixed, and stained as described in A). Dashed lines indicate cell boundary. Scale bar, 10 µm. C) Quantification of the percent of cytochalasin B treated cells with midzone MTs before and after cold treatment as described in A). Data represent mean ± SE, n > 150 cells from three independent experiments.

Figure 3.3 continued C) Quantification of the percentage of blebbistatin-treated cells with midzone MTs before and after cold treatment as described in B). Data represent mean ± SE, n > 200 cells from three independent experiments. D) Maximum z-projections of HeLa cells permeabilized for 30 seconds prior to fixation to extract free tubulin. Cells were otherwise treated, fixed, and stained as described in B). Dashed lines indicate cell boundary. Scale bar, 10 µm.

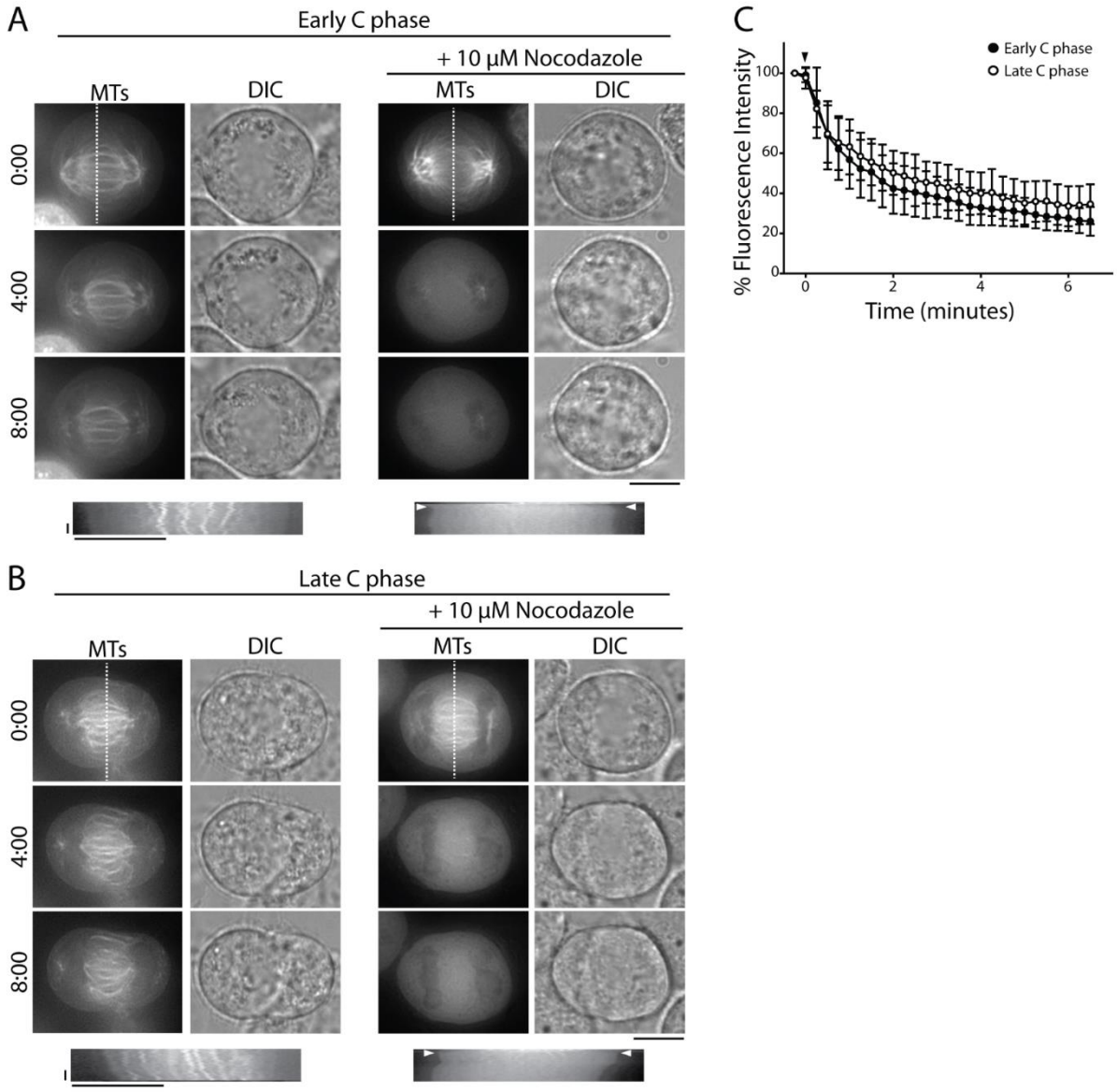

Figure 3.5 Midzone MT stabilization requires furrowing. A) Top: Single z-plane micrographs of HeLa cells expressing mCherry-tubulin in early C phase, as judged by the degree of chromatin condensation. Cells were treated with 100 µM blebbistatin prior to addition of 10 µM nocodazole. Time is indicated in min relative to the initial frame. Dashed lines were used to generate kymographs. Scale bar, 10 µm. Bottom: Kymographs of mCherry-tubulin fluorescence across the division plane during C phase. Arrowheads (white) indicate time of nocodazole addition. Scale bars, 2.5 min (x axis) and 10 µm (y axis). B) Top: Single z-plane micrographs of HeLa cells expressing mCherry-tubulin in late C phase, as judged by the lack of condensed chromatin. Cells were treated with 100 µM blebbistatin prior to addition of 10 µM nocodazole. Time is indicated in min relative to the initial frame. Dashed lines were used to generate kymographs. Scale bar, 10 µm. Bottom: Kymographs of mCherry-tubulin fluorescence across the division plane during C phase. Arrowheads (white) indicate time of nocodazole addition. Scale bars, 2.5 min (x axis) and 10 µm (y axis). C) Quantification of midzone MT fluorescence intensity in early and late C phase cells treated with 100 µM blebbistatin and 10 µM nocodazole. Arrowhead (black) indicates time of nocodazole addition. Data represent mean ± SD. n=14 (early anaphase) and 13 (late anaphase) cells, from three independent experiments.

labile even in cells containing lamin B-labeled chromatin (Figure 3.3 B and C). Similar results were observed in cells treated with 5 μg/ml cytochalasin B, an actin poison (Figure 3.4 A). Again, pre-extraction of free tubulin did not affect these results (Figures 3.3 D and 3.4 B).

We then tested the relative importance of time spent in C phase *versus* contractility for midzone MT stabilization in live cells using our nocodazole shock assay. As blebbistatin has phototoxic effects when imaged with blue light (Kepiro et al., 2014; Mikulich et al., 2012; Sakamoto et al., 2005), we transiently expressed mCherry-tubulin in HeLa cells to visualize midzone MTs. DIC imaging was used to determine the degree of chromatin condensation and distinguish between cells in early or late C phase. Cells were treated with blebbistatin to block furrowing for > 20 min prior to nocodazole addition. Without nocodazole, midzone MTs in early C phase (condensed chromatin as observed by DIC) or late C phase (decondensed chromatin) persisted throughout blebbistatin treatment (Figure 3.5). Addition of nocodazole, however, induced midzone MT disassembly in both early and late C phase. At the terminal time point (6 minutes, 30 seconds), cells in early C phase treated with nocodazole had 26.0 ± 7.2% (n=14 cells) of the initial fluorescence from tubulin polymer. Nocodazole similarly affected cells in late C phase (34.6 ± 9.9%, n=13 cells) indicating that a prolonged C phase does not considerably increase midzone stability in the absence of myosin II contractility (Figure 3.5 C). These observations suggest that midzone MTs do not become stable as a function of time spent in C phase, but rather that their stability is dependent on myosin II contractility.

Spindle elongation during C phase requires furrow ingression

Anaphase B is marked by the elongation of the central spindle to further segregate sister chromosomes into the two proto-daughter cells. Elongation of the spindle midzone is believed to

occur by coupling MT polymerization to motor-dependent sliding (Roostalu et al., 2010; Rozelle et al., 2011; Wang et al., 2013). The timing of central spindle elongation is closely coupled to cleavage furrow ingression and we asked whether these processes were also intrinsically linked. To test this idea, we tracked midzone elongation during C phase by live imaging cells expressing mCherry-tubulin. We observed that when furrow ingression was blocked, by treatment with blebbistatin, the central spindle did not fully elongate (Figure 3.6 A). In cells treated with DMSO, the anaphase spindle elongated to a maximum pole-to-pole distance of 11.3 ± 0.3 microns (mean ± SE, n=16 cells). In cells treated with blebbistatin, the maximum pole to pole distance in C phase was only 9.1 ± 0.5 microns (n=24 cells). To ensure that we did not unintentionally quantify central spindle length in early C phase cells, only cells with decondensed chromatin were included in this analysis. Similar to our observations of midzone stabilization, this finding suggests that spindle elongation during anaphase B depends on acto-myosin contractility and is not related to the duration of C phase.

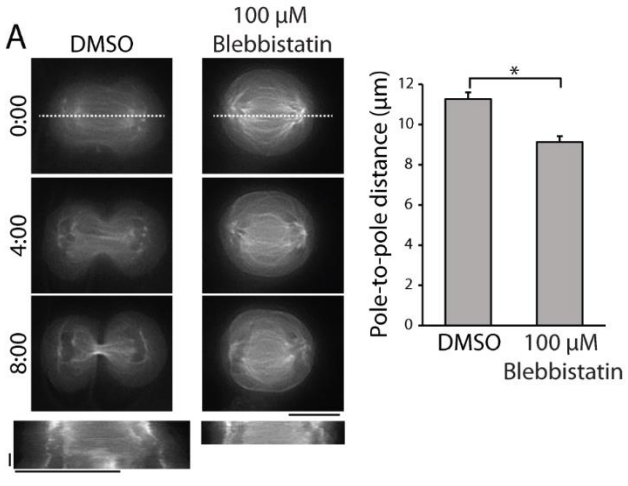

Figure 3.6 Central spindle elongation requires furrow ingression. A) Left, top: Single z-plane micrographs of HeLa cells expressing mCherry-tubulin in C phase, treated with DMSO or 100 µM blebbistatin. Time is indicated in min relative to the initial frame. Dashed lines were used to generate kymographs. Scale bar, 10 µm. Left, bottom: Kymographs of mCherry-tubulin across the spindle axis over time. Scale bars, 10 µm (x axis) and 3 min (y axis). Right: Quantification of the maximum pole-to-pole distance of cells treated with DMSO or Blebbistatin. Data represents mean ± SD. n=16 (DMSO) and 24 (blebbistatin), from three independent experiments, * = $p < 0.05$.

Discussion

Whether actomyosin contractility influences midzone formation during cytokinesis is controversial. Actin disruption eliminates midzone MTs during the meiotic divisions of *Drosophila* spermatocytes (Giansanti et al., 1998) and myosin II inhibition prevents midzone formation during monopolar cytokinesis (Hu et al., 2008). However, similar perturbations in somatic cells undergoing normal, bipolar cytokinesis (Aubin et al., 1981; Cimini et al., 1998; Savoian et al., 1999; Straight et al., 2003) have yielded conflicting results. Our data show that the midzone MTs of HeLa and RPE-1 cells are stabilized upon furrow initiation in a manner that requires actomyosin contraction, suggesting that furrow ingression impacts bipolar midzone stability. These findings are consistent with previous reports showing that midzone MTs in somatic cells acquire resistance to nocodazole (Hu et al., 2011) and pressure (Salmon et al., 1976) during cytokinetic progression. Additionally, our cell analyses demonstrate that myosin II contractility is only required to initiate the feedback signaling that stabilizes midzone MTs; midzones become nocodazole-resistant once furrowing has begun. It is likely that the onset of furrowing thus triggers a unidirectional change in the physiological properties of the midzone.

CHAPTER 4

THE CHROMOSOMAL PASSENGER COMPLEX MEDIATES CYTOSKELTAL FEEDBACK SIGNALING

Introduction

Aurora B kinase (ABK) is the catalytic component of the Chromosomal Passenger Complex (CPC), a protein complex which also consists of INCENP, Borealin, and Survivin, and plays key roles in multiple aspects of cytokinesis (Carmena et al., 2012). While the CPC has well-documented functions in cleavage plane specification (Nguyen et al., 2014) and promoting midzone assembly (Kaitna et al., 2000), its role at the furrow remains unclear. Interestingly, studies of monopolar cytokinesis implicate the CPC in mediating myosin II-dependent cortex-to-MT signaling that promotes the formation of a monopolar midzone (Hu et al., 2008). Moreover, the CPC localizes to actin cables in a MT-free zone that connects the cortex to midzone MTs during monopolar cytokinesis (Canman et al., 2003; Hu et al., 2008). As our data demonstrate a causal relationship between furrow ingression and midzone MT stabilization, we investigated ABK as a potential candidate to mediate cortex-to-MT signaling in bipolar midzones.

A modified version was previously published as:
Landino, J. and Ohi, R. (2016) The Timing of Midzone Stabilization during Cytokinesis Depends on Myosin II Activity and an Interaction between INCENP and Actin. *Curr Biol* 26, 698-706

Stabilization of midzone MTs requires Aurora B kinase activity

To test whether ABK regulates midzone stabilization during C phase, we treated cells for 10 min with 2 μM ZM447439, an ABK inhibitor (Ditchfield et al., 2003), prior to cold treatment. ZM447439 caused a ~5-fold decrease in the percentage of ingressed cells with cold-stable MTs (15 ± 1.7%, mean ± SE, n=85 cells) compared to control cells (79.3 ± 0.9%, n=123 cells) suggesting that ABK activity is required for midzone stabilization after furrow ingression (Figure 4.1 B). Pre-extraction of soluble tubulin did not affect the outcome of this experiment (Figure 4.1 C). To demonstrate this in live cells, GFP-tubulin/mCherry-H2B labeled cells were treated with ZM447439 for 5 min prior to imaging or exposure to nocodazole. Under these conditions, ZM447439 treatment alone did not cause midzone disassembly in either pre- or post-ingression anaphase cells (Figure 4.1 D). Nocodazole addition, however, caused rapid MT disassembly both before and after furrow ingression. Pre-ingression cells treated with ZM447439 maintained only 26.7 ± 10.0% (mean ± SD, n=11 cells) of the initial midzone fluorescence after 6 min in nocodazole (Figure 4.1 E). Likewise, post-ingression midzones maintained only 16.9 ± 7.9% (n=10 cells) of the initial fluorescence after nocodazole addition, demonstrating that myosin II-dependent midzone MT stabilization after the initiation of furrowing also requires active ABK.

We also investigated whether myosin II inhibition might alter midzone stability by disrupting ABK localization. We noted no observable differences in ABK localization in non-ingressed cells compared to ingressed cells suggesting that the change in MT stability observed between these two stages is not due to gross changes in the steady state localization of the kinase (Figure 4.2 A). Additionally, inhibition of myosin II or ABK activity did not prevent ABK from localizing to the division plane (Figure 4.2 B and C) suggesting that changes in midzone stability, induced either through contractility or treatment with small molecules, cannot be attributed to

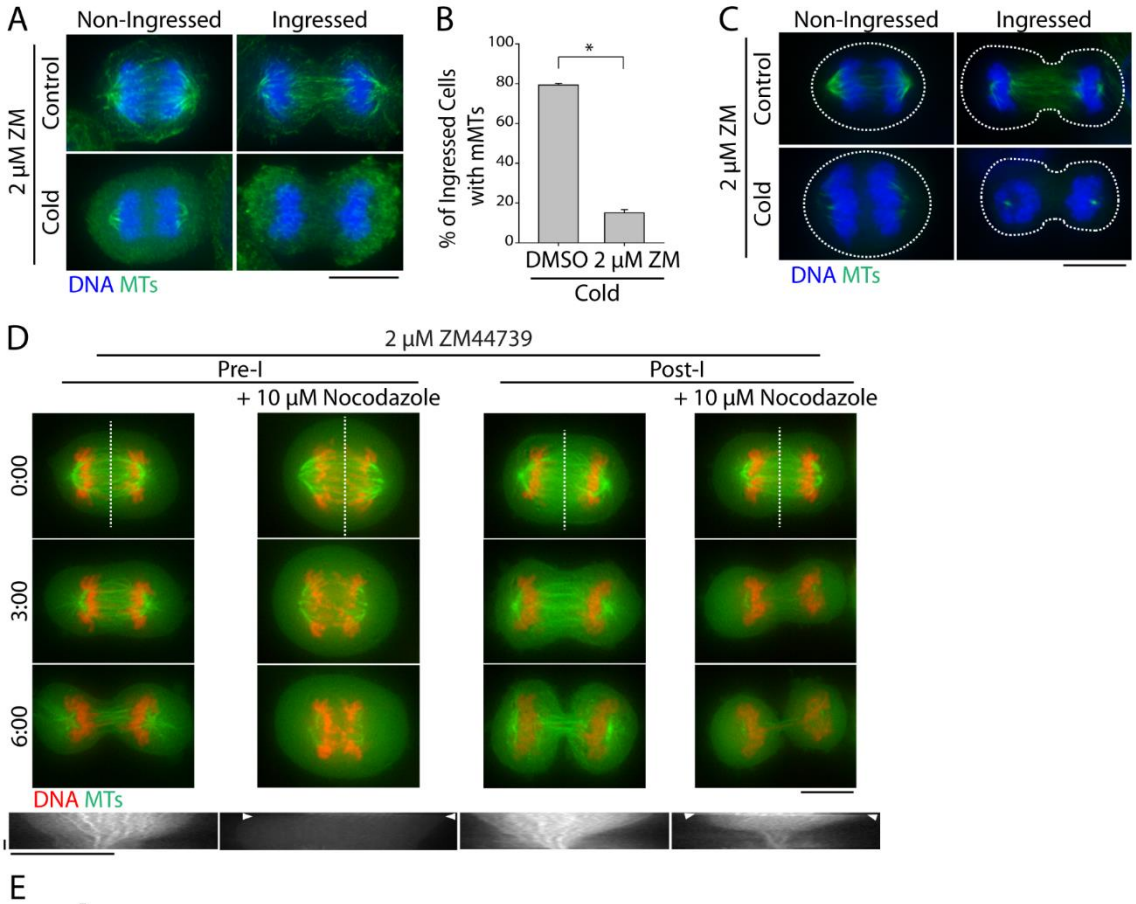

Figure 4.1 ABK activity is required for midzone MT stabilization. A) Maximum z-projections of cells treated with 2 µM ZM447439 (ZM) prior to fixation (top) or cold treatment (bottom). Cells were stained with antibodies to tubulin (green) and DNA was counterstained with Hoechst 33342 (blue). Scale bar, 10 µm. B) Quantification of the percentage of ingressed cells with midzone MTs after treatment with DMSO or 2 µM ZM447439 and cold. Data represent mean ± SE, n > 200 cells from three independent experiments, * = $p < 0.005$. C) Maximum z-projections of HeLa cells treated, fixed and stained as described in A). Cells were permeabilized prior to fixation to remove free tubulin. Dashed lines indicate cell boundary. Scale bar, 10 µm. D) Top: Single z-plane micrographs taken from time lapse movies of pre- and post-ingression HeLa cells expressing GFP-tubulin (green) and mCherry-H2B (red) treated with 2 µM ZM447439 with or without 10 µM nocodazole. Time is indicated in min relative to the initial frame. Dashed lines were used to generate kymographs. Scale bar, 10 µm. Bottom: Kymographs of GFP-tubulin fluorescence across the division plane during C phase. Arrowheads (white) indicate time of nocodazole addition. Scale bars, 2.5 minutes (x axis) and 10 µm (y axis). E) Quantification of midzone MT fluorescence intensity in pre- and post-ingression cells treated with 2 µM ZM447439 and 10 µM nocodazole. Arrowhead (black) indicates time of nocodazole addition. Data represent mean ± SD. n=11 (pre-ingression), and 10 (post-ingression) from three independent experiments.

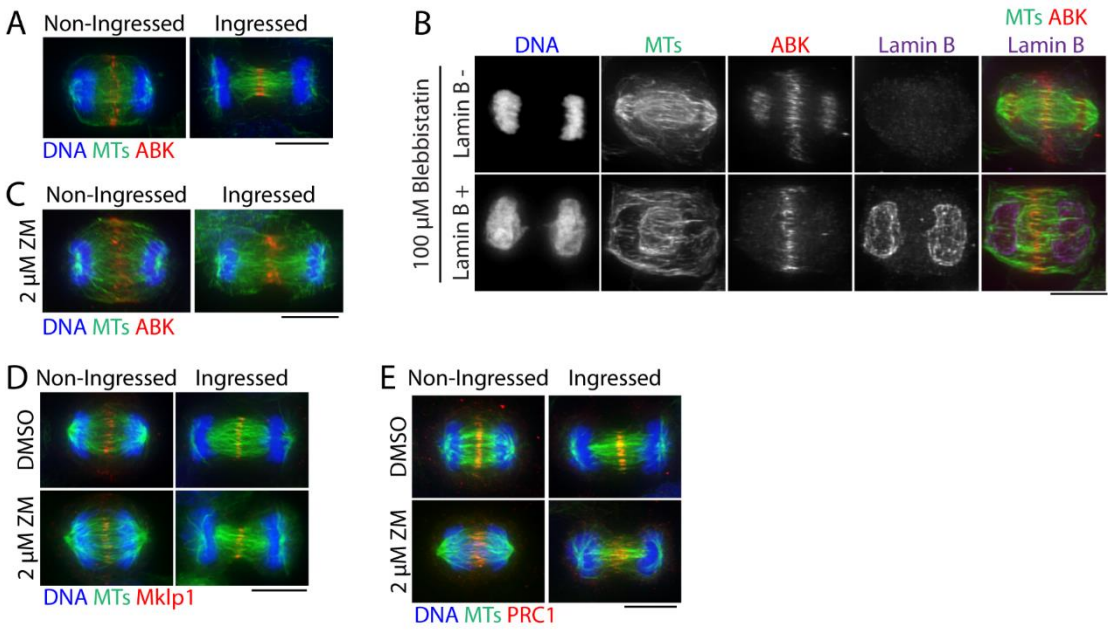

Figure 4.2 ABK localization during C phase. A) Maximum z-projections of HeLa cells stained with antibodies to Aurora B kinase (ABK, red) and tubulin (green). DNA was counterstained with Hoechst 33342 (blue). Scale bar, 10 μm. B) Maximum z-projections of cells treated with 100 μM blebbistatin. Cells were stained with antibodies to ABK (red), lamin B (purple) to mark the nuclear envelope, and tubulin (green). DNA (blue) was counterstained with Hoechst 33342. Scale bar, 10 μm. C) Maximum z-projections of cells treated with 2 μM ZM447439. Cells were stained with antibodies to ABK (red) and tubulin (green). DNA (blue) was counterstained with Hoechst 33342. Scale bar, 10 μm. D) Maximum z-projections of cells treated with DMSO (top) or 2 μM ZM447439 (bottom). Cells were stained with antibodies to Mklp1 (red) and tubulin (green). DNA (blue) was counterstained with Hoechst 33342. Scale bar, 10 μm. E) Maximum z-projections of cells treated with DMSO (top) or 2 μM ZM447439 (bottom). Cells were stained with antibodies to PRC1 (red) and tubulin (green). DNA (blue) was counterstained with Hoechst 33342. Scale bar, 10 μm.

changes in ABK localization. Brief inhibition of ABK also did not displace the midzone organizing factors Mklp1 and PRC1 (Figure 4.2 D and E).

Midzone MT destabilization requires Polo-like kinase 1

Microtubule dynamics are highly regulated throughout mitosis (Belmont et al., 1990), including during C phase, with multiple mitotic kinases working to control cytoskeletal remodeling (Carmena et al., 2012; Green et al., 2012). Polo-like kinase 1 (Plk1) contributes to the formation of an organized midzone during C phase by regulating the localization of the plus-end directed

kinesin Mklp1 (Li et al., 2010), and the MT cross-linker PRC1 (Hu et al., 2012; Schmucker and Sumara, 2014). We investigated whether Plk1 activity regulates midzone stabilization by briefly treating cells with the small molecule inhibitor BI 2536 (100 nM) for 20 min before exposure to cold temperature. In agreement with our previous work, midzone MTs in non-ingressed DMSO-treated cells were sensitive to cold temperature (Figure 4.3 A). However, following Plk1 inhibition, midzone MTs in non-ingressed cells were cold-stable. This finding suggests that Plk1 may function in early C phase, opposite of ABK, to promote midzone MT disassembly or turnover. While we have not pursued studies of Plk1 regulation of midzone stabilization, future investigations should include identifying downstream regulators of early C phase MT dynamics, as well as exploring the relationship between Plk1-dependent and ABK-dependent regulation of midzone MT stabilization.

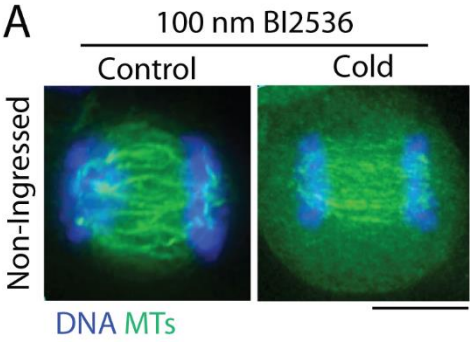

Figure 4.3 Midzone destabilization in early C phase requires Plk1. A) Maximum z-projections of HeLa cells treated with DMSO or 100 nM BI 2536prior or cold-treatment. Cells were stained with antibodies to tubulin (green). DNA (blue) was counterstained with Hoechst 33342. Scale bar, 10 μm.

Human INCENP binds actin directly

The localization of ABK to actin cables during monopolar cytokinesis (Hu et al., 2008) suggests that its function in monopolar midzone formation may require an interaction with actin. Interestingly, *Dictyostelium* INCENP has been shown to associate with actin in cells (Chen et al., 2007), leading us to speculate that human INCENP might also bind actin directly. To examine this possibility, we first analyzed the ability of various GFP-INCENP constructs to co-localize

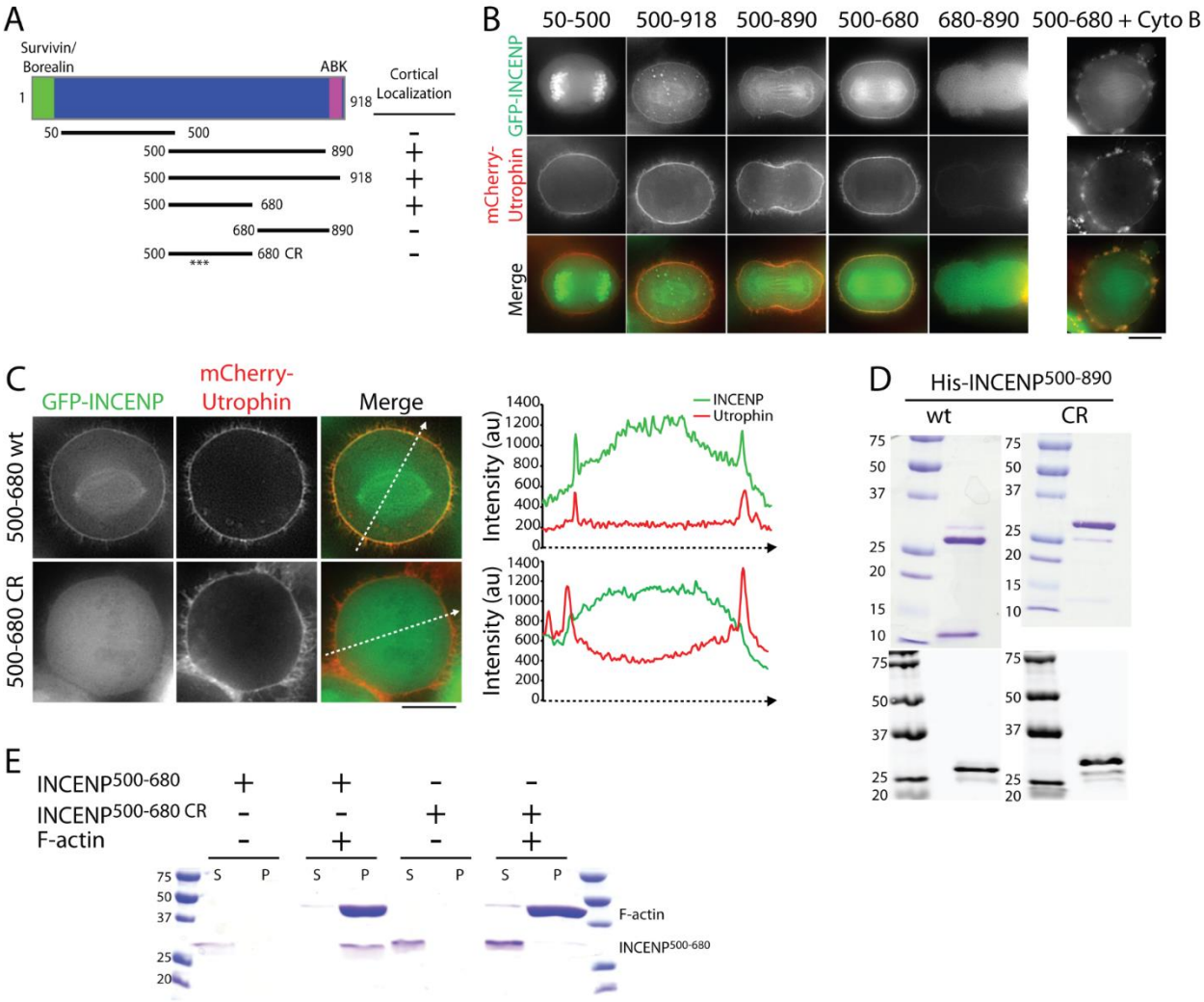

Figure 4.4 Characterization INCENP-actin binding. A) Schematic of GFP-INCENP truncations used to map the actin binding domain in cells. B) Single plane micrographs of HeLa cells expressing GFP-INCENP (green) truncations and mCherry-Utrophin (red). Cells expressing GFP-INCENP 500-680 and mCherry-Utrophin were treated with 10 µg/ml cytochalasin B to confirm that colocalization was specific. Scale bar, 10 µm. C) Single z-plane micrographs of HeLa cells transiently expressing mCherry-Utrophin to mark actin (red) and GFP-INCENP$^{500-680}$ fragments (green) containing the wild type (wt) INCENP sequence or charge reversal (CR) mutations. Dashed lines were used to generate line scans. Scale bar, 10 µm. D) Top: Coomassie-stained gels showing recombinant His$_6$-INCENP$^{500-680}$ and His$_6$-INCENP$^{500-680\ CR}$. Bottom: Anti-His immunoblots of recombinant His$_6$-INCENP$^{500-680}$ and His$_6$-INCENP$^{500-680\ CR}$. Molecular weight standards are indicated in kDa. E) Coomassie-stained gel showing an actin co-sedimentation assay using recombinant wt or CR His$_6$-INCENP$^{500-680}$. Supernatant (S) and pellet (P) fractions are indicated. Molecular weight standards are indicated in kDa.

with actin-based structures, marked with mCherry-Utrophin, when exogenously expressed in

HeLa cells (Figure 4.4 B). A 180 amino acid (aa) fragment of INCENP (hereafter referred to as INCENP$^{500\text{-}680}$) was sufficient to co-localize with actin during both interphase and mitosis. To confirm the specificity of this co-localization, we treated cells expressing GFP-INCENP$^{500\text{-}680}$ with cytochalasin B and found that its localization was disrupted in a manner similar to that of actin (Figure 4.4 C). As INCENP aa residues 500-680 reside in a highly charged region of a single alpha helical domain (Samejima et al., 2015), we hypothesized that INCENP associates with actin through an electrostatic interaction. To test this, and to abrogate a potential INCENP-actin interaction, we generated charge-reversal mutants (lysine/arginine-to-glutamic acid) within amino acid residues 500-680. Charge-reversal of ten residues (K563,R564,R565,R566,K571,K573,R574,R577,R579,K580) abolished co-localization of GFP-INCENP$^{500\text{-}680}$ with mCherry-Utrophin in mitotic cells (Figure 3.11, INCENP$^{500\text{-}680\ CR}$). To determine if INCENP binds actin directly, we purified recombinant His$_6$-INCENP$^{500\text{-}680}$ from *E. coli* (Figure 4.4 D) and performed an actin co-sedimentation assay. His$_6$-INCENP$^{500\text{-}680}$ sediments specifically in the presence of F-actin, indicative of a direct interaction. His$_6$-INCENP$^{500\text{-}680\ CR}$, however, does not co-sediment with actin, indicating that the charge-reversal mutations that abolish actin co-localization in cells also disrupt direct actin binding *in vitro* (Figure 4.4 E).

INCENP-actin binding is required for midzone stabilization

To investigate the role of CPC actin-binding during C phase, we next incorporated the ten charge-reversal mutations into a full-length GFP-INCENP construct (GFP-INCENP CR). We then used a depletion/rescue strategy to substitute endogenous INCENP with either full-length GFP-INCENP or GFP-INCENP CR (Figure 4.5 A). We first analyzed the localization of the CPC in

cells expressing wild type GFP-INCENP or GFP-INCENP CR by imaging GFP and ABK. In agreement with previous work (Earnshaw and Cooke, 1991), GFP-INCENP and ABK both

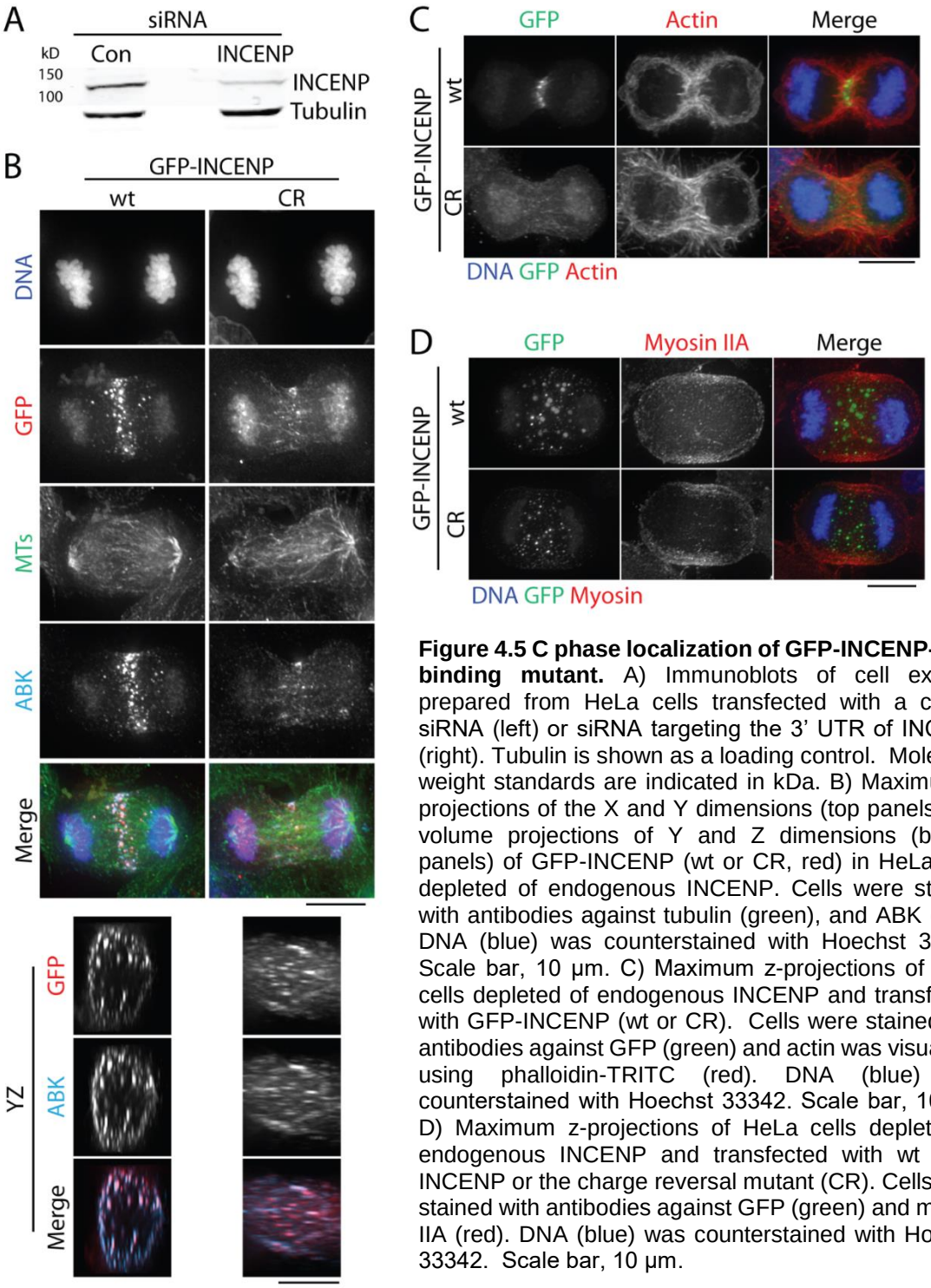

Figure 4.5 C phase localization of GFP-INCENP-actin binding mutant. A) Immunoblots of cell extracts prepared from HeLa cells transfected with a control siRNA (left) or siRNA targeting the 3' UTR of INCENP (right). Tubulin is shown as a loading control. Molecular weight standards are indicated in kDa. B) Maximum z-projections of the X and Y dimensions (top panels) and volume projections of Y and Z dimensions (bottom panels) of GFP-INCENP (wt or CR, red) in HeLa cells depleted of endogenous INCENP. Cells were stained with antibodies against tubulin (green), and ABK (teal). DNA (blue) was counterstained with Hoechst 33342. Scale bar, 10 μm. C) Maximum z-projections of HeLa cells depleted of endogenous INCENP and transfected with GFP-INCENP (wt or CR). Cells were stained with antibodies against GFP (green) and actin was visualized using phalloidin-TRITC (red). DNA (blue) was counterstained with Hoechst 33342. Scale bar, 10 μm. D) Maximum z-projections of HeLa cells depleted of endogenous INCENP and transfected with wt GFP-INCENP or the charge reversal mutant (CR). Cells were stained with antibodies against GFP (green) and myosin IIA (red). DNA (blue) was counterstained with Hoechst 33342. Scale bar, 10 μm.

to the midzone and the cell cortex in cells expressing wild type GFP-INCENP (Figure 4.5 B), with cortical localization examined in volume projections rotated by 90°. In cells expressing

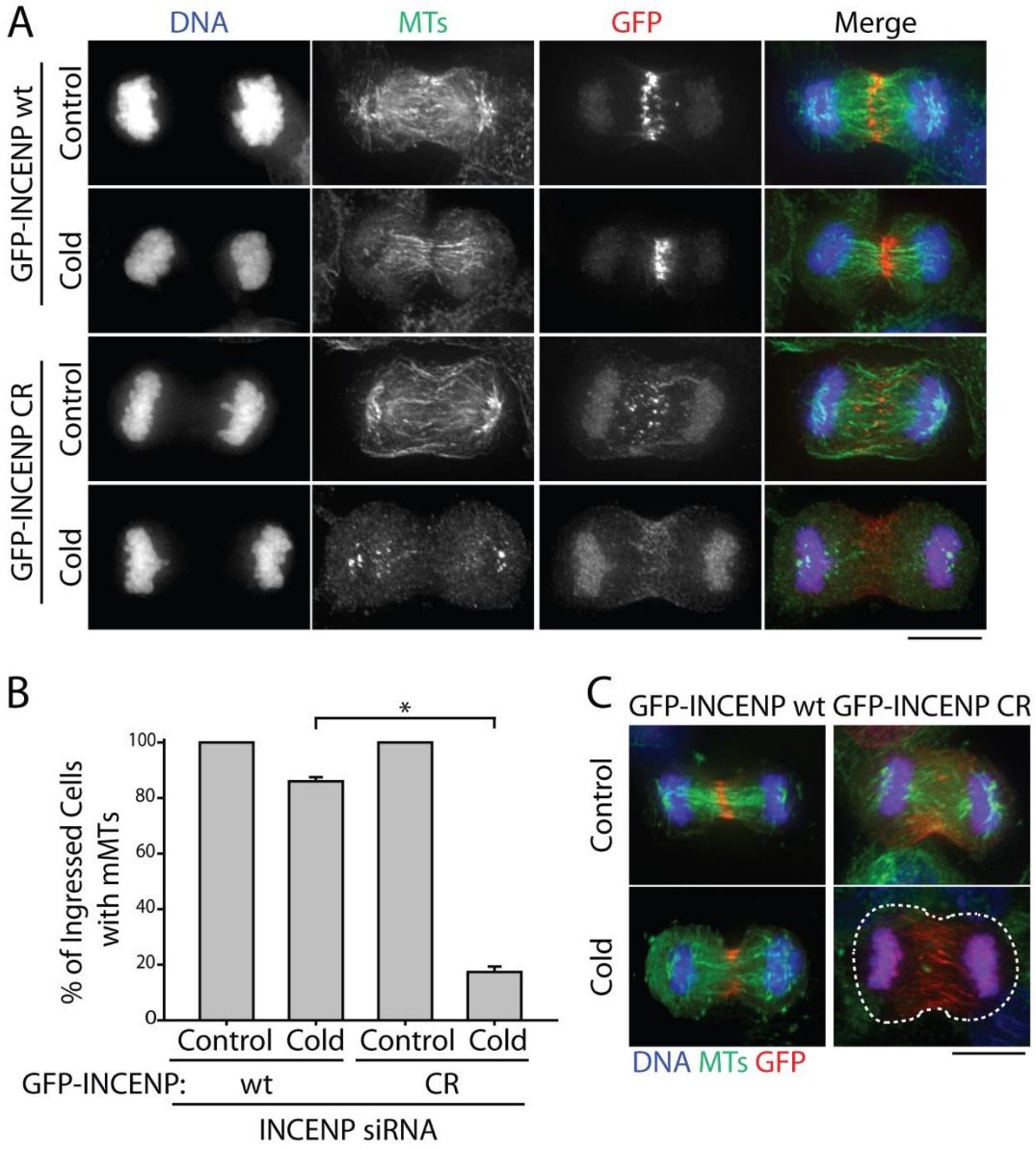

Figure 4.6 INCENP actin-binding promotes midzone MT stabilization. Maximum z-projections of HeLa cells depleted of endogenous INCENP and rescued with full-length GFP-INCENP (top) or GFP-INCENP CR (bottom) prior to fixation or cold-treatment. Cells were stained with antibodies against tubulin (green) and GFP (red). DNA was counterstained with Hoechst 33342 (blue). Scale bar, 10 μm. B) Quantification of the percent of cells with midzone MTs before and after cold-treatment as described in A). Data represent mean ± SE. n = 148 cells from three independent experiments, * = $P < 0.005$. C) Maximum z-projections of HeLa cells treated and stained as described in A). Cells were permeabilized for 30 seconds prior to fixation. Dashed lines indicate cell boundary. Scale bar, 10 μm.

GFP-INCENP CR, GFP-INCENP and ABK still localized to the midzone and to the cell cortex, although this mutation appears to partially disrupt CPC distribution along the midzone. Myosin II and actin localized normally in cells expressing GFP-INCENP CR (Figure 4.5 C and D), indicating that expression of the mutant does not disrupt the organization of the contractile array.

We next assayed midzone MT stability in these cells using exposure to cold temperature (Figure 4.6 A). Similar to unperturbed cells, 86.0 ± 1.5% (mean ± SE, n=84 cells) of ingressed cells expressing wild type GFP-INCENP had cold-stable midzone MTs. However, the percentage of cells with stable midzone MTs decreased ~5-fold in cells expressing GFP-INCENP CR (17.3 ± 3.5%, n=64 cells; Figure 4.6 B). Pre-extraction to remove free tubulin did not change our ability to detect MTs (Figure 4.6 C). This 5-fold decrease in midzone MT stability observed in ingressed cells expressing GFP-INCENP CR mirrors the decrease we observed following ABK inhibition using ZM447439 (Figure 4.1 A), supporting the idea that INCENP-actin interactions are crucial for the CPC to mediate feedback signaling from cortical actin to midzone MTs.

INCENP-actin binding is required for cleavage furrow ingression

To investigate the role of INCENP-actin binding during cleavage furrow ingression, we used live cell imaging to follow cells depleted of endogenous INCENP and rescued with either GFP-INCENP or GFP-INCENP CR throughout C phase. We observed that 100 ± 0.0% of cells expressing wild type GFP-INCENP were successful in cleavage furrow ingression (mean ± SE, n=12 cells), validating our approach. In contrast, only 37.8 ± 2.3% of cells expressing GFP-INCENP CR were able to ingress the furrow and form a midbody (n=16 cells; Figure 4.7 B). As myosin II and actin localized normally in cells expressing GFP-INCENP CR (Figure 4.5 C and

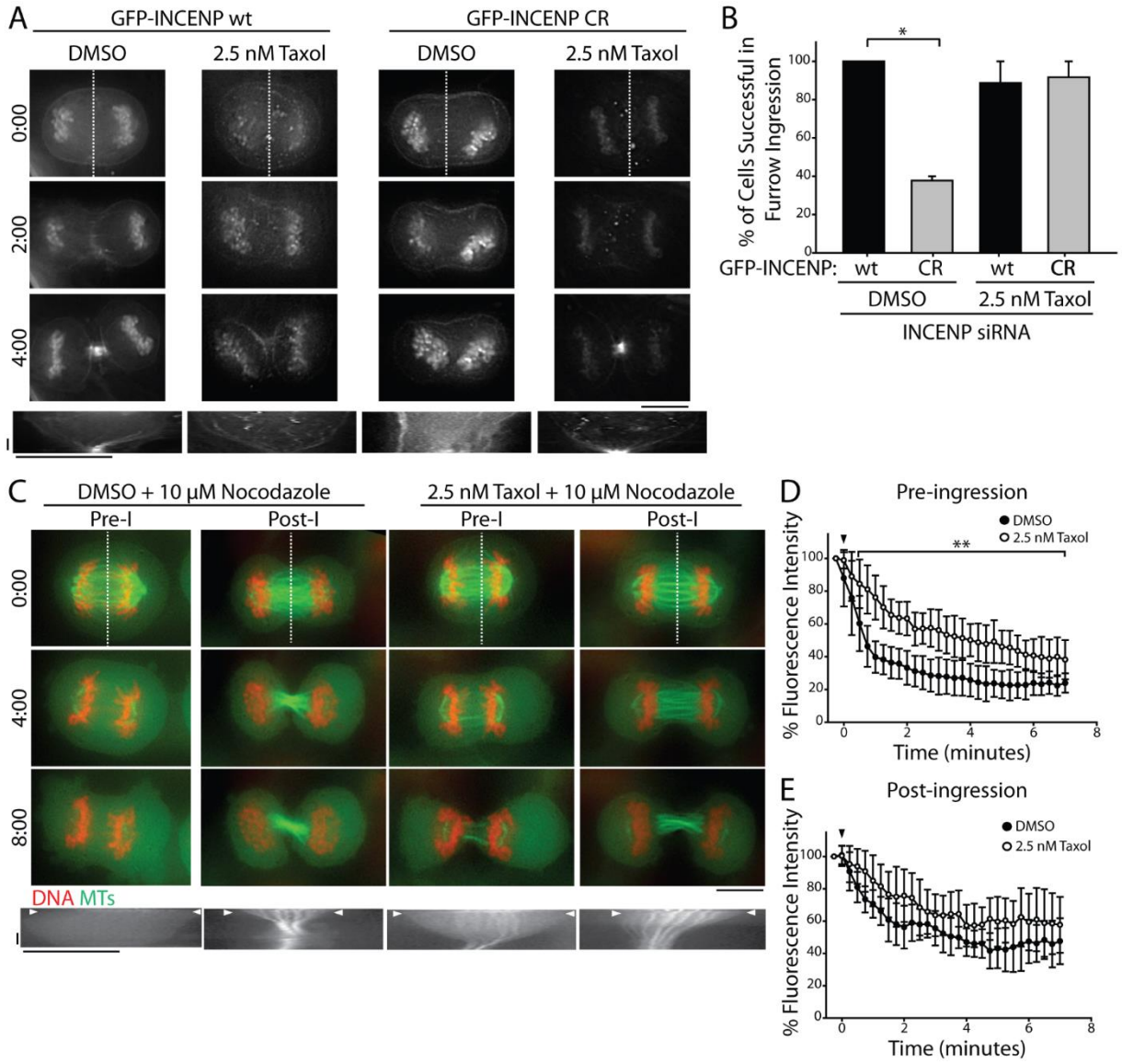

Figure 4.7 INCENP actin-binding promotes furrow closure. A) Top: Single z-plane micrographs taken from time-lapse of HeLa cells depleted of endogenous INCENP and and rescued with GFP-INCENP wt or the charge reversal mutant (CR). Cells were pre-incubated with DMSO or 2.5 nM taxol for 30 mins prior to imaging. Dashed lines were used to generate kymographs. Bottom: Kymographs of GFP-INCENP fluorescence across the division plane during C phase. Scale bars, 2.5 min (x axis) and 10 µm (y axis). B) Quantification of the percentage of cells expressing GFP-INCENP wt or CR that successfully completed furrow ingression as described in A). Data represent mean ± SE. n= 12 (wt, DMSO), 16 (CR, DMSO), 10 (wt, Taxol), and 12 (CR, Taxol) cells from three independent experiments, * = $p < 0.05$. C) Top: Single z-plane micrographs taken from time lapse movies of HeLa cells expressing GFP-tubulin (green) and mCherry-H2B (red) incubated for > 30 mins in DMSO or 2.5 nM Taxol prior to exposure to 10 µM nocodazole. Time is indicated in min relative to the initial frame. Dashed lines were used to generate kymographs. Scale bars, 10 µm. Bottom: Kymographs of GFP-tubulin fluorescence across the division plane during C phase. Arrowheads (white) indicate time point of nocodazole addition. Scale bars, 2.5 min (x axis) and 10 µm (y axis). D, E) Quantification of midzone MT fluorescence intensity in pre-ingression or post-ingression cells incubated with DMSO or 2.5 nM Taxol before exposure to 10 µM nocodazole. Arrowhead (black) indicates the time of nocodazole addition. Data represent mean ± SD. n=11 (pre-I, DMSO), 10 (pre-I, 2.5 nM Taxol), 9 (post-I, DMSO) and 10 (post-I, 2.5 nM Taxol) from three independent experiments, ** = $p < 0.01$.

D), furrow ingression failure in GFP-INCENP CR-expressing cells cannot be a consequence of failed actomyosin accumulation.

As cells expressing GFP-INCENP CR have cold-sensitive midzone MTs, we next investigated whether artificially stabilizing MTs would rescue cleavage furrow ingression in these cells. To test this, we incubated cells in the presence of a low dose of taxol (2.5 nM for 30 minutes, (Gayek and Ohi, 2014)) prior to imaging, a treatment that did not impede C phase progression in cells expressing wild type GFP-INCENP. Cells expressing wild type GFP-INCENP completed cleavage furrow ingression 88.7 ± 11.3% of the time (mean ± SE, n=10 cells) in taxol (Figure 4.7 B). Similarly, cells expressing GFP-INCENP CR also successfully completed cleavage furrow ingression following taxol treatment (91.6 ± 8.3, n=12; Figure 3.14 cells). To confirm that 2.5 nM taxol altered midzone MT stability during C phase, we used the live cell nocodazole shock assay. HeLa cells stably expressing GFP-tubulin and mCherry-H2B were pre-incubated with DMSO or 2.5 nM taxol for 30 minutes before exposure to 10 μM nocodazole (Figure 4.7 C). In cells pre-incubated with low-dose taxol, midzone MTs were more stable when nocodazole was added before cleavage furrow ingression. At the terminal time point (7 min following nocodazole addition), pre-ingression cells incubated with DMSO retained only 23.9 ± 5.9 % (mean ± SD, n=11 cells) of the initial midzone MT fluorescence, whereas pre-ingression cells incubated with taxol retained on average 38.2 ± 11.9% (n=10 cells) of their initial midzone MT fluorescence (Figure 4.7 D). Taken together these results support the notion that INCENP-actin binding is essential for cytokinesis, and that this interaction is important because it promotes midzone MT stabilization.

Disrupting INCENP-MT binding does not affect midzone stabilization

Previous work has shown that the CPC interacts with MTs *via* INCENP (Noujaim et al., 2014; Rosasco-Nitcher et al., 2008; Wheatley et al., 2001b). Of note, the charge reversal mutations that disrupt INCENP actin-binding also appear to disrupt MT localization of GFP-INCENP$^{500\text{-}680}$ in cells (Figure 4.4 A). To confirm that the effect of GFP-INCENP CR expression on midzone stabilization is specific to breaking the CPC-actin interaction and not due to disrupting the CPC-MT interaction we quantified midzone stabilization in cells expressing a second charge reversal mutant (GFP-INCENP MT CR, see Methods and Appendix I). These charge reversal mutations selectively disrupt localization of GFP-INCENP$^{500\text{-}680}$ to MTs in cells without perturbing actin co-localization. We replaced endogenous INCENP with full length GFP-INCENP MT CR using the same depletion/rescue strategy outlined above, and exposed cells to cold temperature to assay midzone stability. In agreement with our previous findings, 90.3 ± 4.0% of ingressed cells expressing wild type GFP-INCENP had cold-stable midzones (mean ± SD, n=52 cells). Midzones were similarly stable in cells expressing GFP-INCENP MT CR as 85.1 ± 4.1 % (n=54 cells) of ingressed cells had midzone MTs after cold treatment (Figure 4.8 A). This result indicates that then CPC-MT interaction is not necessary for midzone MT stabilization after furrow ingression. This finding supports our hypothesis that the CPC-actin interaction is essential and specific for

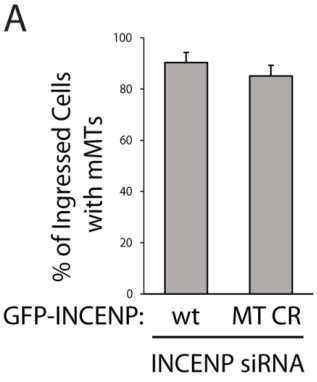

Figure 4.8 INCENP MT-binding is not required for midzone MT stabilization. A) Quantification of the percentage of ingressed HeLa cells depleted of endogenous INCENP and rescued with full-length GFP-INCENP or GFP-INCENP MT CR with midzone MTs after cold-treatment. Data represents mean ± SD. n = 106 cells from two independent experiments.

promoting midzone stabilization after furrow ingression.

Kif2a midzone localization is controlled by Aurora B kinase activity

We next investigated factors that could alter MT dynamics during C phase in order to identify possible effectors that work downstream of ABK signaling to regulate midzone stability. Previous work has shown that the Kinesin-13 Kif2a functions during C phase to regulate midzone MT dynamics and central spindle length (Uehara et al., 2013). Using immunofluorescence we observed that Kif2a localized to the midzone of non-ingressed C phase cells (Figure 4.9 A) and was not detectable on midzone MTs in ingressed cells. Notably, the disappearance of Kif2a immunofluorescence from the midzone is temporally correlated with the appearance of cold- and nocodazole-stable midzone MTs (Figure 3.1 and 3.2). We next investigated whether this displacement of Kif2a from midzone MTs was dependent on acto-myosin contractility. Cells were treated with blebbistatin as described previously (see Chapter 3) to block furrowing. Kif2a immunofluorescence was detectable on midzone MTs in blebbistatin-treated cells, including cells in late C phase, as indicated by decondensed chromatin (Figure 4.9 B). This suggests that Kif2a displacement from the midzone is coupled to cleavage furrow ingression and is not related to the time spent in C phase.

The MT-depolymerizing activity of kinesin-13s is negatively regulated by ABK *in vitro* (Ohi et al., 2007). Kinesin-13s diffuse along the MT lattice through electrostatic interactions with the tubulin E-hook (Helenius et al., 2006) and ABK-dependent phosphorylation blocks the enzymatic activity by decreasing MT binding (Andrews et al., 2004). With this in mind, we investigated whether Kif2a midzone localization was phospho-regulated by treating cells with ZM447439. We observed that in ZM447439-treated C phase cells Kif2a localized to a discrete

band in the center of the midzone regardless of the state of furrow ingression (Figure 4.9 C). This was distinct from the broad midzone localization normally observed in non-ingressed cells (Figure 4.9 A). This central region of the midzone represents the plus end overlap of midzone MTs (Bieling et al., 2010) and we hypothesized that this localization pattern indicated Kif2a accumulation on MT plus ends. We confirmed this by co-staining for the plus end directed

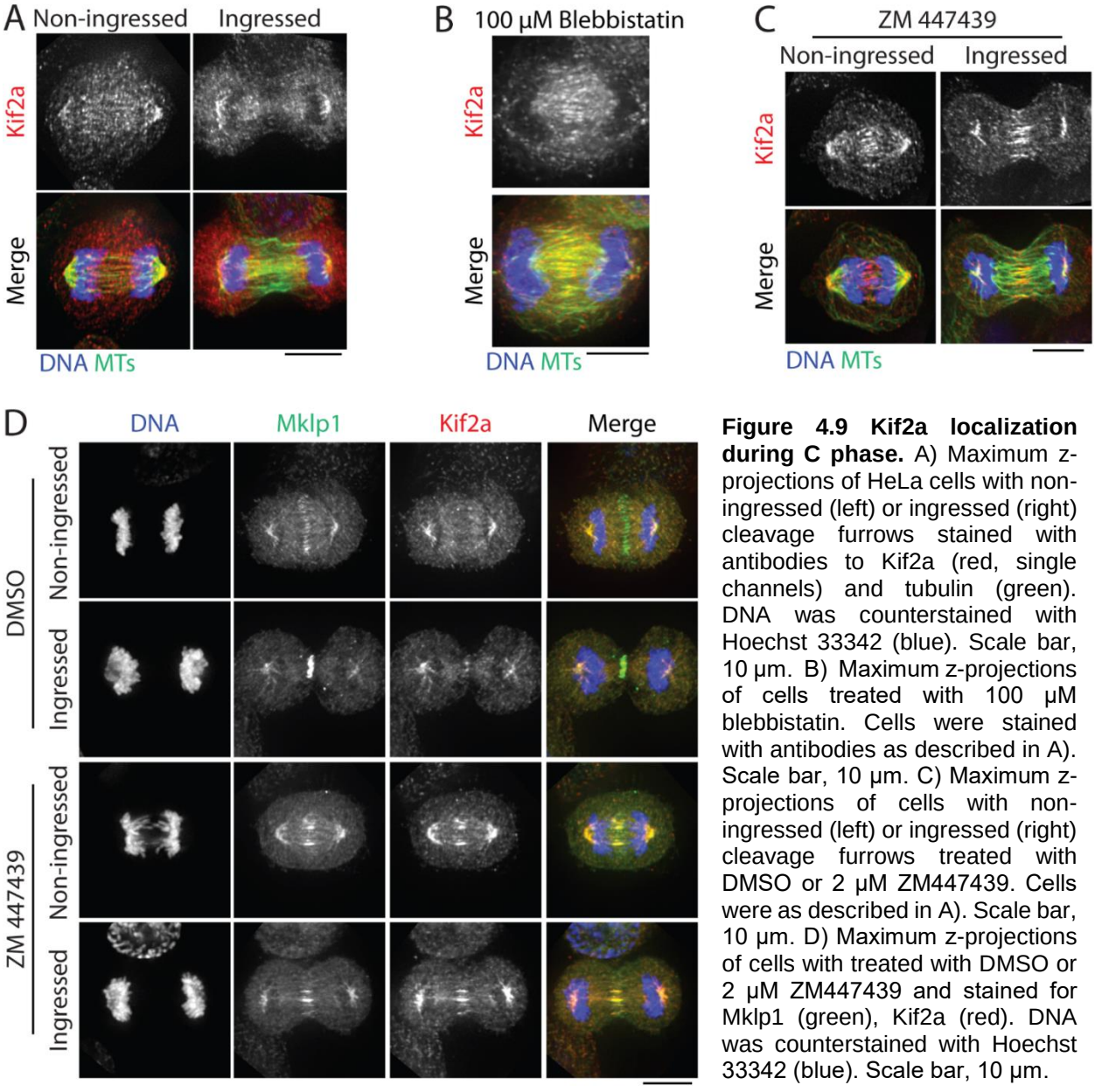

Figure 4.9 Kif2a localization during C phase. A) Maximum z-projections of HeLa cells with non-ingressed (left) or ingressed (right) cleavage furrows stained with antibodies to Kif2a (red, single channels) and tubulin (green). DNA was counterstained with Hoechst 33342 (blue). Scale bar, 10 µm. B) Maximum z-projections of cells treated with 100 µM blebbistatin. Cells were stained with antibodies as described in A). Scale bar, 10 µm. C) Maximum z-projections of cells with non-ingressed (left) or ingressed (right) cleavage furrows treated with DMSO or 2 µM ZM447439. Cells were as described in A). Scale bar, 10 µm. D) Maximum z-projections of cells with treated with DMSO or 2 µM ZM447439 and stained for Mklp1 (green), Kif2a (red). DNA was counterstained with Hoechst 33342 (blue). Scale bar, 10 µm.

anaphase kinesin Mklp1 (Gruneberg et al., 2006; Jang et al., 2005; Neef et al., 2006) and found that Kif2a and Mklp1 only co-localized after ABK inhibition (Figure 4.9 D). These results suggest that ABK functions during C phase to prevent Kif2a accumulation on midzone MTs, especially in ingressed cells. The presence of Kif2a immunofluorescence on midzone MTs in cells treated with ZM447439 may explain the sensitivity of these MTs to cold temperature and nocodazole (Figure 4.1).

Kif2a regulates midzone MT stabilization in non-ingressed cells

To investigate whether Kif2a affects midzone stabilization, we depleted cells of Kif2a using siRNA. Kif2a is notoriously difficult to deplete using RNAi (Uehara et al., 2013) so we analyzed depletion efficiency by Western Blot of whole cell lysates, and by counting the number of cells with Kif2a spindle pole staining after depletion. Normalized to tubulin, Kif2a protein levels were reduced to 26 ± 10.8 % of that in control cells (mean ± SD, n=2 experiments, Figure 4.10 B). Kif2a immunofluorescence was detectable at the spindle pole in 98.2 ± 0.7 % (n=254) of control depleted cells, however, after Kif2a depletion pole staining was only present in 32.1 ± 1.6 % of cells (mean ± SE, n=282) (Figure 4.10 C). These measurements indicate that Kif2a siRNA treatment only partially depletes protein levels in cells. We tested midzone MT stability in Kif2a-depleted cells using cold temperature and non-ingressed cells showed a moderate, but statistically significant, increase in midzone MT stability (Figure 4.11 D). After treatment with control siRNA 32.4 ± 3.6 % (mean ± SE, n=93) of cells had midzone MTs following cold treatment, whereas 56 ± 3.45 % (n=90) of cells treated with Kif2a siRNA had cold stable midzone MTs, suggesting Kif2a affects midzone MT stability during C phase. The moderate increase in midzone MT stability in non-ingressed cells after Kif2a depletion leads us to speculate that Kif2a is likely not the only

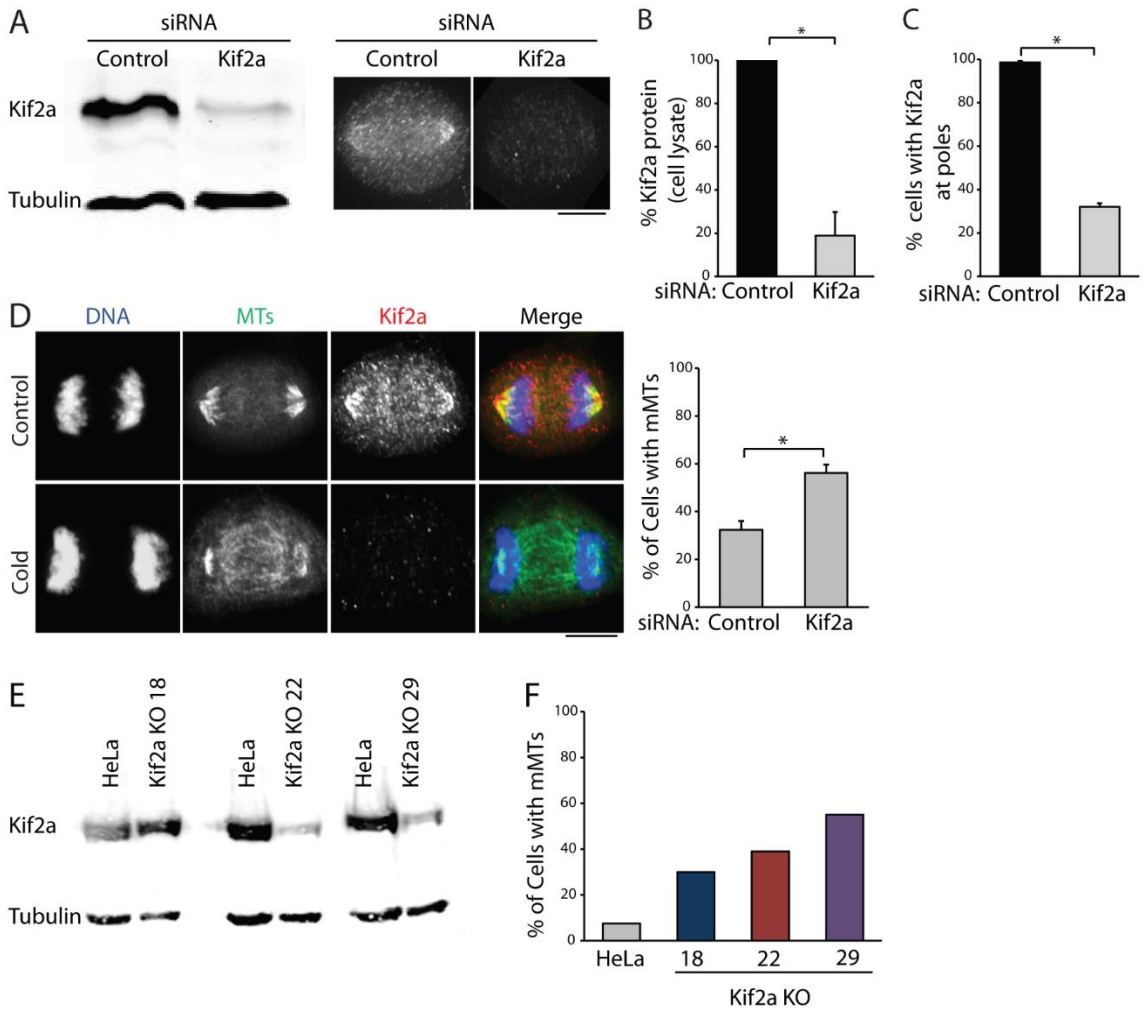

Figure 4.10 Midzone stabilization in cells lacking Kif2a A) Top: Representative Western blot of Kif2a protein levels after control or Kif2a RNAi. Tubulin is shown as a loading control. Bottom: Maximum z-projections of HeLa cells stained with antibodies to Kif2a after control or Kif2a RNAi. Scale bar, 10 μm. B) Quantification of Kif2a protein levels as analyzed by Western blot as described in A). Kif2a protein levels were normalized to tubulin and scored relative to control cells. Data represents mean ± SE. Measurements from two independent experiments, * = $p < 0.05$. C) Quantification of the percentage of cells showing Kif2a spindle pole staining after treatment as described in A). Data represents mean ± SE. $n > 250$ for each condition from four independent experiments, * = $p < 0.05$. D) Left: Maximum z-projections of non-ingressed cells treated as described in A) and stained with antibodies for tubulin (green) and Kif2a (red). DNA was counterstained with Hoechst 33342 (blue) Scale bar, 10 μm. Right: Quantification of the percentage of cells with mMTs after control or Kif2a RNAi and cold treatment. Data represents mean ± SE. n=94 (control) or 174 (Kif2a), * = $p < 0.05$. E) Western blot of Kif2a protein levels in HeLa and Kif2a KO cell lines. Tubulin is shown as a loading control. F) Quantification of the percentage of cells with mMTs in HeLa or Kif2a KO cell lines. n≥100 cells from one experiment.

factor regulating midzone MT dynamics. Taken together with the observation that Kif2a is displaced by ABK activity in ingressed cells, our data suggests that Kif2a may function to

destabilize midzone MTs before ingression, and that ABK-mediated displacement of Kif2a after furrowing promotes midzone stabilization.

Given the non-uniform depletion of Kif2a by RNAi and the unusually high percentage of non-ingressed control cells with cold-stable midzone MTs, we turned to the CRISPR-Cas9 (Mali et al., 2013) system to generate Kif2a knock out cell lines. HeLa cells twice transfected with gRNAs targeting *Kif2a* were clonally selected and screened using immunofluorescence. Three cell lines with reduced Kif2a protein levels (Figure 4.10 E) were selected and analyzed for midzone stability using cold treatment. Similar to Kif2a RNAi treatment, the percentage of non-ingressed C phase cells with cold-stable midzones increased in Kif2a KO cell lines. In HeLa cells 7.5% (n=40) of non-ingressed C phase cells had cold-stable midzone MTs, which more closely mirrors midzone stabilization in non-ingressed cells that we observed in other experiments (Figure 3.1). In Kif2a KO cell lines, 30 % (Kif2a KO 18, n=30), 39 % (Kif2a KO 22, n=36) and 55 % (Kif2a KO 29, n=40) of non-ingressed cells had cold-stable midzones (Figure 4.10 F). Notably, we later determined that the Kif2a KO cell line with the largest increase in midzone stabilization (Kif2a KO 29) was not clonal. We isolated single clones by limiting dilution from Kif2a KO 29 and again screened for a lack of Kif2a by immunostaining, however, these cells have not yet been analyzed for midzone MT stability.

Discussion

Although the mechanism of midzone MT stabilization is not clear, our data identify the CPC as a key mediator of this process; pharmacological inhibition of ABK at any point during cytokinesis results in rapid destabilization of midzone MTs. The importance of CPC actin-binding,

via INCENP, in promoting midzone MT stabilization after furrow ingression further suggests that the CPC may propagate a midzone MT stabilization signal that originates at the equatorial cortex. The idea that the CPC participates in a feedback loop that couples the activities of F-actin and MTs during cytokinesis has been suggested previously; Hu *et al.* showed that ABK activity is required for the formation of a midzone during monopolar cytokinesis (Hu et al., 2008). Our data also suggests that the kinesin-13 Kif2a may be a regulator of midzone stabilization that acts downstream of ABK signaling. Displacement of Kif2a from the midzone requires ABK activity and depletion of Kif2a results in hyper-stable midzone MTs. Finally, the requirement for midzone stabilization to promote furrow closure supports the notion that the activities of the actin and MT cytoskeletal systems are interdependent, and illuminates the fundamental role of cytoskeletal cross-talk during cell division.

CHAPTER 5

RECRUITMENT OF THE CHROMOSOMAL PASSENGER COMPLEX TO THE DIVISON PLANE

Introduction

At the metaphase to anaphase transition the CPC leaves the centromere and is targeted to midzone MT plus ends and the equatorial cortex (Adams et al., 2000; Carmena et al., 2012; Cooke et al., 1987; Earnshaw and Cooke, 1991). This localization depends on the plus end directed kinesin Mklp2; previous work has shown that RNAi of Mklp2 eliminates CPC localization at both midzone plus end and the cortex (Gruneberg et al., 2004; Hummer and Mayer, 2009; Kitagawa et al., 2014). Mklp2-depleted cells are characterized by two phenotypes: first, the CPC remains associated with chromatin throughout C phase, and second, cells fail to complete cleavage furrow ingression (Gruneberg et al., 2004; Kitagawa et al., 2013). Ingression failure in these cells is distinctive in that cells initiate furrowing, but the furrow regresses before midbody formation (Kitagawa et al., 2013). Our work shows that disrupting the INCENP-actin interaction perturbs midzone localization of the CPC during C phase, however the role of actin-binding in regulating CPC recruitment has not been studied. In this chapter, we present evidence for actin-dependent recruitment of the CPC to the equatorial cortex. Cortically localized CPC remains associated with Mklp2 as cell divide, however actin binding is sufficient to enrich CPC at the cortex in the absence

A modified version is in preparation for publication:
Landino, J. and Ohi, R. (2017)

of motor. These findings suggest that the C phase localization of the complex is regulated in two ways: through motor-dependent delivery to MT plus ends, and direct interactions with actin and the equatorial cortex.

Aurora B kinase localizes to the division plane in the absence of Mklp2

In agreement with previous work (Gruneberg et al., 2004), we found that Mklp2 RNAi blocked midzone targeting of ABK and enrichment on chromosomes during C phase (Figure 5.1 A). However, we also observed low levels of ABK at the division plane in cells with no detectable Mklp2 immunofluorescence. To quantify this, we analyzed the fluorescence intensity of ABK at the division plane and observed that Mklp2 RNAi decreased CPC levels ~3-fold (27.9 ± 4.3 AU in control cells, data represent mean ± SE, n=29 cells; 9.7 ± 1.4 AU in Mklp2-depleted cells, n=27 cells, Figure 5.1 B). This finding differs from previous work in that we observed that low levels of ABK immunofluorescence were still detectable at the division plane in the absence of Mklp2 (Figure 5.1 A). We also observed that ABK was present at the equatorial cortex in Mklp2-depleted cells, as viewed using a volume projection (YZ dimensions) of the division plane (Figure 5.1 C). This phenotype is unlikely to be due to partial motor depletion as the bulk of CPC fluorescence is localized to chromatin, a hallmark of Mklp2 RNAi treatment. These results indicate that Mklp2 depletion leads to a reduction, but not a complete loss of the CPC at the division plane. As our previous work indicates a role for actin-binding in regulating CPC localization during C phase, we next investigated whether this residual population of ABK was recruited in an actin-dependent manner. To test this possibility, we briefly treated Mklp2-depleted cells with cytochalasin B (5 μg/ml, 10 min) to disrupt F-actin, and we observed that under these conditions, endogenous ABK is only detectable on chromosomes and no longer concentrates at the division plane (Figure 5.1

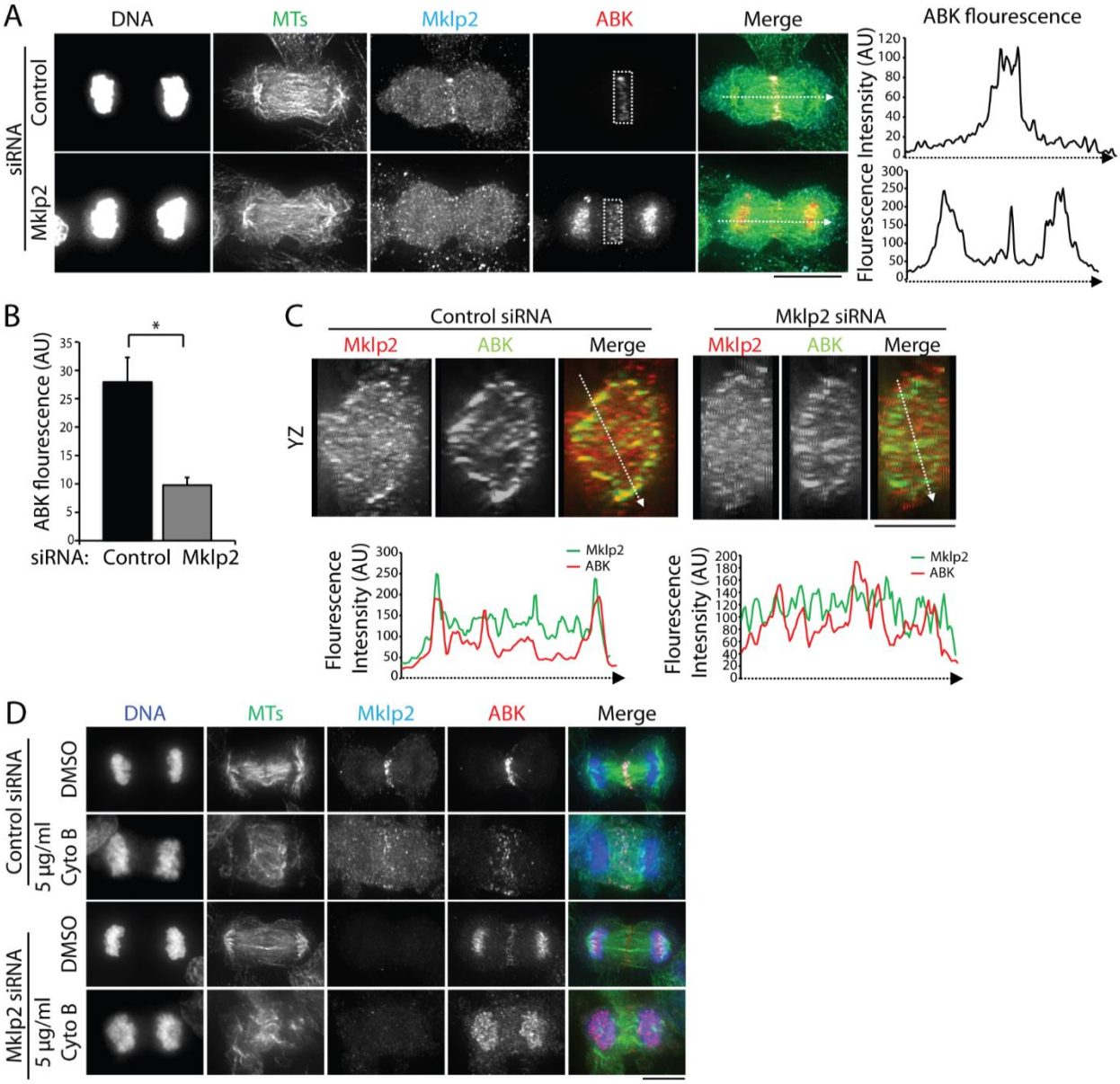

Figure 5.1 The CPC localizes to the division plane in the absence of Mklp2. A) Left: Maximum z-projections of HeLa cells transfected with control (top) or Mklp2 siRNA (bottom). Cells were stained with antibodies to tubulin (green), Mklp2 (teal) and ABK (red). DNA (blue) was counterstained with Hoechst 33342. Dashed boxes indicate regions used for quantitation of ABK fluorescence. Dashed lines were used to generate line scans. Scale bars, 10 µm. Left: line scans of ABK fluorescence intensity along the spindle axis in cells treated with control or Mklp2 siRNA. B) Quantification of ABK fluorescence intensity at the division plane after treatment as described in A). n > 50 cells from three independent experiments. * = $p < 0.05$. C) Top: Volume projections (YZ dimensions) of the division plane of cells treated as described in A). Dashed lines were used to generate line scans. Scale bar 10 µm. Bottom: Line scans of Mklp2 and ABK fluorescence intensity across the YZ projection of the division plane. D) Maximum z-projections of HeLa cells transfected with control or Mklp2 siRNA and treated with DMSO or 5 µg/ml cytochalasin B (Cyto B). Cells were stained with antibodies to tubulin (green), Mklp2 (teal), and ABK (red). DNA (blue) was counterstained with Hoechst 33342. Scale bar, 10 µm.

D). This observation suggests that CPC recruitment to the division plane in the absence of Mklp2 requires actin.

The CPC is enriched at sites of actin-MT overlap during C phase

In agreement with previous work (Earnshaw and Cooke, 1991), we found that ABK localized to the cell periphery in YZ volume projections of the division plane and INCENP immunofluorescence co-localized with actin in similar projections, confirming that the CPC is enriched at the cell cortex during C phase (Figure 5.2 A and B). The equatorial enrichment overlapped with cortically-associated MTs that apparently run along the cell cortex, demonstrating that the CPC localizes to regions where actin and MTs intersect. Notably, we cannot resolve cortically-associated MT plus ends in these cells and therefore cannot specify whether this represents localization to single MT plus ends that terminate at the cortex, or overlapping MT plus ends. We further analyzed the spatial relationship between the CPC, actin, and MTs during C phase using single optical sections of INCENP immunofluorescence at the division plane. We observed that INCENP co-localized with MTs, cortical actin, or both filaments simultaneously (Figure 5.2 C), demonstrating that the CPC can accumulate on cortical actin at sites devoid of furrow-associated MTs. This finding is in agreement with our previous work showing INCENP binds actin *in vitro* and is consistent with the observation that ABK decorates actin cables during monopolar cytokinesis (Hu et al., 2008).

The co-localization of INCENP with both actin filaments and MTs prompted us to investigate the role each filament system plays in positioning the CPC at the division plane. We analyzed the localization of ABK in cells briefly treated with 5 μM nocodazole, 5 μg/ml cytochalasin B, or both drugs simultaneously. In DMSO-treated cells, ABK localized to a

narrowly focused 2.0 ± 0.4 μm wide band (mean ± SD, measured in the X dimension along the spindle axis, n=14 cells, Figure 5.3 B) at the division plane, and prominently to the equatorial

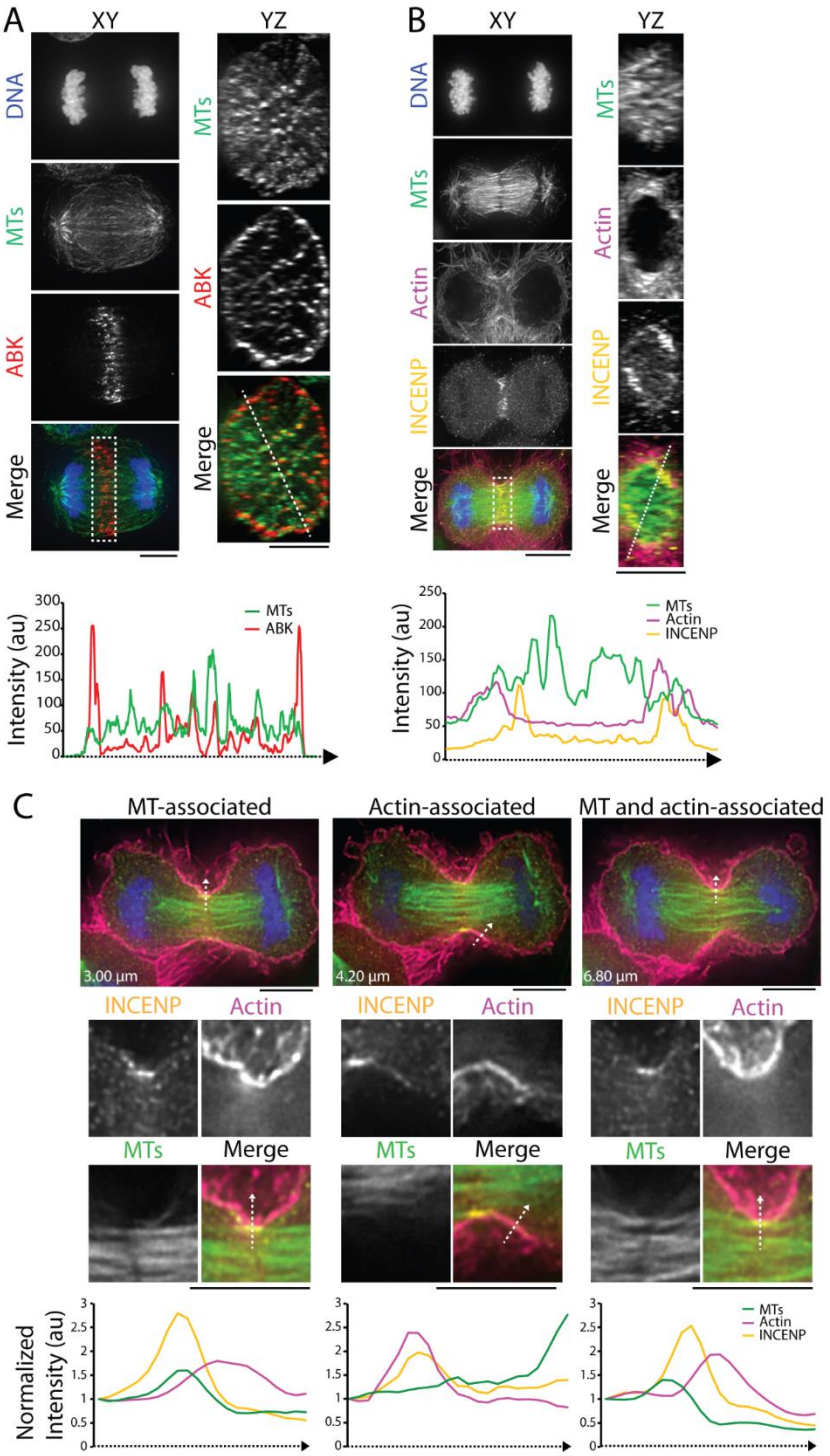

Figure 5.2 The CPC co-localizes with actin and MTs at the cortex during C phase. A, B) Top: Maximum z-projections of the X and Y dimensions of C phase cells (left panels). Dashed box indicates section used to generate a volume projection of Y and Z dimensions (right panels). Dashed lines were used to generate line scans. Cells were stained with antibodies to tubulin (green), ABK (red, A), and INCENP (yellow, B). Actin was visualized with phalloidin-TRITC (pink, B). DNA was counterstained with Hoechst 33342 (blue). Scale bars, 10 μm. Bottom: line scans of MT and ABK fluorescence intensity or MT and Actin and INCENP fluorescence intensity across the YZ projection of the division plane. C) Top: Single optical sections through a C phase cell stained with antibodies to tubulin (green) and INCENP (yellow). DNA (blue) was counterstained with Hoechst 33342. Actin was visualized using phalloidin-TRITC (pink). Dashed arrows were used to generate line scans. Distance of each optical section from the coverslip is indicated at the bottom left. Scale bars, 10 μm. Bottom: line scans of MT and actin and INCENP fluorescence at each optical section, as indicated by dashed arrows in panels shown above.

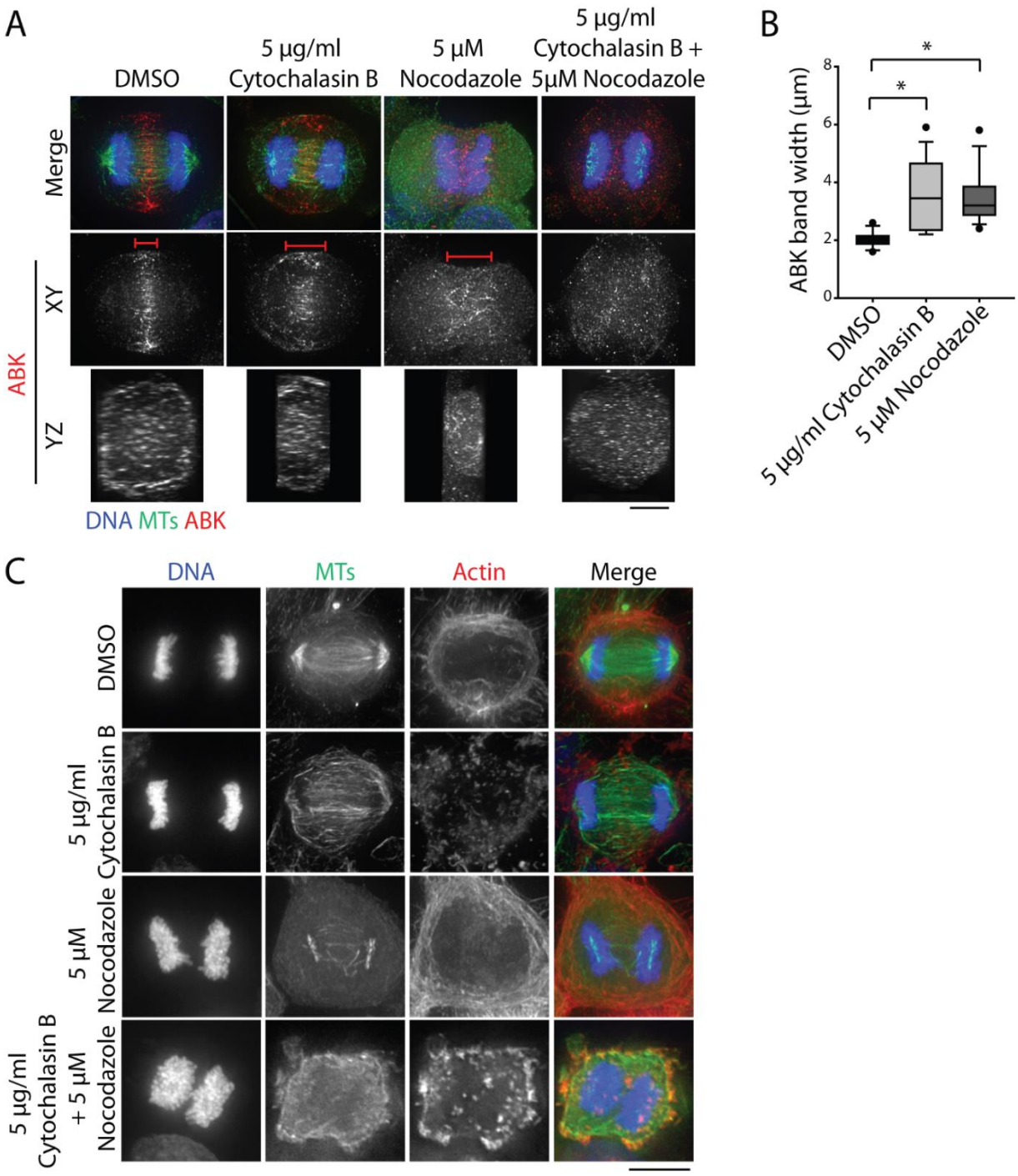

Figure 5.3 CPC localization to the division plane requires MTs and actin. A) Maximum z-projections of the XY dimensions (top) and volume projections of ABK localization in the YZ dimensions (bottom) in cells treated with DMSO, 5 µg/ml cytochalasin B, 5 µM nocodazole, or both drugs simultaneously. Brackets (red) indicate representative regions used to derive "band width" measurements of ABK along the spindle axis. Cells were stained with antibodies to tubulin (green) and ABK (red). DNA (blue) was counterstained with Hoechst 33342 (blue). Scale bar, 10 µm. B) Quantification of ABK band width along the spindle axis in C phase cells treated with DMSO, 5 µg/ml cytochalasin B, or 5 µM nocodazole. Data represent mean ± SD. n = 14 cells per condition, * = $p < 0.05$. C) Maximum z-projections of cells treated as described in A). Cells were stained with antibodies to tubulin (green) and actin was visualized using phalloidin-TRITC (red). DNA (blue) was counterstained with Hoechst 33342. Scale bar, 10 µm.

cortex (Figure 5.3 A). Single drug treatments displaced ABK in two ways. First, the ABK band widened ~2-fold at its maximum points of separation along the spindle axis (4.6 ± 1.8 μm after nocodazole, n=14 cells; 4.2 ± 1.7 μm after cytochalasin B, n=14 cells, Figure 5.3 B). Second, the cortical enrichment of ABK was reduced (Figure 5.3 A). Notably, ABK localization to both the division plane and the cell cortex was only completely abolished when actin filaments and MTs were simultaneously disrupted (Figure 5.3 A and C) suggesting that actin and MTs work cooperatively to properly localize the CPC during anaphase.

INCENP-actin binding targets the CPC to the furrow in the absence of Mklp2

To further characterize the movement and localization of the CPC during C phase, we studied the kinetics of CPC accumulation at the midzone and cortex in live cells transiently expressing GFP-INCENP (Figure 5.4 A). At anaphase onset, GFP-INCENP "streamed" from centromeres to the center of the midzone at a rate of 10.1 ± 2.1 μm/min (mean ± SD, n=52 events). GFP-INCENP then coalesced into numerous puncta (hereafter referred to as "spots") that moved dynamically throughout the midzone at an average rate of 4.4 ± 1.8 μm/min (n=316 spots, Figure 5.4 B). The rate of streaming was determined by measuring the rate at which the fluorescence furthest from the MT-plus end overlap coalesced into a narrow band. This measurement likely represents two oppositely-directed populations of motor-driven transport moving towards each other on the midzone, implying the rate of transport of a single population is approximately half. Therefore, our analysis suggests that streaming and spot movement occur at similar rates. GFP-INCENP spots were notably distinct from the CPC localization pattern visualized using immunofluorescence, and may arise from overexpression. Spots were larger than CPC puncta observed by immunofluorescence, and were not always uniform in size. These spots localized to

both the midzone and the cortex, and can be observed to fuse and split during early mitotic exit. However, upon the initiation of furrowing GFP-INCENP took on an appearance indistinguishable

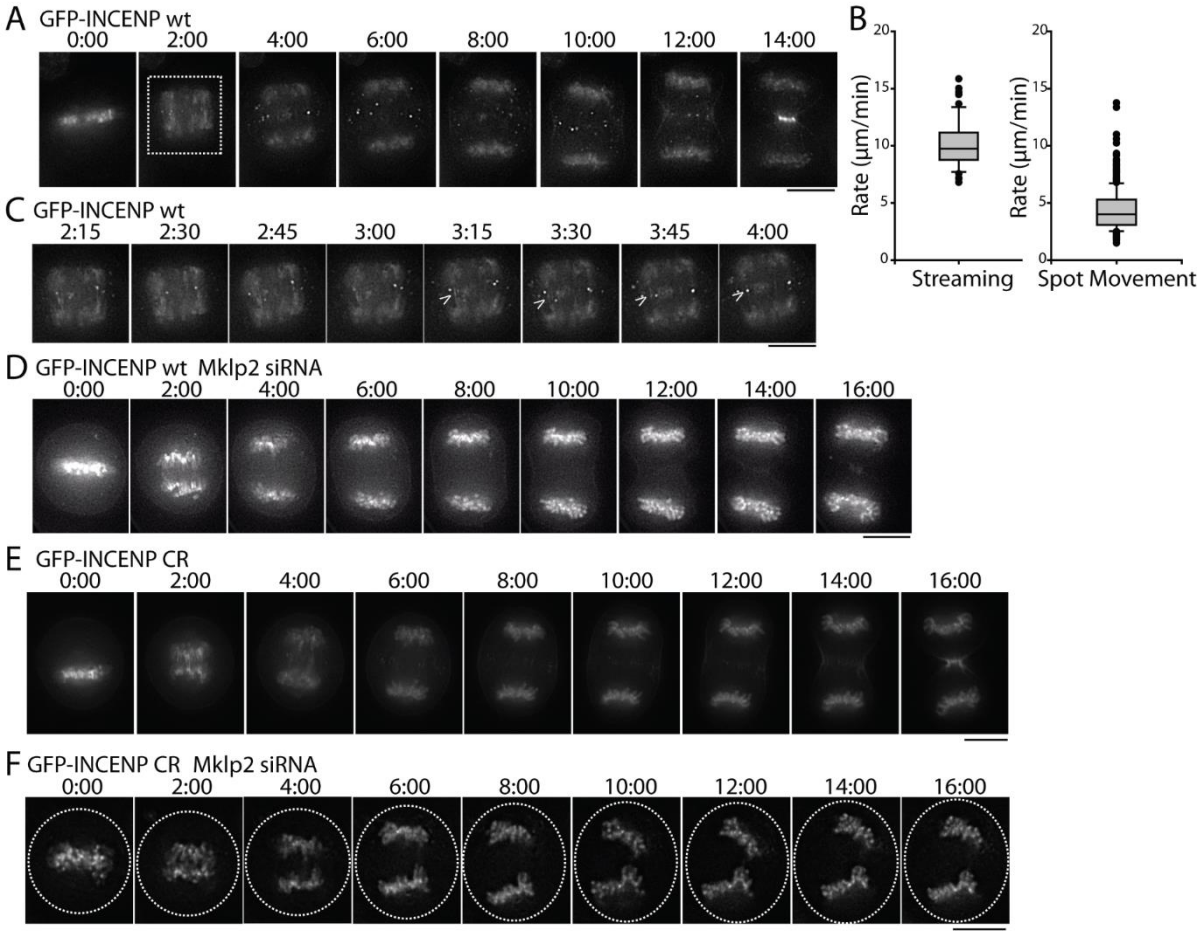

Figure 5.4 Characterization of GFP-INCENP movements during C phase. A) Single z-plane micrographs taken from a time-lapse movie of a HeLa cell transiently expressing GFP-INCENP. Time is indicated in minutes relative to the initial frame. Box indicates region used to demonstrate streaming in panel C). Scale bar, 10 µm. B) Quantification of the rate of GFP-INCENP streaming (left) and GFP-INCENP spot movement (right). Spot movement analysis includes spots that moved uni-directionally for at least two consecutive frames. Data represent mean ± SD. n=52 events (streaming) and 316 spots (spot movement). C) Single z-plane micrographs taken from the time-lapse movie shown in A). Time is indicated in minutes:seconds relative to the initial frame. Arrows indicate streaming of GFP-INCENP along a midzone MT, leading to coalescence into a single spot. Scale bar, 10 µm. D) Single z-plane micrographs taken from a time-lapse movie of a GFP-INCENP expressing cell depleted of Mklp2. Note the lack of midzone-localized GFP-INCENP. Time is indicated in minutes relative to the initial frame. Scale bar, 10 µm. E) Single z-plane micrographs taken from a time-lapse movie of a GFP-INCENP CR-expressing cell. Time is indicated in minutes relative to the initial frame. Scale bar, 10 µm. F) Single plane micrographs taken from a time-lapse movie of a GFP-INCENP CR-expressing HeLa cell depleted of Mklp2. Note lack of midzone-localized GFP-INCENP CR. Time is indicated in minutes relative to the initial frame. Dashed lines represent the cell boundary. Scale bar, 10 µm.

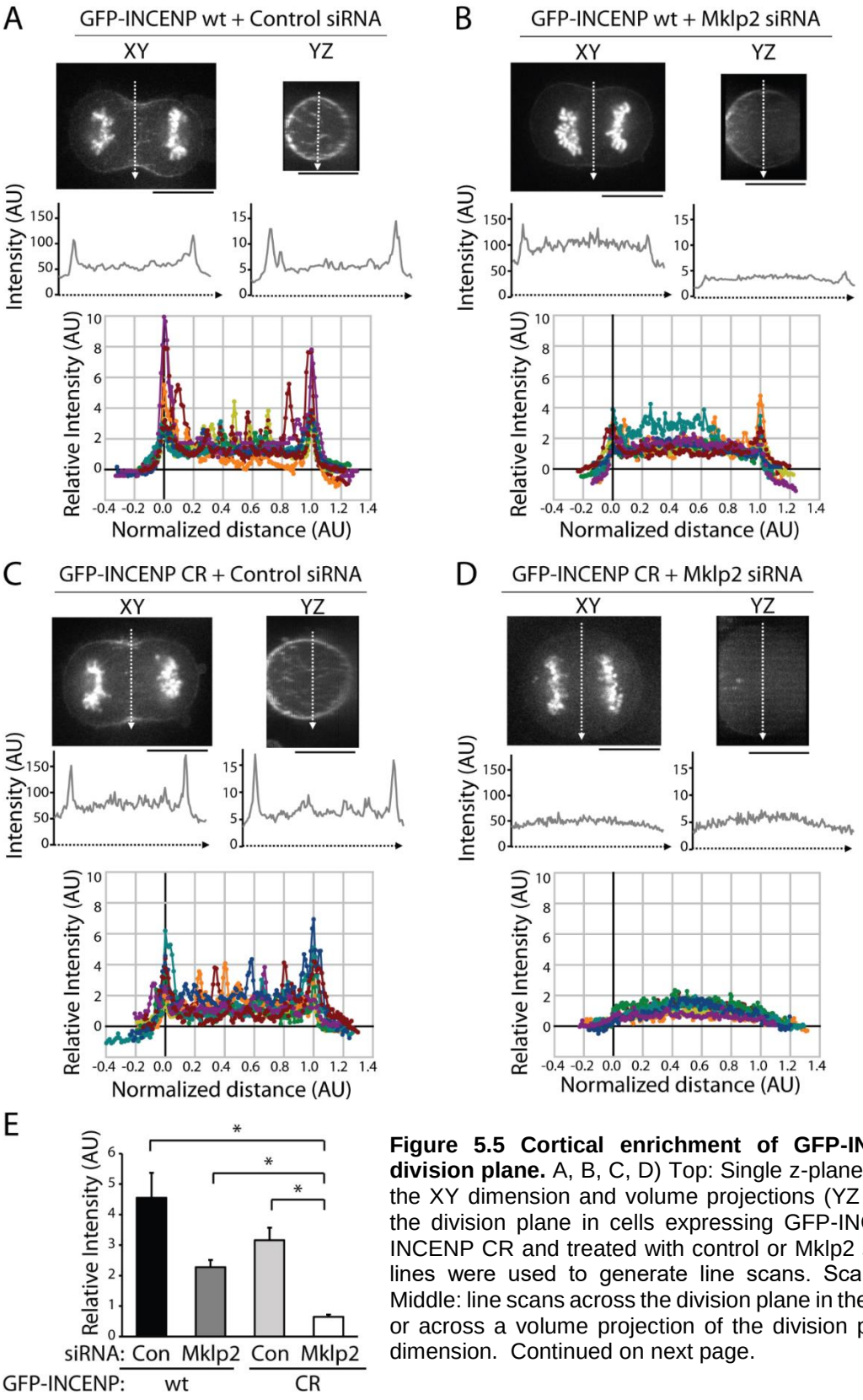

Figure 5.5 Cortical enrichment of GFP-INCENP at the division plane. A, B, C, D) Top: Single z-plane micrographs in the XY dimension and volume projections (YZ dimensions) of the division plane in cells expressing GFP-INCENP or GFP-INCENP CR and treated with control or Mklp2 siRNA. Dashed lines were used to generate line scans. Scale bar, 10 μm. Middle: line scans across the division plane in the XY dimension, or across a volume projection of the division plane in the YZ dimension. Continued on next page.

from endogenous CPC in fixed cells. RNAi of Mklp2 in GFP-INCENP-expressing cells abolished streaming and puncta formation, indicating that these events depend on motor activity (Figure 5.4 C).

In addition to midzone localization, and in agreement with our observations from fixed cells, we observed an accumulation of GFP-INCENP at the cortex during C phase (Figure 5.5 A). We analyzed the enrichment of GFP-INCENP at the equatorial cortex using line scans of fluorescence intensity across YZ projections of the division plane. Intensity values were normalized to cytoplasmic (non-midzone) fluorescence to control for variable expression, and three peak intensity values were averaged to determine the relative increase in fluorescence at the cortex. In cells expressing GFP-INCENP the cortical intensity was 4.5 ± 0.8-fold higher than the cytoplasmic signal (Figure 5.5 E). Similar to our fixed cell analysis, the cortical enrichment of GFP-INCENP was reduced but not absent in Mklp2-depleted cells. Cortical GFP-INCENP fluorescence was increased 2.3 ± 0.2-fold relative to cytoplasmic GFP-INCENP (Figure 5.5 E). Importantly, these cells did not show any midzone MT localization, confirming successful RNAi of Mklp2. The partial reduction of cortical GFP-INCENP in Mklp2-depleted cells suggests the motor is involved in cortical delivery of the CPC, perhaps *via* furrow-associated astral MTs. However, the presence of cortical GFP-INCENP fluorescence after Mklp2 depletion suggests that there are alternative mechanisms that work to recruit the CPC to the cortex.

To test whether this Mklp2-independent cortical accumulation of GFP-INCENP requires an interaction with actin, we utilized our previously described (see Chapter 4) INCENP-actin binding mutant (full length GFP-INCENP CR) and analyzed its localization in the presence and absence of Mklp2. Similar to wild type GFP-INCENP, GFP-INCENP CR localizes to the

Figure 5.5 Continued. A, B, C, D) Bottom: normalized line scans of cells expressing GFP-INCENP or GFP-INCENP CR and treated with control or Mklp2 siRNA. n=10 cells (GFP-INCENP wt + control siRNA or Mklp2 siRNA, GFP-INCENP CR + control sRNA) or 9 cells (GFP-INCENP CR + Mklp2 siRNA). E) Quantification of cortical GFP-INCENP peak intensities as described in A-D). Three adjacent peak intensity values were averaged for each individual cell, n=10 or 9 cells as described previously, * = $p < 0.05$.

centromeres during metaphase and moves as spots along the midzone during anaphase, suggesting that this construct associates with other CPC components and Mklp2 (Figure 5.4 E). Also, like wild type INCENP, GFP-INCENP CR movements on the midzone are abolished by Mklp2 depletion (Figure 5.4 F). Quantitation of cortical fluorescence revealed that GFP-INCENP CR was enriched 3.2 ± 0.4-fold (Figure 5.5 E) compared to cytoplasmic fluorescence, which is significantly lower than the cortical enrichment of wild type GFP-INCENP. These cells also showed punctate localization in the cell middle, suggesting that the CPC can still localize to midzone MTs in the absence of actin binding. The reduction in cortical enrichment compared to wild-type GFP-INCENP demonstrates that direct actin binding is required to fully recruit the CPC to the cortex during C phase, even in the presence of Mklp2. However, disrupting the INCENP-actin interaction is not sufficient to fully abolish cortical enrichment. There are two possible explanations for this: Mklp2 may transport the CPC along to the plus ends of furrow-associated MTs or Mklp2 could bind the cortex directly through an interaction with myosin (Kitagawa et al., 2013). Both mechanisms have the potential to promote CPC cortical localization even when actin-binding is disrupted. With these possibilities in mind, as well as our observation that Mklp2-depletion reduces cortical enrichment of wild type GFP-INCENP, we next asked if GFP-INCENP CR could localize to the cortex in the absence of motor. In Mklp2-depleted cells expressing GFP-INCENP CR the cortical fluorescence was lower than the cytoplasmic signal (0.6 ± 0.1 fold enrichment, Figure 5.5 E) indicating a loss of cortically-localized CPC under these conditions.

These results demonstrate that cortical enrichment of the CPC during C phase requires both INCENP-actin binding and transport by Mklp2. Moreover, our data suggests that a direct interaction with actin is sufficient to recruit the CPC to the cortex in the absence of motor.

The CPC and Mklp2 move together during C phase

Cortical localization of the CPC has been observed previously (Earnshaw and Cooke, 1991), although the mechanism of cortical recruitment has not been investigated. Our analysis of GFP-INCNEP cortical enrichment demonstrates that the CPC can target the equatorial cortex in the absence of Mklp2, in a manner that depends on INCENP-actin binding. Additionally, we observed that actin-dependent recruitment by itself is inefficient at promoting cortical enrichment. This result might indicate that cortical recruitment of the CPC is a two-step process where MT-dependent transport by Mklp2 delivers the CPC to the cortex and the complex is then "off-loaded" onto cortical actin. Alternatively, transport by Mklp2 and INCENP-actin binding may work cooperatively to position the CPC at the division site. As previous investigations of the CPC-Mklp2 relationship have primarily focused on midzone targeting, we asked whether cortically-localized CPC was associated with Mklp2 in live cells. Cells transiently expressing GFP-INCENP and Mklp2-mCherry were plated on 100 μg/ml fibronectin (Taneja et al., 2016) to flatten mitotic cells on the basolateral side and create a large cortical surface for imaging. As expected, spots of GFP-INCENP and Mklp2-mCherry were co-localized on the midzone during C phase (Figure 5.6 B). In addition, we observed that spots of GFP-INCENP were co-localized with Mklp2-mCherry at the cell cortex (Figure 5.6 A). These spots are also dynamically associated as they move in unison when tracked over time by kymograph (Figure 5.6 A and B). The co-localization of GFP-INCENP and Mklp2-mCherry on both the midzone and the cortex argues against an "off-loading"

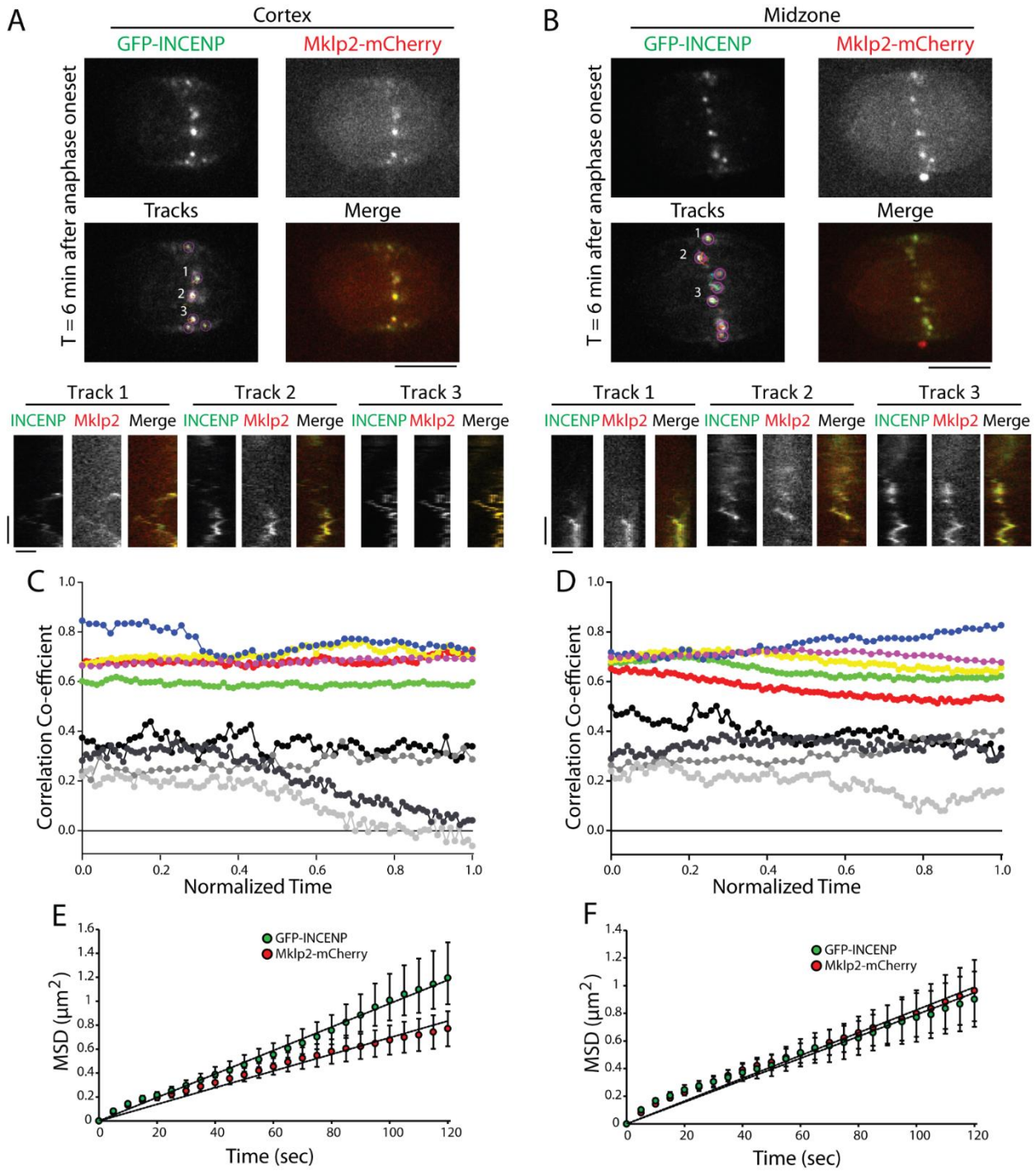

Figure 5.6 GFP-INCENP and Mklp2-mCherry are co-localized on the cell cortex. A, B) Top: Single z-plane micrographs of the cell cortex or midzone taken from a time-lapse movie of a HeLa cell transiently expressing GFP-INCENP and Mklp2-mCherry plated on 100 μg/ml fibronectin. Micrographs represent a time point 6 minutes after anaphase onset. The "tracks" panel highlights examples of spots and tracks used to quantify MSD. Numbers indicate tracks that correspond to kymographs below. Scale bar, 10 μm. Bottom: Kymographs of GFP-INCENP and Mklp2-mCherry generated from the spots indicated above. Scale bars, 100 seconds (y axis) and 1 μm (x axis). C, D) Pearson's correlation co-efficient of GFP-INCENP and Mklp2-mCherry on the cell cortex or midzone (colored circles). Co-localization was quantified from immediately after anaphase onset (normalized time=0) to immediately before cleavage furrow ingression (normalized time=1).

model where cortically localized CPC represents a population that moves independent of the motor.

To quantify the association of GFP-INCENP and Mklp2-mCherry across multiple cells we tracked the Pearson's correlation co-efficient (Manders et al., 1992) at the cortex and on the midzone during C phase (Figure 5.6 C and D). GFP-INCENP and Mklp2-mCherry were positively correlated on the midzone at anaphase onset (0.68 ± 0.02, data represents mean ± SD, normalized time=0) and immediately before cleavage furrow ingression (0.72 ± 0.11, normalized time=1, n=5 cells Figure 5.6 D) in agreement with fixed cell observations (Gruneberg et al., 2004). At the cortex, GFP-INCENP and Mklp2-mCherry were similarly positively correlated at anaphase onset (0.68 ± 0.09, normalized time=0) and immediately before cleavage furrow ingression (0.68 ± 0.05, normalized time=1, n=5 cells, Figure 5.6 C). Control cells co-expressing GFP-INCENP and mCherry did not show a strong positive correlation on the cortex (0.25 ± 0.03, normalized time=0; 0.07 ± 0.15, normalized time=1, n=3 cells) or on the midzone (0.26 ± 0.02, normalized time=0; 0.30 ± 0.14, normalized time=1, n=3 cells). This result indicates that GFP-INCENP and Mklp2-mCherry localization is positively correlated during early mitotic exit.

We next investigated whether the CPC and Mklp2 have similar dynamic properties on the cortex and at the midzone. To analyze the movement of GFP-INCENP and Mklp2-mCherry we used automated tracking to determine the XY position of spots over time (Tinevez et al., 2016) (Figure 5.6 A and B) and then quantified the mean-squared displacement (MSD) of these tracks

Figure 5.6 Continued. Control cells expressing GFP-INCENP and mCherry are represented by gray-scale circles. n=3 cells (control) and 5 cells (experimental) from three independent experiments. E, F) Mean squared displacement (MSD) of GFP-INCENP (green circles) and Mklp2-mCherry (red circles) spots on the cortex and midzone during C phase. Data represents mean ± SE. Linear regression represents best fit used to calculate the diffusion co-efficient. n=625 tracks (GFP-INCENP, cortex), 537 tracks (Mklp2-mCherry, cortex), 626 tracks (GFP-INCENP, midzone), or 424 tracks (Mklp2-mCherry, midzone) from 6 cells from three independent experiments.

(Tarantino et al., 2014a). At the cortex, the MSD of GFP-INCENP was best fit using a linear regression, as was the MSD of Mklp2-mCherry, indicating that cortical movement is largely diffusive. The diffusion co-efficient of GFP-INCENP was 2.5 x 10^3 $\mu m^2/s$ (n=625 tracks from 6 cells), and the diffusion co-efficient of Mklp2-mCherry was similar at 1.7 x 10^3 $\mu m^2/s$ (n=537 tracks from 6 cells, Figure 5.6 E). The quantitative difference in GFP-INCENP and Mklp2-mCherry cortical diffusion is likely due to the fact that mCherry fluorescence is relatively dim compared to GFP, and more difficult to detect by automated tracking. While the movement of GFP-INCENP and Mklp2-mCherry was primarily diffusive, there were rare instances of directed movement detected during our analysis (see Figure 5.6 A and B kymographs). These events comprised approximately 2-6% of the total time tracked, and are therefore unlikely to significantly alter the diffusion co-efficient. The movements of midzone-localized GFP-INCENP and Mklp2-mCherry were also best fit by linear regression. Importantly, this analysis largely represents time points after which the CPC has coalesced into discrete spots, and does not include directed "streaming" events in early anaphase. The diffusive behavior of Mklp2 and CPC on the midzone may indicate that motor activity is shut off after the complex reaches midzone MT plus ends, or once the complex coalescence into spots. The diffusion co-efficients of GFP-INCENP and Mklp2-mCherry were nearly identical on the midzone (GFP-INCENP=1.9 x 10^3 $\mu m^2/s$, n=626 tracks from 6 cells; Mklp2-mCherry=2.1 x 10^3 $\mu m^2/s$, n=424 tracks from 6 cells, Figure 5.6 F) demonstrating that the two proteins have the same dynamic behavior during early mitotic exit. Combined with our observation that GFP-INCENP and Mklp2-mCherry localization is positively correlated, we propose that the CPC and Mklp2 are always associated during C phase.

Dynamic cortical movement of the CPC depends on actin and MTs

Our analysis of GFP-INCENP and Mklp2-mCherry cortical movement indicates that the CPC diffuses on the cell cortex during C phase. Additionally, our quantification of GFP-INCENP cortical enrichment demonstrates that robust recruitment of the CPC depends on actin-binding. We next asked whether cortical diffusion of the CPC is affected by cortical F-actin. To test this, we treated cells expressing GFP-INCENP, plated on 100 μg/ml fibronectin, with DMSO or 5 μg/ml cytochalasin B, to induce F-actin disassembly; and tracked the XY position (Tinevez et al., 2016) of GFP-INCENP spots on the cortex. In agreement with our previous findings, GFP-INCENP cortical movement in cells treated with DMSO was best fit by linear regression, and the diffusion co-efficient was 1.9×10^3 $\mu m^2/s$ (n=256 tracks from 6 cells, Figure 5.7 A). Treatment with cytochalasin B prior to imaging dampened the movement of GFP-INCENP on the cortex, and significantly decreased the diffusion co-efficient (1.1×10^3 $\mu m^2/s$, n=249 tracks from 5 cells, Figure 5.7 A). This observation suggests that rapid diffusion of cortical GFP-INCENP requires actin filaments. Moreover, this finding argues against a model where cortical F-actin acts as a static tether for equatorial CPC.

Furrow-associated astral MTs are thought to stably interact with the equatorial cortex (Canman et al., 2003). We therefore investigated whether MTs also influence cortical diffusion of the CPC. We treated cells expressing GFP-INCENP, plated on 100 μg/ml fibronectin, with DMSO or 5 μM nocodazole to depolymerize MTs. In order to ensure that we did not disrupt MT-dependent delivery of the CPC to the cortex, nocodazole was only added after cortical GFP-INCENP was detectable. The behavior of cortical GFP-INCENP in DMSO-treated cells was similar to our previous experiment and the diffusion co-efficient well matched (1.9×10^3 $\mu m^2/s$, n=626 tracks from 6 cells, Figure 5.7 B). Treatment with 5 μM nocodazole altered the movement

of cortical GFP-INCENP and partially decreased the diffusion co-efficient (1.4 x 10^3 μm^2/s n=424 tracks from 9 cells, Figure 5.7 B) indicating that MTs also promote diffusion of the CPC along the cortex. Notably, depolymerizing MTs had a smaller effect on cortical diffusion than disassembly of actin filaments (nocodazole ~26% decrease of the diffusion co-efficient; cytochalasin B ~42%

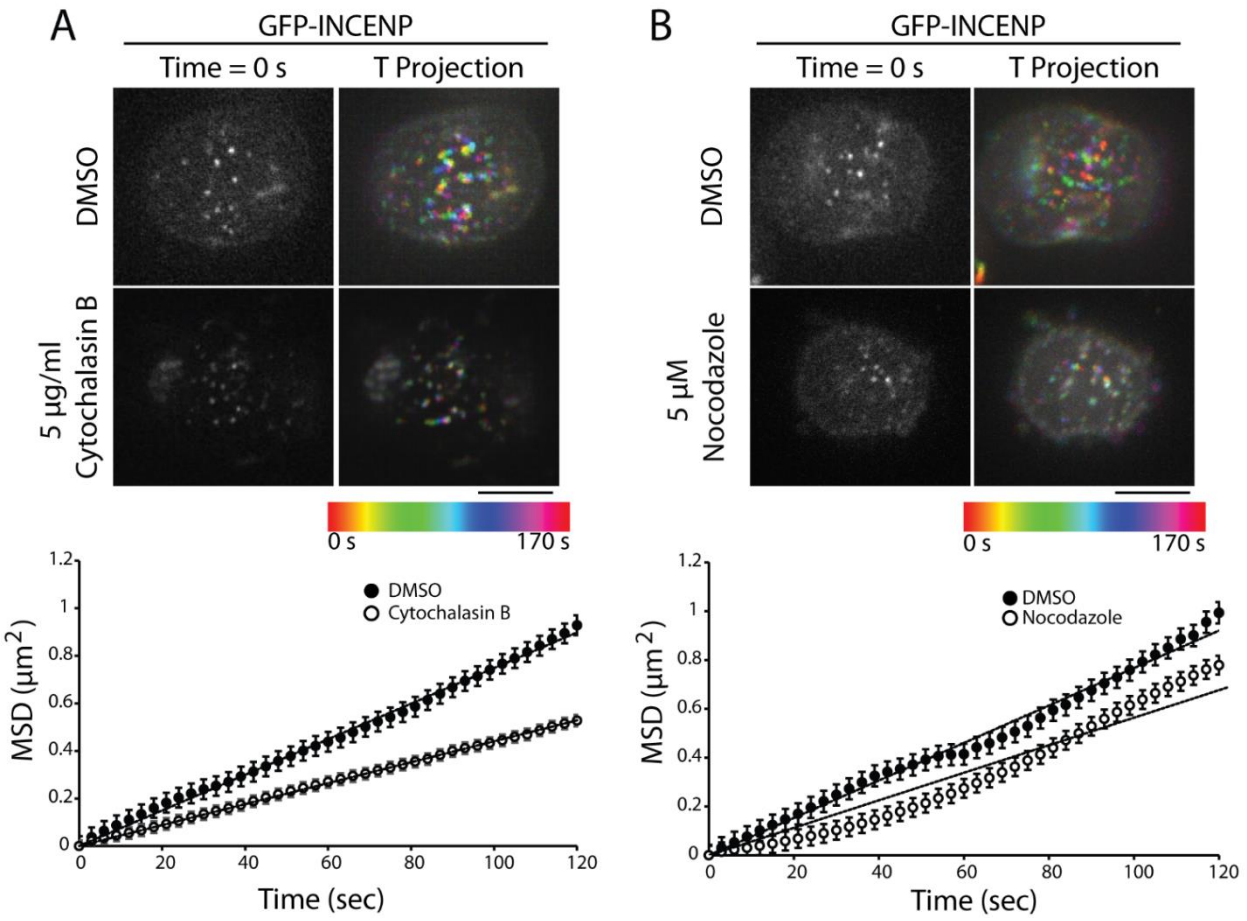

Figure 5.7 GFP-INCENP cortical movement depends on actin and MTs. A, B) Top left: Single z-plane micrographs of the cell cortex or midzone taken from a time-lapse movie (time=0 seconds) of a HeLa cell transiently expressing GFP-INCENP plated on 100 µg/ml fibronectin treated with DMSO, 5 µg/ml cytochalasin B, or 5 µM nocodazole prior to imaging. Top right: Micrograph time projections of GFP-INCENP fluorescence over the course of 170 seconds. Scale bar, 10 µm. Time projection scale, 0 seconds to 170 seconds. Bottom: Mean squared displacement (MSD) of GFP-INCENP spots on the cortex and midzone in cells treated with DMSO (open circles), or 5 µg/ml cytochalasin B (closed circles), or 5 µM nocodazole (closed circles). Data represents mean ± SE. Linear regression represents best fit used to calculate the diffusion co-efficient. n=256 tracks (DMSO) from 6 cells, 249 tracks (cytochalasin B) from 5 cells from three independent experiments as described for A). n=626 tracks (DMSO) from 6 cells, or 424 tracks (nocodazole) from 9 cells from three independent experiments as described for B).

decrease of the diffusion co-efficient). This comparison suggests that while actin and MTs both influence cortical diffusion of the CPC, actin plays a larger role in promoting movement on the cortex.

INCENP overexpression rescues cleavage furrow ingression in Mklp2-depleted cells

We next investigated whether cortically-localized CPC was functional during C phase. We tested this by observing the success of cleavage furrow ingression in Mklp2-depleted cells. In agreement with a previous study (Kitagawa et al., 2013), we observed that ~47% of Mklp2-depleted cells (n=7/15 cells) successfully completed cleavage furrow ingression (Figure 5.8 A), as judged by imaging mCherry-Utrophin to mark the furrow. Cells that failed to complete furrowing did so as a consequence of furrow regression rather than a failure to initiate ingression, mirroring the phenotype others have observed (Kitagawa et al., 2013). In contrast, 92% of control cells (n=11/12 cells) completed furrow ingression, resulting in the formation of a midbody. Surprisingly, transient overexpression of GFP-INCENP rescued the ability of Mklp2-depleted cells to complete cytokinesis: 92% (n=11/12) of cells expressing GFP-INCENP completed furrow ingression, similar to control transfected cells (100%, 8/8 cells; Figure 5.8 B). The timing and rates of furrow ingression were similar between control-depleted cells and Mklp2-depleted cells expressing GFP-INCENP (Figure 5.9 A and B). In control siRNA-transfected cells expressing GFP-INCENP, furrow ingression started 6.01 ± 1.12 min (mean ± SD) after anaphase onset (n=5 cells), and proceeded at a rate of 1.48 ± 0.36 μm/min (n=8 cells). Mklp2-depleted cells expressing GFP-INCENP began furrow ingression 5.89 ± 1.29 min after anaphase onset, and ingression progressed at a rate of 1.51 ± 0.42 μm/min (n=12, Figure 5.9 B and C). Transient expression of GFP-INCENP led to a 2.5-fold increase in INCENP protein levels, as assessed by Western blotting

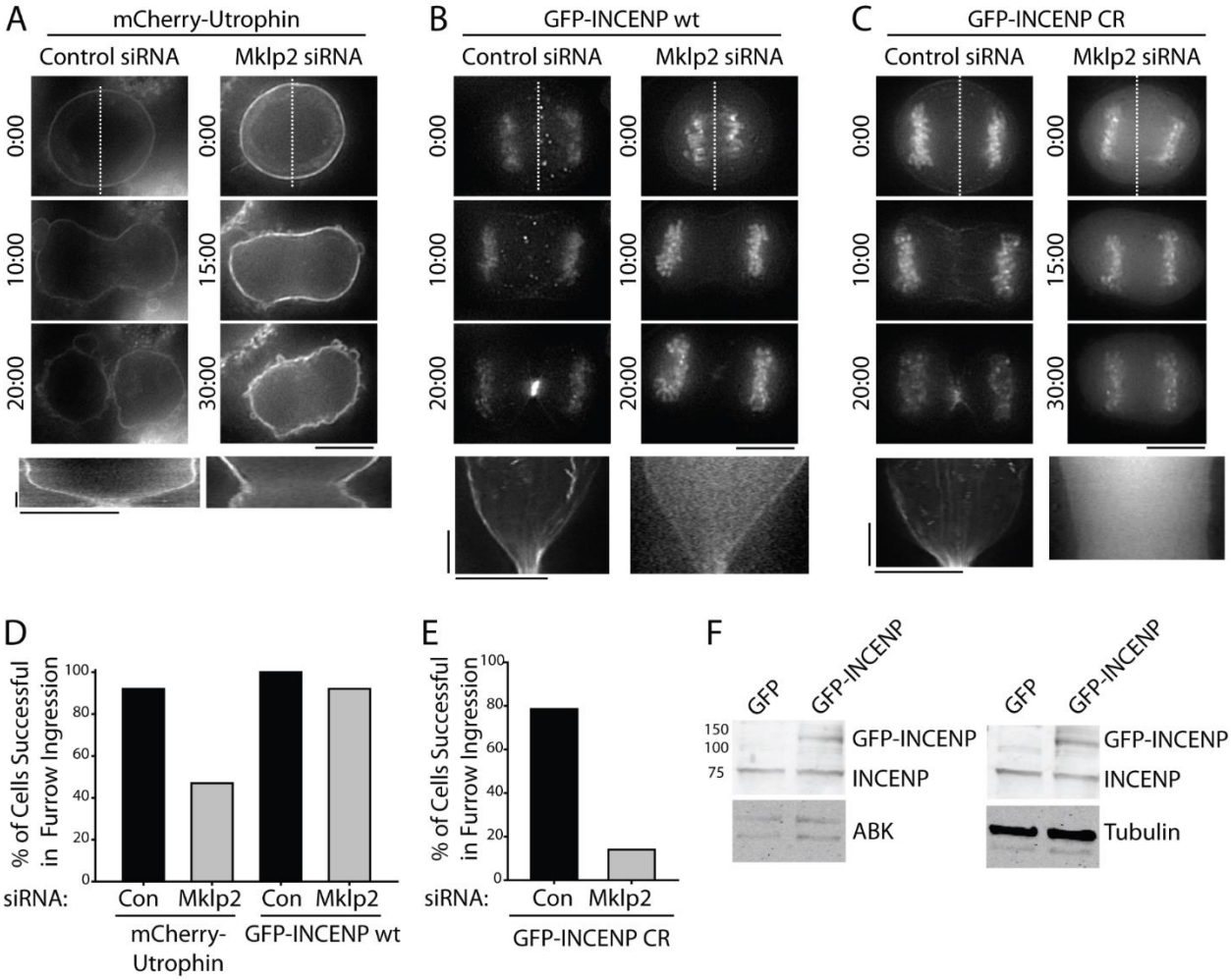

Figure 5.8 Overexpression of GFP-INCENP rescues cleavage furrow ingression in Mklp2-depleted cells. A, B, C) Top: Single z-plane micrographs taken from time-lapse movies of cells transiently expressing mCherry-Utrophin, GFP-INCENP, or GFP-INCENP CR in the presence or absence of Mklp2. Time is indicated in minutes. Dashed lines were used to generate kymographs. Scale bars, 10 μm. Bottom: Kymographs of mCherry-Utrophin, GFP-INCENP, or GFP-INCENP CR fluorescence across the division plane. Scale bars, 2.5 minutes (y axis) and 10 μm (x axis). D) Quantification of the percentage of cells from A) and B) that successfully completed furrow ingression. For mCherry-Utrophin-expressing cells, n=12 (control) and 15 (Mklp2 siRNA) cells. For GFP-INCENP-expressing cells, n=8 (control) and 12 (Mklp2 siRNA) cells. E) Quantification of total percentage of cells from C) that successfully completed furrow ingression. n=14 cells per condition. F) Immunoblots of cell extracts prepared from HeLa cells transfected with GFP or GFP-INCENP. ABK levels are unchanged when GFP-INCENP is overexpressed. Tubulin is shown as a loading control. Molecular weight standards are indicated in kDa.

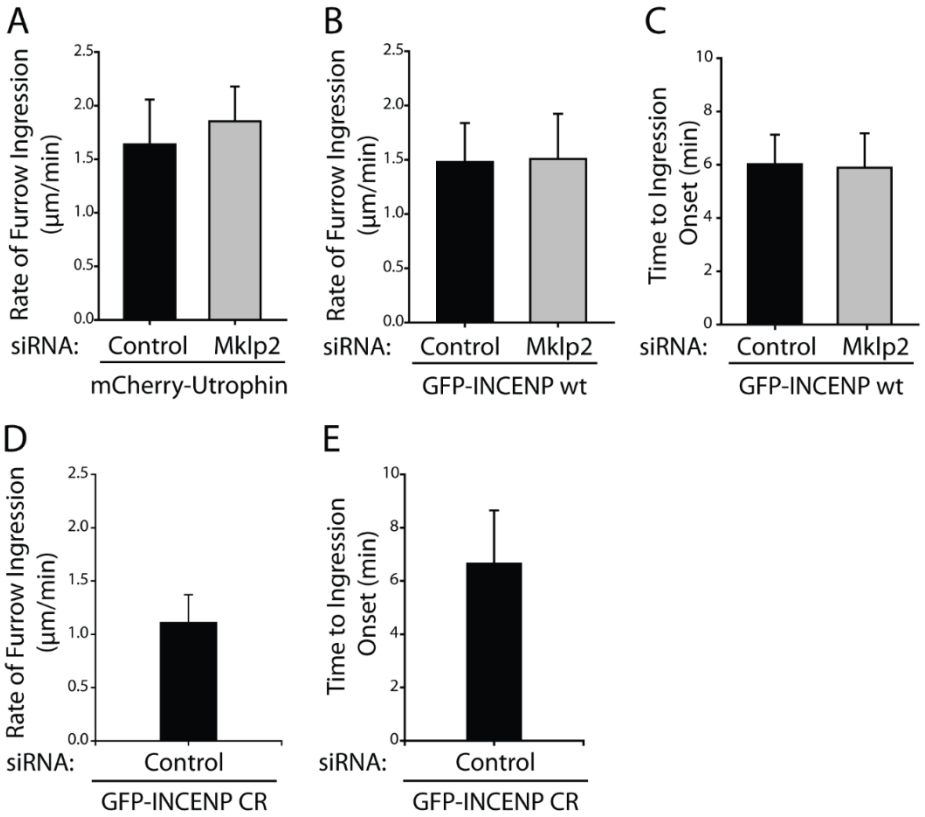

Figure 5.9 Dynamics of C phase in cells expressing GFP-INCENP. A) Quantification of the rate of cleavage furrow ingression in cells expressing mCherry-Utrophin. Cells were transfected with a control or Mklp2-targeting siRNA. Cells that failed to complete furrow ingression were not scored. Data represent mean ± SD. n=12 (control) and 6 (Mklp2 siRNA) cells. B) Quantification of the rate of furrow ingression in cells expressing GFP-INCENP. Cells were transfected with siRNA as described in A). Cells that failed to complete furrow ingression were not scored. n=6 (control) and 12 (Mklp2 siRNA) cells. C) Quantification of the time to ingression onset, measured relative to anaphase onset. Cells were treated as described in B). Data represent mean ± SD. n=5 (control) and 6 (Mklp2 siRNA) cells. D) Quantification of the rate of cleavage furrow ingression in cells expressing GFP-INCENP CR and transfected with a control siRNA. Cells that failed to complete furrow ingression, including cells transfected with an Mklp2-targeted siRNA, were not scored. n=8 cells. E) Quantification of the time to ingression onset measured relative to the time of anaphase onset in cells expressing GFP-INCENP CR as described in D). Data represent mean ± SD. n=6 cells.

(Figure 5.8 F), but did not result in a gross overexpression of ABK (1.2-fold increase), demonstrating that INCENP overexpression does not concomitantly increase expression of other CPC components.

Furrow ingression rescue requires INCENP-actin binding

Using the INCENP CR mutant, we next tested whether actin-dependent furrow enrichment of INCENP can explain its ability to rescue cytokinesis in Mklp2-depleted cells. Control or Mklp2-depleted cells were transfected with GFP-INCENP CR and imaged during C phase. 78% of control-depleted cells expressing GFP-INCENP CR (n=11/14 cells) progressed through C phase normally and completed furrow ingression, forming a midbody (Figure 5.8 C). The time from anaphase onset to furrow ingression was identical to control cells (6.64 ± 2.01 min, Figure 5.9 D), and the rate of furrow ingression in cells expressing GFP-INCENP CR was comparable to cells expressing wild type GFP-INCENP (1.11 ± 0. 26 μm/min, n=8, Figure 5.9 E). In contrast, only 14% of Mklp2-depleted cells expressing GFP-INCENP CR (n=2/14 cells) successfully completed furrow ingression (Figure 5.8 E), indicating that INCENP overexpression rescues furrow ingression in Mkp2-depleted cells in a manner that requires actin binding. Interestingly, furrows did not initiate ingression in Mklp2-depleted cells expressing GFP-INCENP CR, strongly suggesting that actin-dependent targeting of the CPC to the cortex is required to initiate cleavage furrow ingression in the absence of Mklp2.

Cleavage furrow ingression in cell lines stably expressing GFP-INCENP

As transient expression of GFP-INCENP could affect the success of cleavage furrow ingression in a manner dependent on the level of protein expression we generated stable cell lines that uniformly express GFP-INCENP in a doxycycline-inducible manner (see Materials and Methods). These cells expressed GFP-INCENP in addition to endogenous INCENP, although overexpression of INCENP was lower than transient transfection (1.79-fold for GFP-INCENP, 1.64-fold for GFP-INCENP CR, Figure 5.10 F). As a control, we tracked the success of cleavage

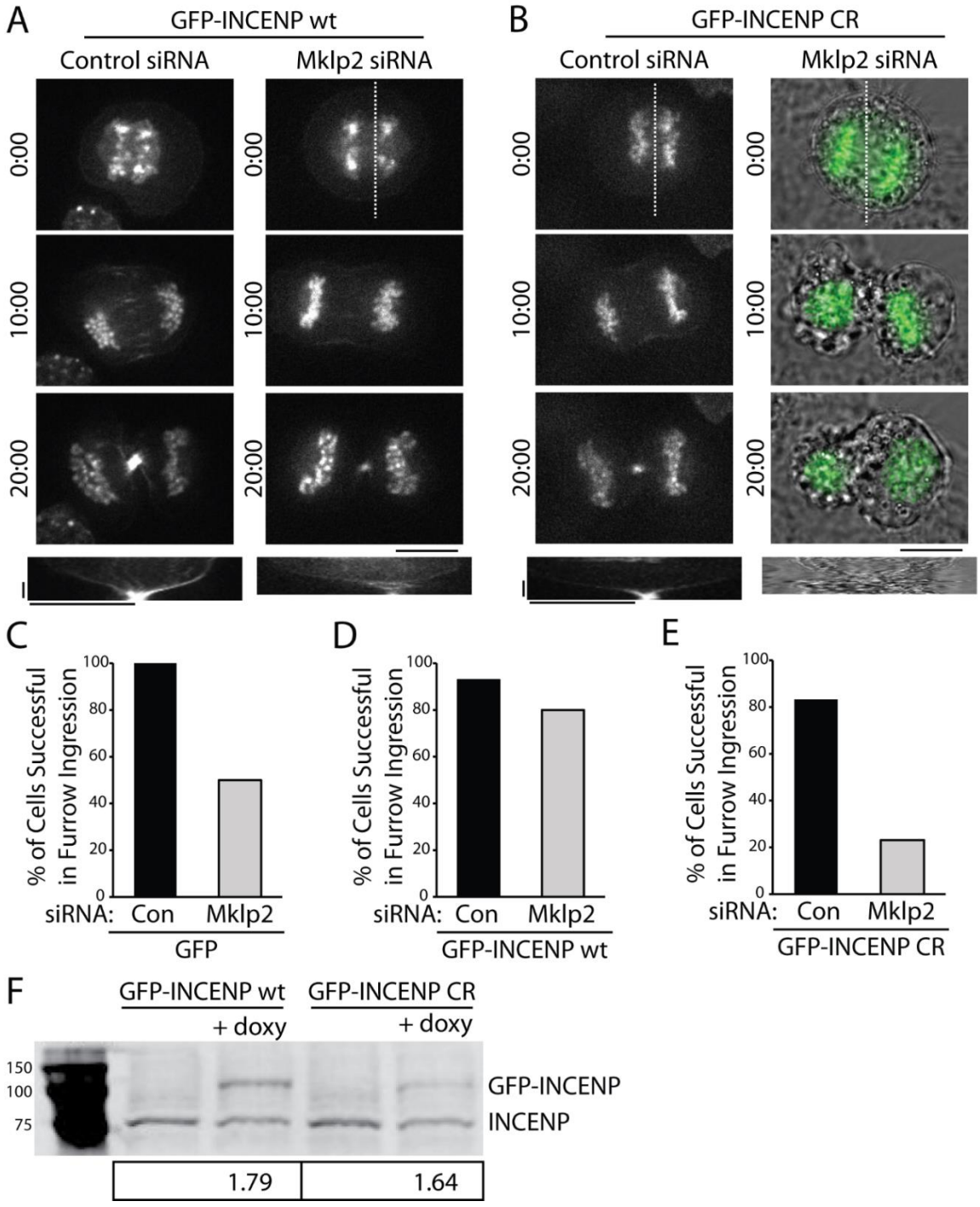

Figure 5.8 Stable overexpression of GFP-INCENP rescues cleavage furrow ingression in Mklp2-depleted cells. A, B,) Top: Single z-plane micrographs taken from time-lapse movies of cells stably expressing GFP-INCENP or GFP-INCENP CR, after 24 hours in 2 µg/ml doxycycline, in the presence or absence of Mklp2. Time is indicated in minutes. Dashed lines were used to generate kymographs. Scale bars, 10 µm. Due to the dim cortical signal of GFP-INCENP CR (green) after Mkp2 depletion, we tracked furrow ingression by DIC. Bottom: Kymographs of GFP-INCENP, GFP-INCENP CR fluorescence, or DIC imaging across the division plane. Scale bars, 2.5 minutes (y axis) and 10 µm (x axis). Continued on next page.

Figure 5.8 Continued. C) Quantification of the percentage of cells stably expressing GFP successful in cleavage furrow ingression in the presence or absence of Mklp2. n=8 (control) and 10 (Mklp2 siRNA) cells. D, E) Quantification of the percentage of cells successful in cleavage furrow ingression as described in A) and B). For GFP-INCENP-expressing cells, n=14 (control) and 10 (Mklp2 siRNA) cells. For GFP-INCENP CR-expressing cells, n=12 (control) and 13 (Mklp2 siRNA) cells. F) Immunoblots of cell extracts prepared from cells stably expressing GFP or GFP-INCENP CR after 24 hours in 2 μg/ml doxycycline. Molecular weight standards are indicated in kDa. Boxes (bottom) represent the fold change in INCENP expression after doxycycline relative to non-induced cells.

furrow ingression in a cell line expressing GFP alone in the presence and absence of Mklp2. In agreement with our previous findings, 100% of GFP-expressing cells treated with a control siRNA successfully completed furrowing (n=8/8 cells), while only 50% of Mklp2-depleted cells (n=5/10 cells) completed furrow ingression (Figure 5.10 C). Stable expression of GFP-INCENP also showed a similar phenotype to transient transfection. Control-depleted cells completed furrow ingression 92% (n=13/14 cells) of the time, and Mklp2-depleted cells expressing wild type GFP-INCENP were similarly successful (80%, n=8/10 cells) demonstrating that even low level overexpression of INCENP can rescue furrowing after Mklp2 RNAi (Figure 5.10 A and D). Stable expression of GFP-INCENP CR, however, was not sufficient to rescue furrowing after Mklp2 depletion. 83% (n=10/12 cells) of GFP-INCENP CR-expressing cells transfected with control siRNA completed furrowing, while only 23% (n=3/13 cells) of cells transfected with Mklp2 siRNA completed furrow closure (Figure B and E). A portion of these cells were able to initiate furrowing, but this event was soon followed by furrow regression. Other cells were unable to initiate furrowing, in agreement with our observations from transient transfection. These findings demonstrate that even low level overexpression of INCENP can rescue cleavage furrow ingression, and that regardless of expression level, the INCENP-actin interaction is required for furrowing in the absence of Mklp2. Taken together, the general observation that overexpression of INCENP

rescues furrowing in a manner that depends on actin-binding, suggests that the cortical population of the CPC is functional during C phase, and is sufficient to promote the final steps of cell division.

Discussion

While it is well accepted that the CPC traffics to the spindle midzone *via* Mklp2-dependent transport (Cesario et al., 2006; Gruneberg et al., 2004; Hummer and Mayer, 2009; Jang et al., 2005; Nguyen et al., 2014), how the CPC concentrates at the equatorial cortex had remained largely uncharacterized. As with midzones, MT association provides one plausible explanation. MTs lining the equatorial cell perimeter are abundant, as are those whose plus-ends terminate there. Indeed, our data shows co-localization of the CPC with cortically-associated MTs at the division plane. However, the CPC also localizes to cortical actin, and disrupting the INCENP-actin interaction perturbs normal C phase localization. Moreover, ABK and GFP-INCENP both localize to the equatorial cortex in cells depleted of Mklp2. Our work suggests that the CPC-actin interaction regulates the recruitment of the complex to the equatorial cortex and is sufficient to promote cortical localization in the absence of motor. We found that proper CPC localization during C phase requires both actin and MTs; single disruptions of either cytoskeletal system, by filament disassembly, or by abolishing the interaction between the CPC and cytoskeletal filaments, are insufficient to fully displace the CPC from the midzone or the equatorial cortex. It is important to note that CPC interactions with F-actin and furrow-associated MTs do not appear to statically link the complex to the cortex. The CPC diffuses on the cell cortex during early mitotic exit and cytoskeletal perturbations diminish cortical diffusion. However, the CPC remains at the cortex after single filament disruption, suggesting tethering mechanisms, such as Mklp2-myosin (Kitagawa et al., 2013) or Mklp2-lipid interactions (Fung et al., 2017), may be involved in

maintaining cortical localization. Our studies suggest that cortical diffusion is primarily dependent on actin filaments, indicating that the behavior of the CPC once it reaches the cortex does not depend on motor activity. This is distinct from the proposed mechanism of Mklp2-based transport to target midzone MT plus ends. Collectively, these findings lead us to propose that the CPC concentrates at the equatorial cortex because F-actin and MT plus-ends overlap there. Finally, cortical CPC is functional to promote cleavage furrow ingression in the absence of Mklp2, suggesting that successful cell division does not necessarily require midzone-localized CPC.

CHAPTER 6

CONCLUDING REMARKS

Cytoskeletal coordination during C phase

A variety of essential cellular functions depend on active cooperation between the actin and microtubule cytoskeletons (Rodriguez et al., 2003). During cell migration, actin and MTs cooperate to drive forward motility (Ballestrem et al., 2000). In neurons, cytoskeletal dynamics are synchronized during pathfinding to prevent "wandering" growth cone extensions (Schaefer et al., 2002; Zhou et al., 2002). The activities of actin and microtubules are highly coordinated throughout the process of cell division as well. For example, actin and myosin interact with astral MTs to position centrosomes (Hwang et al., 2003; Kwon et al., 2015). As cells exit mitosis, furrow-associated astral MTs specify the division site by serving as tracks to deliver factors that promote assembly of the contractile array (Mandato et al., 2000; Mishima, 2016). With respect to mitotic exit, it has remained unclear whether cytoskeletal cross-talk occurs in the reverse direction; that is, does cortical actin regulate MT dynamics? Work using monopolar cytokinesis as a model suggests that acto-myosin contractility is required for midzone formation (Hu et al., 2008), however, efforts to investigate this relationship during bipolar cytokinesis have produced conflicting results (Cimini et al., 1998; Straight et al., 2003). Actin-to-microtubule communication could allow plasticity in positioning the division plane before furrowing, or ensure that the midzone does not form a barrier before chromosomes have fully segregated.

In this study we have demonstrated that acto-myosin contractility is required for bipolar midzone stabilization, suggesting there is signaling which links the activities of cortical actin to midzone MTs. Moreover, we have identified the CPC as a key mediator of this feedback signaling.

This finding parallels the cytoskeletal coordination that occurs during monopolar cytokinesis (Hu et al., 2008) and supports the idea that cross-talk occurs in the cortex-to-midzone direction. Additionally, we observed that cleavage furrow ingression fails in cells with unstable midzones (see Chapter 4). This finding is particularly exciting as it suggests MT stabilization is an essential step in cytokinesis. An intriguing possibility is that positive feedback from the midzone promotes furrow closure, creating a double feedback loop of cytoskeletal communication. Whether this feedback is representative of bi-directional signaling *via* the CPC is yet to be determined. Nevertheless, our work underscores the notion that cytokinetic processes cannot be studied as a linear series of events as they involve feedback loops that dynamically connect the spatio-temporal activities of acto-myosin and midzone MTs.

Monopolar cytokinesis as a tool for studying feedback signaling

A number of previous studies have investigated the localization and function of C phase proteins using monopolar cytokinesis as a model system (Hu et al., 2008; Kitagawa et al., 2013; van der Horst et al., 2015). While myosin II and ABK inhibition block *monopolar midzone formation*, these perturbations do not affect midzone formation in bipolar cells, and instead alter *bipolar midzone stabilization*, an outcome which we suggest reflects a fundamental difference in the properties of monopolar *vs.* bipolar midzones. This is somewhat unsurprising as the plus ends of MTs in bipolar midzones are cross-linked within the anti-parallel overlap, due to the activity of PRC1 (Bieling et al., 2010; Subramanian et al., 2010) and associated factors, such as Kif4A (Kurasawa et al., 2004). Our findings lead us to propose that relative to monopolar midzones, bipolar midzones may be more organizationally robust. In accordance with this idea, PRC1 and Mklp1 are delocalized in monopolar midzones that do manage to form in the presence of an ABK

inhibitor (Hu et al., 2008), whereas PRC1 and Mklp1 localizations are qualitatively unaffected by ABK inhibition during bipolar cytokinesis (See Chapter 4). Despite the organizational differences, there appears to be comparable feedback signaling that exists in both monopolar and bipolar C phase cells. However, the outcome of this signaling pathway differs; i.e. midzone formation *vs.* stabilization. This observation indicates that monopolar cytokinesis could be a useful tool beyond studying protein localization. Our work predicts that signaling factors which affect bipolar midzone stability would also regulate monopolar midzone formation, and vice versa. This may present an opportunity to rapidly screen for factors involved in cytoskeletal cross-talk during C phase.

Midzone stabilization during mitotic exit

An important goal for the future will be to determine the significance of midzone MT stabilization during bipolar cytokinesis. One obvious possibility is that midzone stabilization ensures that cells will undergo abscission properly, through the formation of a functional midbody that in turn recruits abscission factors, such as the ESCRT machinery (Green et al., 2012). However, cells with unstable midzones, such as cleaving cells treated with nocodazole (Wheatley and Wang, 1996), fail in cytokinesis prior to abscission, implying that midzone stability may play an earlier role in promoting cleavage furrow ingression. Here, we used the INCENP-actin binding mutant to selectively block midzone stabilization after furrowing and found that furrow ingression failed before midbody formation (see Chapter 4). Midzone stabilization appears to be the underlying factor as furrow closure was rescued by treating cells with low dose taxol. Unfortunately, we cannot rule out the possibility that the ABK phospho-gradient (Afonso et al., 2014; Fuller et al., 2008) is also disrupted in these cells, as the actin-binding mutations also affect

CPC midzone localization. Addressing the function of midzone stabilization in furrowing cells will require a more precise experimental approach to perturb C phase MT dynamics in a manner that does not broadly disrupt CPC localization and function.

While our work suggests that midzone stabilization in mammalian cells is required for successful furrow closure, the function of MT stabilization during C phase may be cell-type specific. Studies of midzones in millimeter-sized urchin embryos have suggested that stabilization - assessed by nocodazole resistance - can occur prior to cleavage furrow ingression (Foe and von Dassow, 2008). It has also been proposed that the midzone array of urchin embryos generates MT-dependent signaling that specifies the cleavage plane (Bement et al., 2005), which may explain why midzone MTs are stabilized earlier relative to mammalian cells. Investigations of midzone organization and stability in *C. elegans* indicate that MTs are generally required for successful cleavage furrow ingression (Guse et al., 2005; Raich et al., 1998), however, an organized midzone is dispensable for cytokinesis (Verbrugghe and White, 2004). This may point to a role for furrow-associated MTs in driving furrow closure in this system. Cleavage plane specification in smaller somatic cells is a function that has been ascribed to furrow-associated astral MTs (Canman et al., 2003; Shannon et al., 2005), potentially negating the requirement for highly stable midzones in early anaphase in mammalian cells. Taken together with work presented in this study, these findings indicate that the timing and function of midzone stabilization differs among organisms and cell types. One plausible explanation for this phenomenon is that cell size may dictate the function and therefore stability of C phase MT subsets. Urchin embryos are significantly larger than somatic cells, and a stable midzone array may be more efficient at propagating diffusion-based signaling (Nguyen et al., 2014). Another possibility is that midzone stability is tied to MT geometry. For example, the MT array in *C. elegans* embryos is comprised

of a compact midzone and large astral MTs (Raich et al., 1998) while midzones in mammalian cells are much larger relative to cell size and astral MTs are less dominant in C phase (Rankin and Wordeman, 2010). These ideas are not mutually exclusive and many factors may work in concert to influence midzone stabilization. In the future, determining the relative importance of astral MTs and midzone MTs in positioning the cleavage furrow and promoting ingression may provide insight as to why the timing of midzone stabilization varies among different cell types. This will require strategies that selectively alter or eliminate specific sub-populations of C phase MTs.

Aurora B kinase mediates cytoskeletal cross-talk

While the CPC is known to regulate many aspects of cytokinesis, the specific function of the CPC at the cell cortex has remained elusive (Carmena et al., 2012). We have shown that the CPC coordinates the initiation of furrowing with midzone MT stabilization. Significantly, the ability of INCENP to bind actin is essential for this function of the CPC. This key finding strongly suggests that CPC-mediated cytoskeletal feedback signaling initiates at the cortex. Determining the mechanism(s) by which ABK coordinates midzone stabilization with furrowing is an important area of future work. We find that perturbations of the CPC, either through pharmacological inhibition of ABK or through disrupting INCENP-actin binding, specifically alters midzone stability after cleavage furrow ingression, suggesting ABK signaling is likely to function downstream of myosin II activity (see Chapter 4). An exciting possibility is that INCENP-actin binding enables the CPC to respond to physical changes in the furrow as it ingresses. Furrow ingression could impact ABK activity at a molecular level in a number of ways. For example, CPC clustering and MT binding both increase ABK activity *in vitro* (Kelly et al., 2007; Noujaim et al., 2014; Rosasco-Nitcher et al., 2008), and cleavage furrow ingression may mimic a "reduction

in dimensionality" by bringing neighboring complexes close enough to activate feedback signaling. One way to test whether acto-myosin activates ABK through clustering would be to measure the activity of recombinant ABK *in vitro* in the presence of F-actin or an acto-myosin contractile meshwork (Kasza and Zallen, 2011). Previous studies of MT-dependent CPC activation (Noujaim et al., 2014; Rosasco-Nitcher et al., 2008) lead us to predict that contraction-dependent clustering of the CPC would hyper-activate ABK. Another model that might explain ABK activation after furrowing, is that as the circumference of the cortex shrinks the midzone-bound substrates of ABK become more accessible to cortically-localized CPC. In contrast to this model, we do not observe that MTs closest to the cortex become stabilized first. In other words, MTs in the center of the midzone are cold-stable even in the early stages of ingression. However, it is plausible that reducing the distance between the cortex and midzone, through furrowing, may allow for more efficient transmission of ABK signaling across the midzone (Nguyen et al., 2014). Finally, cleavage furrow ingression could induce conformational changes in INCENP which activate ABK signaling. The structure of full-length INCENP remains unsolved, however, the C-terminal half is primarily comprised of a single-alpha helical (SAH) domain which has been proposed to function as a flexible "dog-leash" during prometaphase (Samejima et al., 2015). This model suggests that the flexibility of the SAH domain allows ABK to reach substrates at the outer kinetochore, even while the N-terminus of INCENP is anchored at the centromere. It is conceivable that flexibility conferred by the SAH domain allows for conformational changes of INCENP at the cortex as well. Distinguishing between these possibilities will be important for elucidating the mechanism of ABK feedback signaling during cleavage furrow ingression. Generally, we anticipate that the INCENP actin-binding mutant described here will be a useful tool to probe these models.

Microtubule dynamics regulators and midzone stabilization

Our work clearly indicates that there is a transition from unstable to stable midzones as cells progress through C phase. We have identified the CPC as a mediator of cytoskeletal cross-talk that drives midzone stabilization, however, we have yet to fully identify substrates of ABK that regulate MT dynamics at this stage of division. Our preliminary investigation of Kif2a suggests that it may be one effector of feedback signaling. Kif2a is displaced from the midzone after ingression in a manner that depends on ABK activity, and eliminating Kif2a results in a moderate increase in midzone stabilization before furrowing. The generation of Kif2a KO cell lines presents an opportunity to further characterize the role of Kif2a in regulating midzone MT stability. An analysis of midzone stabilization in this cell line using our "nocodazole shock" assay would allow us to more carefully quantify small changes to MT stability in the absence of Kif2a. For example, the addition of high dose of nocodazole may show that midzones in Kif2a KO cells depolymerize more slowly than the parent cell line. This result would not be revealed by analyzing cells exposed to cold temperature. Another informative experiment would be to express Kif2a phospho-mutants (Ohi et al., 2007; Uehara et al., 2013) in the KO cell line and examine Kif2a C phase localization and midzone MT stability. Based on our preliminary experiments, we predict a non-phosphorylatable mutant of Kif2a will localize robustly to midzone MT plus ends throughout C phase. This may also cause midzones to become cold and nocodazole-sensitive after furrowing, thereby pheno-copying ABK inhibition. Alternatively, an ABK phospho-mimetic would be expected to prevent Kif2a midzone localization. Our Kif2a RNAi experiments suggest this would likely cause midzones to become hyper-stable before furrow ingression. These experiments have the potential to reveal how ABK feedback signaling directly regulates midzone MT stability.

It is worth mentioning that we have searched for other microtubule-associated factors that may be involved in regulating midzone MT dynamics. To do this we have screened the C phase localization of candidate proteins before and after cleavage furrow ingression, and before and after ABK inhibition. For example, PRC1 and Kif4A have roles in regulating midzone organization and length immediately after anaphase onset, however, both proteins are associated with midzone MT plus ends regardless of the state of cleavage furrow ingression (Kurasawa et al., 2004; Shrestha et al., 2012; Subramanian et al., 2013). We have also investigated the C phase localization of kinesins that associate with the midzone such as Mklp1, Mklp2, Kif18a, and Eg5 (Zhu et al., 2005b). Unfortunately, the steady state localization of these proteins does not reflect pattern that would explain changes in midzone stability. Even so, these proteins may still be involved in regulating midzone MT dynamics. Importantly, we do not believe that depleting these proteins by RNAi is a useful approach for testing their role in midzone stabilization, as this is likely to cause major disruptions to cell cycle progression and midzone organization, which would complicate the interpretation of any observed effect on midzone stabilization. Investigating whether these factors influence midzone stabilization may instead require an analysis of protein dynamics within the plus end overlap. It is possible that the turnover of plus-end associated proteins decreases after the initiation of furrowing, and this could stabilize MT plus ends without broadly changing the steady state protein localization. This question could be addressed using FRAP (De Los Santos et al., 2015) or photo-activation (McKinney et al., 2009) of proteins localized to the plus-end overlap before and after furrowing. A decrease in protein turnover might suggest that MT plus ends become stably embedded in a cross-linked matrix after cleavage furrow ingression. This could affect midzone MT stability by making the plus ends inaccessible to destabilizing factors (Walczak et al., 2013). Using this approach, it would be possible to investigate whether factors that regulate

midzone formation in early C phase also impact midzone MT stabilization after furrowing. Moreover, this analysis could be coupled to investigations of depletion phenotypes using the monopolar cytokinesis model system. Factors that appear to stabilize bipolar midzone MTs would be predicted to promote monopolar midzone formation.

The role of actin in CPC C phase localization

Previous studies of CPC recruitment to the plus end overlap and the equatorial cortex have focused primarily on Mklp2-dependent transport along MTs (Gruneberg et al., 2004; Hummer and Mayer, 2009; Kitagawa et al., 2013) while the mechanism of cortical localization of the CPC has remained largely unexplored (Earnshaw and Cooke, 1991). This is somewhat surprising given the number of cytokinetic functions attributed to ABK (Carmena et al., 2012) and the proposed requirement for proper localization in carrying out those functions (Afonso et al., 2014; Fuller et al., 2008). We find that the CPC distributes more broadly along the midzone in cells expressing an INCENP actin-binding mutant (GFP-INCENP CR, see Chapter 4) and this result led us to speculate that this interaction may be involved in CPC localization during C phase. In agreement with this idea, we found that actin-binding is sufficient to recruit the complex to the cortex in the absence of Mklp2. We have also observed that cortically localized CPC can rescue furrow closure in Mklp2-depleted cells indicating that this population of CPC is functional for cytokinesis. Our investigation shows that the CPC diffuses along the cell cortex before furrow ingression, in a manner that depends primarily on actin filaments. Therefore, we propose that direct interactions between the Mklp2-CPC complex and acto-myosin underlie cortical recruitment.

Our work implies that there is cooperation between actin and MTs in localizing the CPC during normal C phase, however, what remains unanswered is how INCENP-actin binding can

promote recruitment to the division site in the absence of Mklp2. We generally do not observe cortical enrichment of GFP-INCENP near the spindle poles, and we can clearly detect CPC at the equatorial cortex and midbody of Mklp2-depleted cells by immunofluorescence and live-cell imaging (see Chapter 5). As cortical actin is only moderately enriched (~1.5-fold) at the site of the presumptive furrow in mammalian cells (Murthy and Wadsworth, 2005; Rankin and Wordeman, 2010), we predict that the mechanism of actin-based recruitment to the cell equator is more complex. One way the CPC could become enriched in the cell middle is through cortical flow towards the division site (Bray and White, 2017), however, our study suggests that the movement of GFP-INCENP on the cortex is primarily diffusive. We cannot rule out the possibility that cortical diffusion switches to flow after RNAi of Mklp2, and this hypothesis could be tested using lectins to block cortical flow during C phase (Rosenblatt et al., 2004). Unfortunately, cells lacking Mklp2 do not have enough cortically localized GFP-INCENP to accurately track and characterize spot movement. Other explanations for medial CPC enrichment include the possibilities that the CPC reaches the cortex through cytoplasmic diffusion, or is targeted there through yet unknown direct interactions with factors within the contractile array. Differentiating between these possibilities has the potential to reveal the physiological relevance of Mklp2-independent recruitment of the CPC to the cortex.

CPC movement during C phase

The behavior and transport of the CPC observed in live cells is strikingly complex. The movement of Mklp2-CPC can be described in two phases. First, the CPC off-loads from centromeric chromatin at anaphase onset, and is rapidly transported to the plus end overlap of the nascent midzone. Second, the CPC diffuses on the cortex and midzone until the onset of cleavage

furrow ingression. Transport on the early midzone to MT plus ends appears to depend on motor activity, as this event is absent in Mklp2-depleted cells. The window of time where off-loading and plus-end directed transport occurs is short (< 2 min after anaphase onset) and future characterization of these events would benefit from high-speed imaging. It is encouraging that the rate of streaming measured in our system is comparable to CPC plus end-directed streaming on MT asters in vitro (Nguyen et al., 2014). A number of unanswered questions about these early events remain. Why does the CPC off-load onto the newly formed midzone, as opposed to other populations of MTs? Are there regulatory factors that function to couple centromere off-loading to Mklp2-CPC complex formation? Monopolar cytokinesis may be the best model system for addressing these questions as one complication of studying this process in bipolar cells is that the chromosome masses mask the GFP-INCENP signal on the early midzone. It would also be useful to track CPC off-loading using a photo-convertible INCENP probe (Bancaud et al., 2010) which would allow us to follow the movement of a specific sub-population of centromeric CPC and analyze its behavior as cells transition into C phase. This type of analysis could potentially provide more detailed and quantitative information about the first steps of Mklp2-dependent CPC transport on the midzone.

Our data indicates that once streaming is complete motor activity no longer dominates C phase movement of the CPC. Midzone-localized Mklp2-CPC is diffusive after streaming, suggesting that motor activity is shut off. One explanation is that the bulk of Mklp2-CPC remains stably associated with MT plus ends, either due to the inherent properties of the motor or perhaps through interactions with other factors at the plus end overlap. In this scenario, the midzone diffusion of Mklp2-CPC would be correlated to diffusive movement of the entire MT filament within the midzone. Alternatively, Mklp2-CPC spots could transiently interact with midzone MT

ends and move laterally along the plus end overlap. This model is in agreement with *in vitro* studies of ABK plus end localization using centrosome-nucleated asters (Nguyen et al., 2014). Previous studies have indicated that the MT-binding activity of INCENP promotes Mklp2 midzone localization (van der Horst et al., 2015), however, it is not clear which phase of CPC transport requires this interaction. It is possible to envision models where INCENP-MT binding is necessary for any one of the following events: CPC off-loading, Mklp2-CPC complex formation, plus end-directed transport on the early midzone, or association with midzone MT plus ends. High-speed imaging of an INCENP-MT binding mutant during monopolar cytokinesis may help answer this question. Our analysis of CPC behavior on the midzone suggests that motor activity promotes plus end accumulation very early in C phase, and once Mklp2-CPC coalesces in the center of the cell, directed movement stops.

Our work suggests that delivery of GFP-INCENP spots to the cortex occurs *via* Mklp2. While actin-binding can promote cortical recruitment in the absence of motor, the enrichment of CPC at the cortex is low compared to control-depleted cells. Additionally, cortical GFP-INCENP spots are too dim to accurately image and track after Mklp2 depletion. Surprisingly, Mklp2 and the CPC diffuse together, indicating the Mklp2-CPC complex remains stably associated on the cortex. Moreover, the diffusive behavior suggests that once Mklp2-CPC reaches the cortex, movement no longer depends on motor activity. In agreement with this idea, we find that F-actin disassembly causes a decrease in the diffusion co-efficient of GFP-INCENP. This result indicates that actin filaments do not function to tether the CPC to the cortex, and are instead required for movement. One possibility is that electrostatic interactions between the CPC and F-actin allow the complex to rapidly diffusive along the cortex, and when those filaments are disrupted Mklp2-CPC becomes statically attached to the membrane, perhaps through lipid interactions (Fung et al.,

2017). Our work suggests that MTs also contribute to Mklp2-CPC diffusion on the cortex. This could occur if Mklp2-CPC diffuses along the lattice of MTs that run parallel to the cortex or if Mklp2-CPC is stably bound to the plus ends of MTs that terminate there. Importantly, disassembly of either filament does not appear to cause Mklp2-CPC to switch filament tracks. For example, actin disassembly does not result in directed movement along MTs, and MT disassembly does not cause an increase in actin-based diffusion. This suggests that actin and MTs work cooperatively to promote cortical diffusion of Mklp2-CPC, and this agrees with our finding that actin and MTs are both required to promote cortical localization of the CPC. In the future it will be interesting to uncouple cortical CPC diffusion from cleavage furrow ingression in order to test whether this dynamic CPC movement is required for cytokinesis.

Cross-linking actin and MTs at the cortex

It is exciting to consider the potential for higher-order complex formation between cytoskeletal filaments and Mklp2-CPC at the equatorial cortex. Mklp2 has been proposed to interact directly with myosin II (Kitagawa et al., 2013) in addition to the CPC (Carmena et al., 2012); and Mklp2 bundles MTs *in vitro* (Neef et al., 2003). We have demonstrated that INCENP binds actin at the cortex, and others have shown that recombinant INCENP binds directly to MTs (Noujaim et al., 2014; Samejima et al., 2015). Furthermore, INCENP has been proposed to multimerize in cells during C phase (van der Horst et al., 2015) suggesting higher-order complex formation is possible. Using live-cell imaging we have observed that Mklp2-mCherry and GFP-INCENP move together as discrete spots on the cortex and the midzone. Notably, these spots are much larger than we would predict for single molecules, potentially supporting the hypothesis that these proteins assemble into larger complexes in cells. Previous studies have shown that

multimerization increases the affinity of INCENP for MTs (van der Horst et al., 2015) suggesting weak electrostatic interactions between the Mklp2-CPC complex and cytoskeletal filaments may be enhanced by forming multimers. As Mklp2 and the CPC can *each* interact with *both* actin and MTs, we hypothesize that multimeric "teams" of Mklp2-CPC may function as a tether that links furrow-associated astral MTs to cortical actin. This model is particularly intriguing because this MT sub-population has been proposed to be highly stable compared to MTs at the polar cortices (Canman et al., 2003) and physically cross-linking MT plus ends to the cortex might explain this stabilization.

It is imperative to determine whether INCENP can multimerize *in vitro* and to identify the mechanism(s) and/or protein domains that are necessary for this process. Previous work in cells has shown that an N-terminal fragment of INCENP can "piggyback" on endogenous protein to target the division plane (van der Horst et al., 2015). Deleting this region of INCENP in cells is challenging as this would disrupt interactions with Survivin and Borealin and likely affect cellular processes that precede C phase (Carmena et al., 2012). It would be most useful to identify point mutations that abolish multimer formation without disrupting the interaction between INCENP and Survivin and Borealin. This approach is potentially more informative than generating mutants that abolish the interaction between Mklp2 and the CPC as recruitment of these proteins to the division plane is interdependent (Gruneberg et al., 2004; Kitagawa et al., 2013; van der Horst et al., 2015). Expression of an INCENP multimerization mutant in cells would allow us to test whether GFP-INCENP spots represent the formation of higher-order complexes. Moreover, by examining astral MT stability in these cells it would be possible to determine whether multimeric Mklp2-CPC promotes tethering of furrow-associated MTs to the cortex. These studies have the

potential to shed light on how C phase astral MTs that extend toward the cleavage furrow are stabilized as well as reveal the function of astral MT stabilization during mammalian cytokinesis.

APPENDIX

THE ROLE OF INCENP WITHIN THE CHROMOSOMAL PASSENGER COMPLEX

Fixed Cell Imaging

To visualize Mad1 and CREST cells were fixed at -20^{o} C in MeOH for 10 min and stained as previously described (see Chapter 2). Serum containing anti-Mad1 was used at a 1:10 dilution and anti-CREST (Immunovision) was used at a 1:100 dilution. To visualize phospho-Hec1 coverslips were first rinsed in 1X PHEM buffer (60 mM PIPES, 25 mM K-HEPES, 10 mM EGTA, 4 mM $MgSO_4$, pH=6.9) at 37^{o} C. Fresh lysis buffer (1X PHEM, 1% TX-100, and 100 nM microcystin) was sonicated for 5 min before use. Coverslips were incubated in lysis buffer for 5 min at 37^{o} C. Cells were then fixed in 2% PFA in 1X PHEM for 20 min at 37^{o} C. Coverslips were washed with 1X PHEM and blocked with 1X PHEM + 20% BSA for 1 hour at room temperature. Antibodies were diluted in 1X PHEM-T (1X PHEM + 0.1% TX-100). Anti-phospo-ser44 (anti-phosphoHec1, a gift from Jennifer DeLuca) was used at 1:30. Imaging was performed as previously described (see Chapter 2).

Molecular Biology

To construct the CPC triple helix complex full-length human Borealin (CDCA8, NCBI accession: KJ894139) and Survivin (BIRC5, NCBI accession: CR541740) ORFs were synthesized as G blocks (IDT) and cloned into pETDuet-1 restricted with *EcoRI* and *HindII* or *NdeI* and *KpnI*, respectively. Borealin was cloned into the first MCS of pETDuet so as to add a His_6 tag for purification. An N-terminal fragment (amino acids 1-50) of INCENP was assembled with the amplified mCherry ORF (from pmCherry-C1) into pST39 restricted with *EcoRI* and *HindIII*. That

fragment was amplified using PrimeStar GXL (Takara) and cloned into pGEX6P1 restricted with *EcoRI* and *SalI*.

Full-length human Mklp2 (Kif20a) cDNA (Thermo Scientific, Clone ID: 3604291, NCBI accession: BC) was used to prepare all Mklp2 DNA constructs. Amplification of the ORF was performed using Phusion polymerase (New England Biolabs). The Mklp2 ORF was cloned into pmCherry-N1 restricted with *XhoI* and *BamHI*. Mklp2 ORF was also cloned into pEGFP-N1 restricted with *EcoRI* and *KpnI*. Bacculovirus construction was performed by assembling the amplified Mklp2-GFP ORF into pFASTBAC-1 restricted with *EcoRI* and *HindIII*. This construct was used with the Bac-to-Bac expression system (Invitrogen) to create bacculovirus that expresses full length Mklp2-His_6-GFP.

Protein Expression and Purification

His_6-INCENP$^{500\text{-}680\ MT\ CR}$ was expressed in BL21 DE3 RIPL cells with 0.4 mM IPTG for 16 hours at 16^{o}C and purified as previously described for His_6-INCENP$^{500\text{-}680}$ (see Chapter 2).

To generate the CPC triple helix construct, GST-mCherry-INCENP$^{1\text{-}50}$, His_6-Borealin, and Survivin were expressed in Bl21 DE3 RIPL cells with 0.4 mM IPTG for 16 hours at 16^{o}C. For purification, cells pelleted and resuspendend in lysis buffer lysis buffer (1X PBS, 0.5 M NaCl, 5 mM β-mercaptoethanol (β-ME), 1% NP40, and protease inhibitors [1 mM phenylmethylsufonyl fluoride, 1 mM benzamidine, and 10 μg/ml each of leupeptin, pepstatin, and chymostatin]). Cells were enzymatically lysed, sonicated, and clarified by centrifugation as described previously. The clarified supernatants were mixed at 4^{o}C for 1 hour before a 1 hour incubation with 2 ml of GST bind resin (Millapore). Resin was washed extensively with wash buffer (PBS, 0.5 M NaCl, 5 mM β-ME) and protein was eluted with (50 mM Tris-Cl pH=8.0, 300 mM KCl, 5mM Glutathione).

Peak fractions were desalted using a PD-10 column (GE Healthcare) equilibrated in 10 mM K-HEPES, pH=7.7, 1 mM DTT, 300 mM KCl, and 10 % glycerol. Protein was aliquoted, frozen in liquid nitrogen and stored at -80^{o}C.

His_6-GFP-Mklp2 was expressed in Sf9 cells for 72 hours. For purification, cells were pelleted and resuspended in PNI, 5 mM β-mercaptoethanol (β-ME), 100 μM $MgCl_2$, 100 μM ATP, 1 % NP40, 10 % glycerol and protease inhibitors. Cells were then sonicated, and clarified by centrifugation as described previously. Clarified supernatant was incubated with Ni^{++}-NTA agarose (Qiagen) for 1 hour at 4^{o}C and washed with wash buffer (PNI, 5 mM β-ME, 100 μM $MgCl_2$-ATP, 10 % glycerol). Protein was eluted with PNI, 5 mM β-ME, 100 μM $MgCl_2$-ATP, 10 % glycerol and 180 mM imidazole. Peak fractions were combined and subjected to size exclusion chromatography on a Hiload 16/60 Superdex 200 preparatory grade column (GE Healthcare). The bed volume for this column is 120 mls, and the void volume is 56 mls. Gel filtration buffer contained 10 mM K-HEPES, pH=7.7, 1 mM DTT, 0.1 mM MgATP, 300 mM KCl, and 10 % glycerol. Protein concentration was measured by Bradford assay, accounting for dimerization of Mklp2. Peak fractions were combined (17-19) and protein was aliquoted, frozen in liquid nitrogen and stored at -80^{o}C.

MT assays

For gliding assays with Mklp2-His_6-GFP, flow cells were constructed with double-stick tape and infused with 1 μM Mklp2-His_6-GFP at 1.9 μM for 3 minutes, 1% Pluronic F-127 in BRB80 for 1 minute, and Alexa 594-labeled GMPCPP MTs at 1 μM tubulin in BRB80 for 3 minutes. Flow cells were washed between each infusion with 3 volumes wash buffer (WB; BRB80 + 1 mM MgATP + 500 μg/ml casein). For the final infusion, the MTs were diluted in flow cell

buffer (FCB; BRB80 + 1 mM MgATP + 500 μg/ml casein + Oxygen Scavenging Mix [200 μg/ml glucose oxidase, 35 μg/ml catalase, 25 mM glucose, 70 mM β-ME]). MT motility was recorded at 3 s intervals by timelapse microscopy. Images were acquired at ambient temperatures by widefield fluorescence microscopy on an Eclipse 90i (Nikon) equipped with a 100X 1.4 NA (Nikon) objective and a Cool SnapHQ2 CCD camera (Roper). Nikon Elements was used for acquisition and ImageJ for subsequent image processing (adjusting levels, rotating, and cropping).

For imaging single molecules, flow cells were prepared in the same way. Alexa-594- and biotin-labeled GMPCPP MTs were adhered to coverslips coated with biotin-BSA and neutravidin. Flow cells were washed with WB, and the final mixture contained 1X BRB80, 0.5 mg/ml casein, 100 mM MgATP, 1X OS and a 1:2 dilution of Mklp2-GFP from cell lysates.

MT co-sedimentation and Immunoblotting

Prior to use, His_6-INCENP$^{500-680}$ and His_6-INCENP$^{500-680\ MT\ CR}$ were pre-clarified by centrifugation at 90K rpm for 30 minutes at 4^{o}C in a TLA-100 Ultracentrifuge (Beckman). Co-pelleting was performed with GFP-INCENP$^{500-680}$ or GFP-INCENP$^{500-680}$ at 1 μM in 100 μl reaction buffer (10 mM HEPES, pH=7.7, 50 mM KCl, 1mM DTT) with tubulin or taxol-stabilized MTs at 1 μM. Reactions were incubated for 15 minutes at room temperature and centrifuged at 90K rpm for 20 minutes at 22^{o}C. Taxol was included to 1 μM in reaction buffer. 100 μl of supernatant was collected and mixed with and equivalent volume of 2X Laemmli buffer. Pellets were resuspended in 200 μl of 2X Laemmli buffer. 20 μl of each fraction was boiled, separated on a 10% SDS-PAGE gel, and transferred to nitrocellulose for immunoblotting. Immunoblots were blocked with 5% w/v milk in PBS-T and then probed with anti-His (Sigma) or DM1α followed by

fluorescently tagged anti-mouse secondary antibodies (Invitrogen). Bound antibodies were detected using an Odyssey fluorescence detection system and images were cropped using ImageJ.

Preparation of Mklp2-GFP from cell lysates

Cos7 cells were transfected with Mklp2-GFP as previously described (see Chapter 2) 24 hours before collection. To synchronize cells in C phase, cells were treated with 10 µM STLC for 16 hours at 37^{o}C and then transferred to 10 µM STLC + 30 µM Purvalanol A for 30 min at 37^{o}C to induce exit from mitosis. Lysates were collected by adding 0.05% Trypsin-EDTA to cells for 2 min at room temperature, and cells were then transferred to a conical tube on ice. Cells were pelleted by centrifuging at 1500 rcf for 3 min at 4^{o}C. After centrifugation, tryspin was removed and cells were washed with 1 ml of DMEM, and pelleted again by centrifugation. After centrifugation, DMEM was removed and cells were resuspended in lysis buffer (25 mM HEPES pH=7.4, 115 mM KOAc, 5 mM NaOAc, 5 mM $MgCl_2$, 0.5 mM EGTA, 1% TX-100) + 1 mM ATP. Lysates were centrifuged for 10 min at 140,000 rpm at 4^{o}C and supernatant was aliquoted and store at -80^{o}C.

Co-immunoprecipitation of Mklp-His_6-GFP and triple helix

To immunoprecipitate Mklp-His_6-GFP, anti-GFP beads were blocked with 1X P12 Buffer, 1% BSA, 0.5 mg/ml casein, for 1 hour. Beads were washed extensively with 1X P12, and 4 µg Mklp-His_6-GFP was incubated with the beads end-over-end for 1 hour a 4^{o}C. Again, beads were washed extensively with 1XP12, and 4 µg of CPC triple helix was incubated with bound Mklp-His_6-GFP for 1 hour a 4^{o}C. Protein was eluted using high salt (3.6 M MgCl) according to

manufacturer instructions. Protein was separated by SDS-PAGE, and transferred to a nitrocellulose membrane. Bound protein was detected using anti-mCherry (Invitrogen) at 1:1000, and anti-Survivin (Abcam), and species-appropriate fluorescently tagged secondary antibodies, and an Odyssey fluorescence detection system.

INCENP binds MTs directly

Previous studies of CPC activation have shown that the C-terminal half of INCENP bound to ABK can bind MTs *in vitro* (Noujaim et al., 2014). We set out to investigate which regions of INCENP were sufficient for MT-binding. To do this, we exogenously expressed a fragment of INCENP in cells (GFP-INCENP$^{500\text{-}680}$) along with fluorescently tagged α-tubulin (mCherry-tubulin). We observed that GFP-INCENP$^{500\text{-}680}$ co-localized with MTs in mitotic cells, and GFP-INCENP$^{500\text{-}680}$ fluorescence was diminished after a 10 min treatment with 5μM Nocodazole (Figure A1.1 A). As INCENP aa residues 500-680 reside in a highly charged region of a single alpha helical domain (Samejima et al., 2015), we predicted that INCENP MT-binding occurs through an electrostatic interaction. We generated charge reversal mutations (lysine/arginine-to-glutamic acid) to abrogate MT co-localization. Charge-reversal of eight residues (K622E, K624E, K625E, K626E, K630E, K631E) abolished the MT co-localization of GFP-INCENP$^{500\text{-}680}$ in cells suggesting they disrupt INCENP-MT binding (Figure A1.1 A, GFP-INCENP$^{500\text{-}680\ \text{MT CR}}$). To determine if INCENP binds MTs directly, we purified recombinant His$_6$-INCENP$^{500\text{-}680}$ from *E. coli* and performed an MT co-sedimentation assay. Free tubulin dimers mixed with His$_6$-INCENP$^{500\text{-}680}$ do not sediment, however, His$_6$-INCENP$^{500\text{-}680}$ does co-sediment wtih MTs, confirming there is a direct interaction. His$_6$-INCENP$^{500\text{-}680\ \text{CR MT CR}}$, however, does not co-sediment with MTs, indicating that these charge-reversal mutations disrupt MT-binding *in vitro*

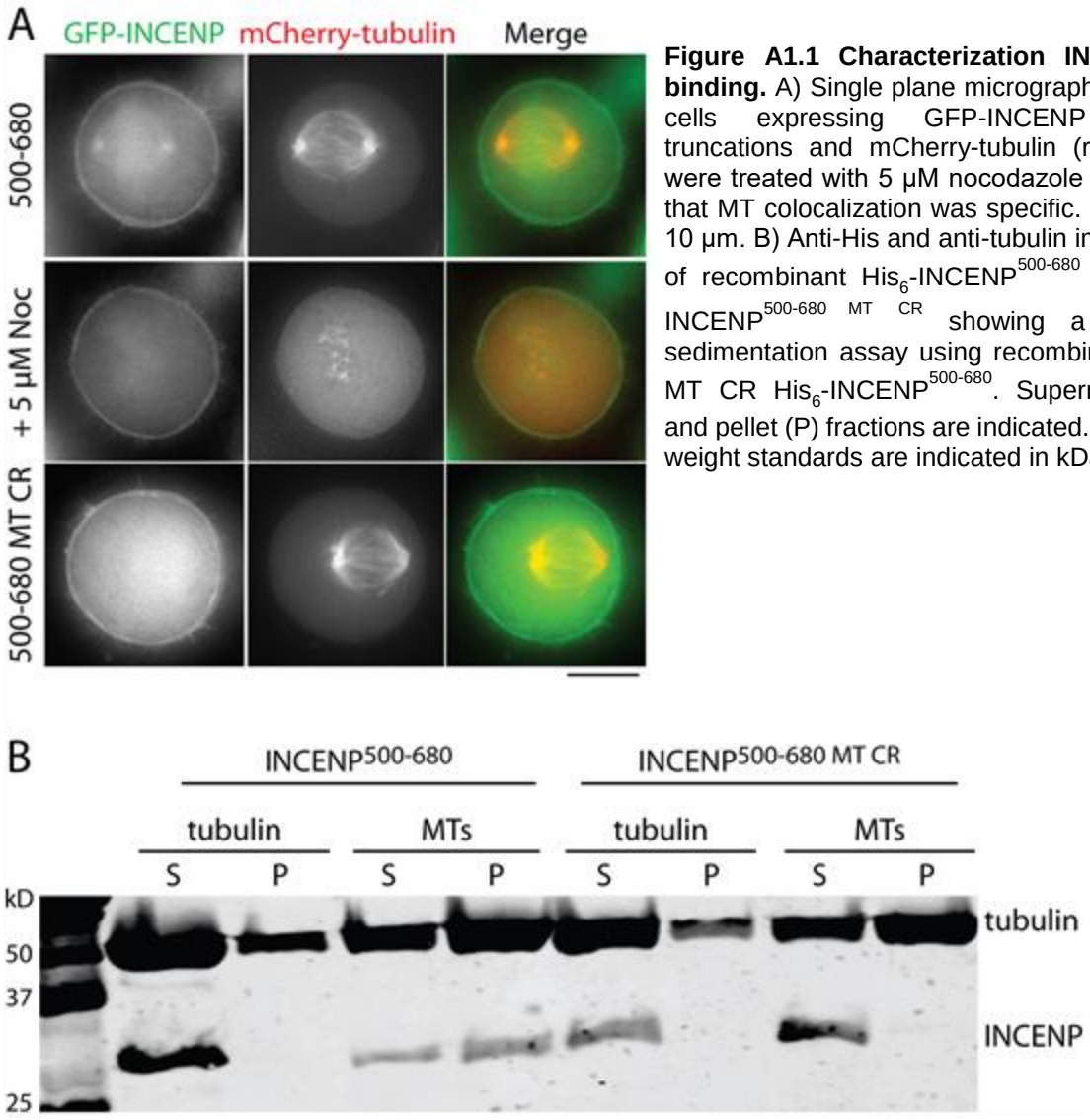

Figure A1.1 Characterization INCENP-MT binding. A) Single plane micrographs of HeLa cells expressing GFP-INCENP (green) truncations and mCherry-tubulin (red). Cells were treated with 5 µM nocodazole to confirm that MT colocalization was specific. Scale bar, 10 µm. B) Anti-His and anti-tubulin immunoblot of recombinant His_6-$INCENP^{500-680}$ and His_6-$INCENP^{500-680\ MT\ CR}$ showing a MT co-sedimentation assay using recombinant wt or MT CR His_6-$INCENP^{500-680}$. Supernatant (S) and pellet (P) fractions are indicated. Molecular weight standards are indicated in kDa.

(Figure A1.1 B). These mutations were incorporated into full-length GFP-INCENP to test whether INCENP-MT binding was required to promote midzone stabilization (see Chapter 4). This construct (GFP-INCENP MT CR) was also used to investigate the role of MT-binding at the centromere (see below).

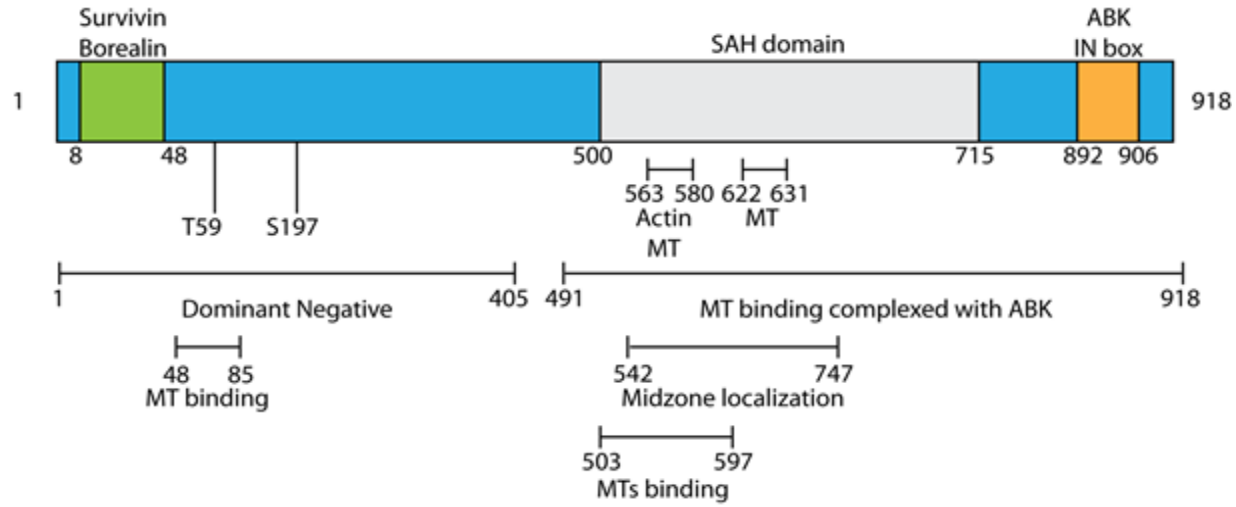

Figure A1.2 Summary of INCENP sites that mediate cytoskeletal interactions.

Amino acids 8-48: These residues interact with Survivin and Borealin through the formation of a triple helix (Jeyaprakash et al., 2007). They are also sufficient to allow for exogenously expressed INCENP to "piggyback" on endogenous INCENP and reach midzone MT plus ends (van der Horst et al., 2015).

Amino acid 59: This residue is phosphorylated by Cdk1 and de-phosphorylated by cdc14 to regulate interactions with Mklp2 (Hummer and Mayer, 2009).

Amino acid 197: Phosphorylation of this residue by Plk3 is required for midbody localization of the CPC (Yang et al., 2007).

Amino acids 1-405: These residues function as a dominant negative when expressed in cells and disrupt midzone localization of the CPC (Wheatley et al., 2001a).

Amino acids 491-918: These residues bind MTs in vitro when complexed with ABK, and when bound to MTs, can lead to ABK activation through a "reduction in dimensionality". Experiments performed using *X. laevis* protein (Noujaim et al., 2014).

Amino acids 500-715: These residues make up a single alpha helical (SAH) domain which binds MT *in vitro* (Samejima et al., 2015).

Amino acids 503-597: These amino acids are sufficient for *in vitro* MT binding (Samejima et al., 2015).

Amino acids 542-747: These amino acids are necessary for midzone localization in cells. They are not, however, required for interactions with Mklp2 (van der Horst et al., 2015).

Amino acids 563-580: Charge reversal mutations of lysine and arginine residues within this region abolish actin and MT co-localization in cells. These mutations also disrupt actin-binding *in vitro*.

Amino acids 622-631: Charge reversal mutations of lysine and arginine residues within this region abolish MT co-localization in cells. These mutations do not disrupt actin co-localization in cells. These mutations also abolish MT binding *in vitro*.

Amino acids 892-906: These residues represent the highly conserved IN box where ABK binds.

Mapping INCENP

Investigations of CPC function during cell division have largely focused on ABK, as it represents the active component of the complex. However, ABK activity is largely regulated by

the scaffolding protein INCENP, which functions to activate low-level kinase activity through binding, and regulates the sub-cellular localization of active ABK (Carmena et al., 2012). While the structure of INCENP is not known, previous studies have identified a number of key residues and protein domains that modulate interactions with the cytoskeleton and are involved in regulating CPC localization. Those findings, in addition to the characterization of INCENP described in this study are summarized in Figure A1.2. It is important to note that this is not a comprehensive list of INCENP regulatory sites, rather it highlights those domains which appear to control CPC-cytoskeletal interactions or CPC localization, especially during C phase.

The interactions between the SAH domain of INCENP and cytoskeletal filaments are not well understood. One of the major discrepancies is how actin and MT interactions are differently regulated. Our work, along with the work of others, suggest that INCENP can interact with F-actin and MTs directly through electrostatic interactions (Samejima et al., 2015; van der Horst et al., 2015). However, mutating residues to disrupt these interactions produces varied results. For example, we find that generating charge reversal mutations in two discrete regions of the SAH domain abolishes co-localization of GFP-INCENP$^{500\text{-}680}$ with MTs. Charge reversal mutations of lysine and arginine residues from amino acids 563-580 (10 residues) or 622-631 (8 residues) can abolish MT co-localization. Other investigations report that charge reversal mutations of either 8 or 27 lysine/arginine residues spanning amino acids 543-746 also lowered the affinity of INCENP for MTs (van der Horst et al., 2015). Together, these findings seem to indicate that INCENP MT-binding is not confined to a specific site. Instead, MT-binding may require a threshold of positively charged residues within the SAH. This is distinct from what we have found for INCENP-actin binding. Charge reversal mutations spanning amino acids 622-631 did not disrupt actin co-localization of GFP-INCENP$^{500\text{-}680}$ in cells. This may indicate that actin-binding is mediated

through a specific site within amino acids 563-580, rather than requiring a threshold of positively charged residues. An important future direction will be to determine if it is possible to disrupt INCENP-actin binding with a more specific set of mutations. It is not clear how INCENP differentiates between cytoskeletal filaments and identifying a more discrete mutation that abolishes actin-binding, without disrupting MT binding, may help explain why charge reversal perturbations of INCENP affect filament interactions differently.

The role of INCENP-MT binding during prometaphase

The localization of the CPC to centromeric DNA is essential for regulating MT-attachments at the kinetochore (Carmena et al., 2009). Previous studies have suggested that increasing the local concentration of the CPC leads to *trans*-activation of ABK (Wang et al., 2011) and both the centromere and MTs are thought to functionally activate ABK through clustering (Noujaim et al., 2014; Rosasco-Nitcher et al., 2008). However, whether MTs function to promote ABK activity at the centromere is unclear. MTs have been proposed to regulate the dynamics of the centromere-localized CPC as centromeric turnover of the CPC decreases in cells treated with nocodazole (Beardmore et al., 2004). This finding is at odds with *in vitro* studies suggesting MTs promote centromere activation: if MTs promote turnover of the CPC, this should dampen ABK activity by reducing the local concentration. To test the role of INCENP-MT binding at the centromere in cells we analyzed chromosome alignment and K-MT attachment in cells over-expressing full-length wild type GFP-INCENP or full-length GFP-INCENP MT CR. While misaligned chromosomes were relatively rare in cells over-expressing GFP-INCENP wt (23.7 ± 4.8% of cells, data represents mean ± SE, n=174 cells), of percentage of cells with unaligned chromosomes increased to 57.5 ± 4.4% in cells expressing GFP-INCENP MT CR (n=194 cells)

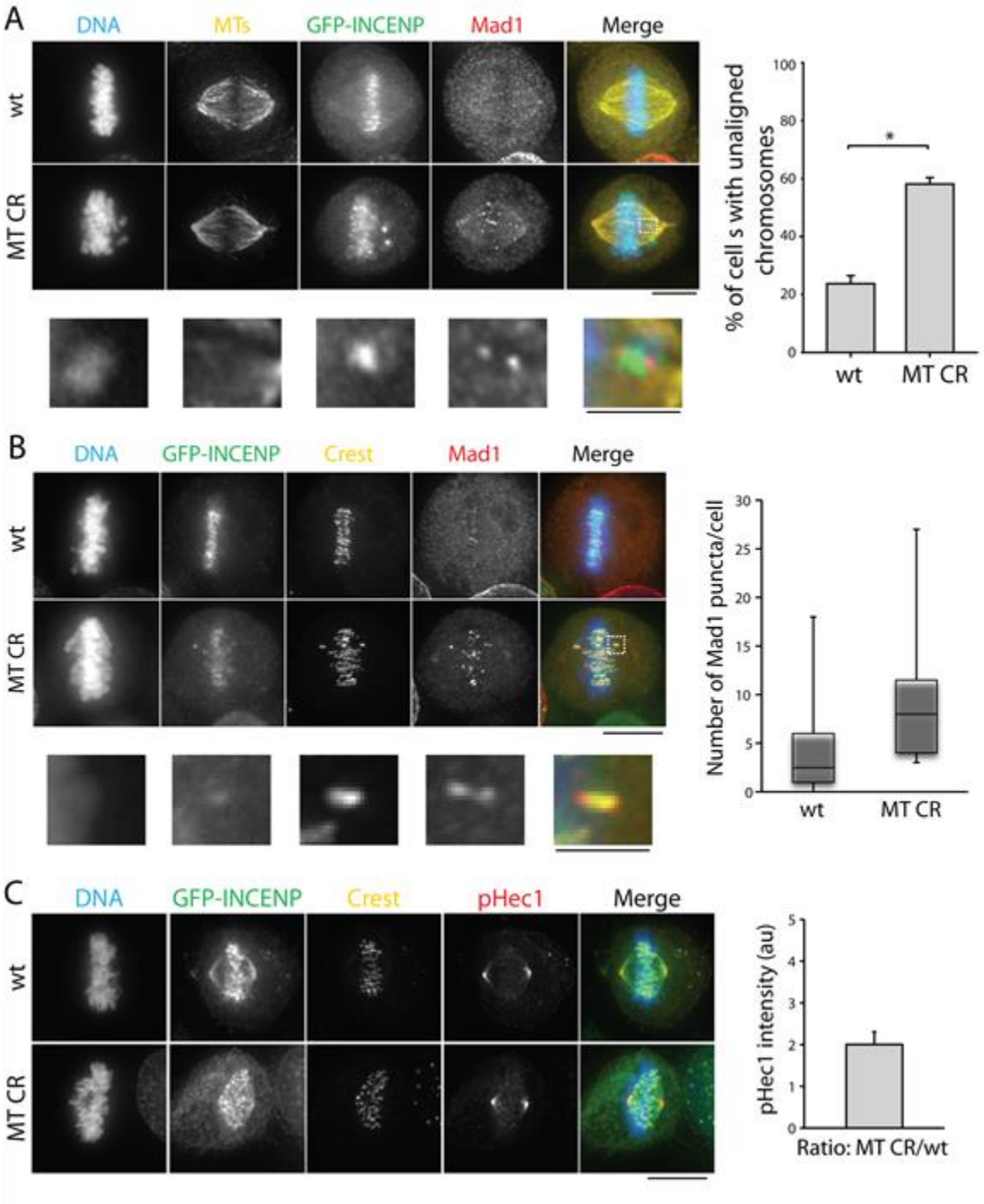

Figure A1.3 INCENP-MT binding in pro-metaphase. A) Left: Maximum Z projections of HeLa cells expressing GFP-INCENP wt or GFP-INCENP MT CR. Cells were fixed and stained with antibodies to tubulin (yellow), GFP (green) and Mad1 (red). DNA was counterstained with Hoescht. Scale bar, 10 μm. Bottom: enlarged micrographs corresponding to the dashed box shown above. Scale bar, 2.5 μm. Right: Quantification of the number of cells with unaligned chromosomes in cells expressing GFP-INCENP wt or GFP-INCENP MT CR. Data represents mean ± SE, n>300 cells, * = p<0.005. B) Left: Maximum Z projections of cells expressing GFP-INCENP wt or GFP-INCENP MT CR. Cells were stained with antibodies to GFP (green), Crest (yellow), and Mad1 (red). DNA was counterstained with Hoescht. Scale bar, 10 μm. Bottom: enlarged micrographs corresponding to the dashed box shown above. Scale bar, 2.5 μm. Continued on next page.

suggesting that INCENP-MT binding is required for chromosome alignment (Figure A1.3 A). We also observed that unaligned chromosomes were generally positive for Mad1 suggesting these cells had errors in K-MT attachment. We quantified the number of Mad1 puncta in cells co-stained with CREST to accurately position the kinetochore, and found that GFP-INCENP MT CR over-expression caused ~2-fold increase in the number of Mad1 puncta per cell. Cells expressing wild type GFP-INCENP had 4.2 ± 4.7 Mad1-positive kinetochores per cell (data represents mean ± SD, n=31 cells), while cells expressing GFP-INCENP MT CR had 8.7 ± 7.0 Mad1-positive kinetochores per cell (n=27 cells, Figure 1.3 B). This finding is consistent with phenotypes of hyper-active ABK (Wang et al., 2011), suggesting that INCENP-MT binding decreases centromeric ABK activity. We next investigated whether ABK substrates were hyper-phosphorylated in cells expressing the MT-binding mutant. ABK phosphorylates the kinetochore component Hec1 to regulate MT attachment to the kinetochore (DeLuca et al., 2006; Zaytsev et al., 2015). Using a phospho-specific antibody for Hec1, we found that cells expressing wild type GFP-INCENP, showed relatively low phospho-Hec1 immunoflourescence at metphase, which is consistent with our observation that these cells had few Mad1-positive kinetochores. Ratiometric analysis revealed that phospho-Hec1 fluorescence was increased approximately 2-fold (data represents mean ± SE, n=48 cells) in cells expressing GFP-INCENP MT CR (Figure A1.3 C). This result indicates that ABK activity is increased when INCENP-MT binding is disrupted and suggests that MTs reduce the centromeric ABK activity. This is consistent with the idea that MTs

Figure A1.3 Continued. Right: Quantification of the number of Mad1-positive puncta/cell. Data represents mean ± SD, n =58 cells. C) Left: Maximum Z projections of HeLa cells expressing GFP-INCENP wt or GFP-INCENP MT CR. Cells were otherwise fixed and with antibodies to GFP (green), Crest (yellow), pHec1 (red). DNA was counterstained with Hoescht. Scale bar, 10 μm. Right: Ratiometric analysis of pHec1 fluorescence intensity at the centromere is cells expressing wt GFP-INCENP or GFP-INCENP MT CR. n=48 cells.

increase turnover of centromeric CPC and dampen ABK activity by decreasing the local concentration at the centromere. In the future, it will be useful to quantify the centromeric turnover of tagged INCENP containing MT-binding mutations. To this end, we have generated photo-convertible probes of INCENP for mammalian expression (mEOS-INCENP wt, mEOS-INCENP MT CR). One interesting idea is that iMTs which are laterally associated with the centromere promote low-level CPC off-loading during pro-metaphase to fine-tune ABK activity. This may allow the spindle to modulate CPC activity, thereby creating a feedback loop where spindle MTs regulate ABK activation, and ABK regulates MT attachment to the kinetochore.

INCENP regulates Mklp2 midzone targeting

The MT-binding activity of INCENP has been proposed to promote midzone localization of Mklp2 during C phase (van der Horst et al., 2015). Disrupting MT binding does not affect direct interactions between the CPC and Mklp2 (van der Horst et al., 2015), suggesting that the MT-binding activity of INCENP does more than just promote Mklp2-CPC complex formation. Investigations of centralspindlin using *in vitro* MT gliding assays suggest that MgcRacGAP functions to activate Mklp1 walking on MTs (Tao et al., 2016). We investigated whether INCENP could also be involved in activating Mklp2 in cells by exogenously expressing fragments of GFP-

GFP-INCENP (aa)	Endogenous Mklp2	Mklp2-mCherry
1-680	Midzone	Midzone
1-500	Cytoplasmic	Midzone (sometimes
50-680	Cytoplasmic	Cytoplasmic
50-500	Cytoplasmic	Cytoplasmic

Table A1.1 Localization of Mklp2 in cells expressing GFP-INCENP fragments

INCENP and examining the C phase localization of endogenous or transiently expressed Mklp2. The results of this analysis are summarized in Table A1.1. Briefly, we observed that both the triple helix-forming domain of INCENP (aa 1-50) and the MT-binding region of the SAH (aa 500-680) were required to promote midzone localization of Mklp2. This led us to hypothesize that Mklp2 binds the CPC through the triple helix, and INCENP-MT binding may serve to increase processivity of Mklp2 on MTs.

We next investigated the single molecule properties of Mklp2-GFP expressed in Cos7 cells. Lysates were collected from interphase or C phase (monopolar cytokinetic) cells (Hu et al., 2008) over-expressing Mklp2-GFP and lysate was introduced into flows cell containing bound GMPCPP stabilized MTs. We observed that Mklp2-GFP was motile and moved at a constant velocity towards the MT end. Mklp2-GFP from interphase lysates walked with a velocity of 6.3 ± 0.4 μm/min (data represents mean ± SE, n=121 tracks) and Mklp2-GFP from C phase lysates moved with a similar speed (8.2 ± 0.6 μm/min, n=96 tracks). We were encouraged that these velocities were in the range measured for CPC streaming on the early midzone during anaphase onset. Single molecules of Mklp2-GFP had a dwell time of 11.1 ± 0.9 sec (interphase lysate, n=121 tracks) and 8.6 ± 0.6 (C phase lysate, n=96 tracks) demonstrating that Mklp2-GFP is only briefly associated with the MT lattice. In agreement with this, single molecules had a relatively short run length at 1.2 ± 0.1 μm for Mklp2-GFP from interphase lysates (n=121 tracks) and 1.1 ± 0.1 μm for Mklp2-GFP from C phase extracts. These results show that regardless of cell cycle state, Mklp2-GFP from cell lysates walks processively along stabilized MTs. However, the motor generally does not remain associated with the lattice for long and as such is usually unable to travel far enough to reach the MT end. These findings created a foundation for us to understand and probe the dynamic properties of Mklp2 *in vitro*.

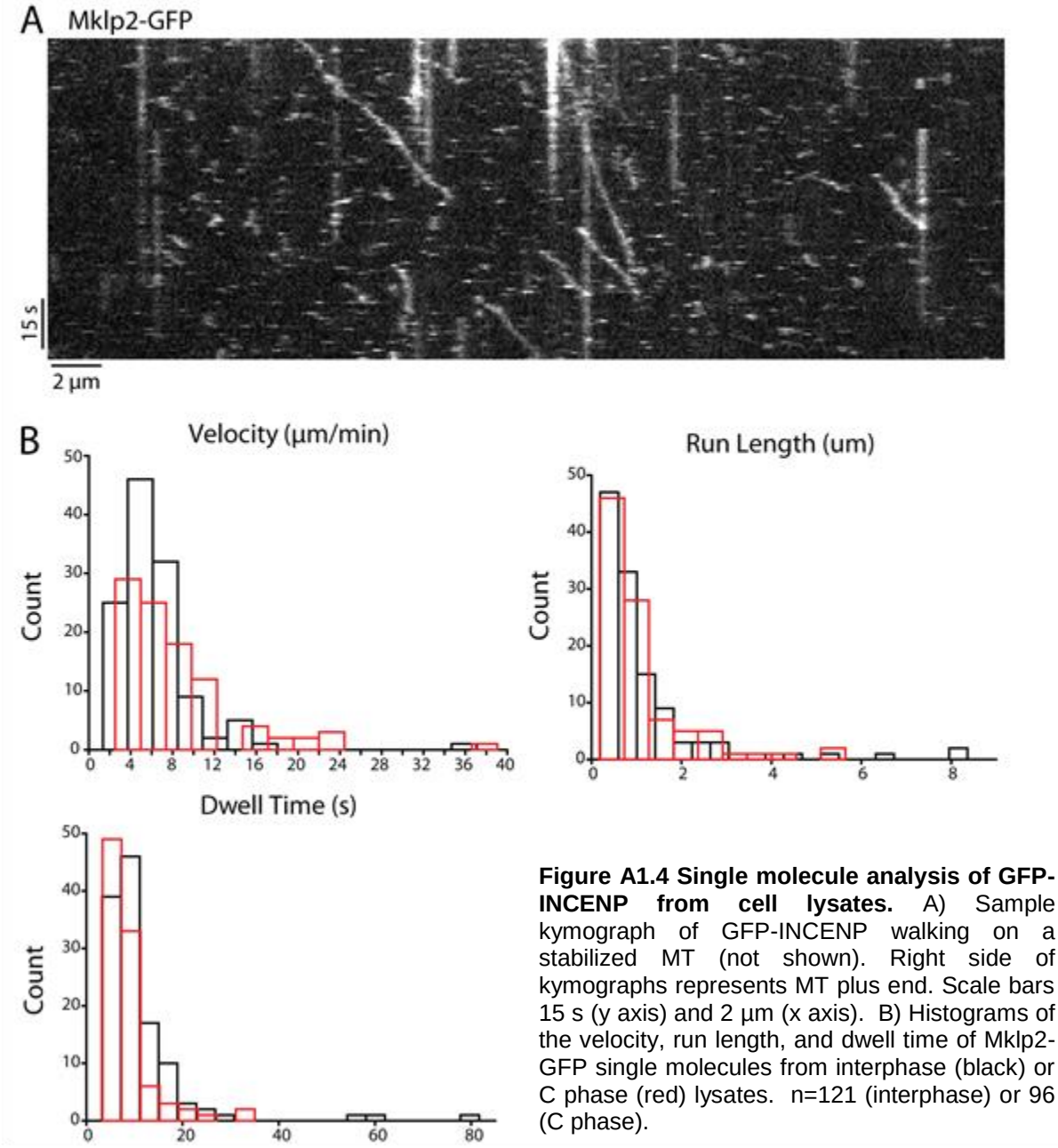

Figure A1.4 Single molecule analysis of GFP-INCENP from cell lysates. A) Sample kymograph of GFP-INCENP walking on a stabilized MT (not shown). Right side of kymographs represents MT plus end. Scale bars 15 s (y axis) and 2 µm (x axis). B) Histograms of the velocity, run length, and dwell time of Mklp2-GFP single molecules from interphase (black) or C phase (red) lysates. n=121 (interphase) or 96 (C phase).

Using the cell lysate system we could not confirm whether processive Mklp2-GFP molecules were associated with the CPC. To investigate whether CPC binding affects the behavior of the motor, we decided to use recombinant protein. Mklp2-His_6-GFP was expressed and purified from insect cells in order to examine motor properties with and without the CPC (Figure A1.5 A).

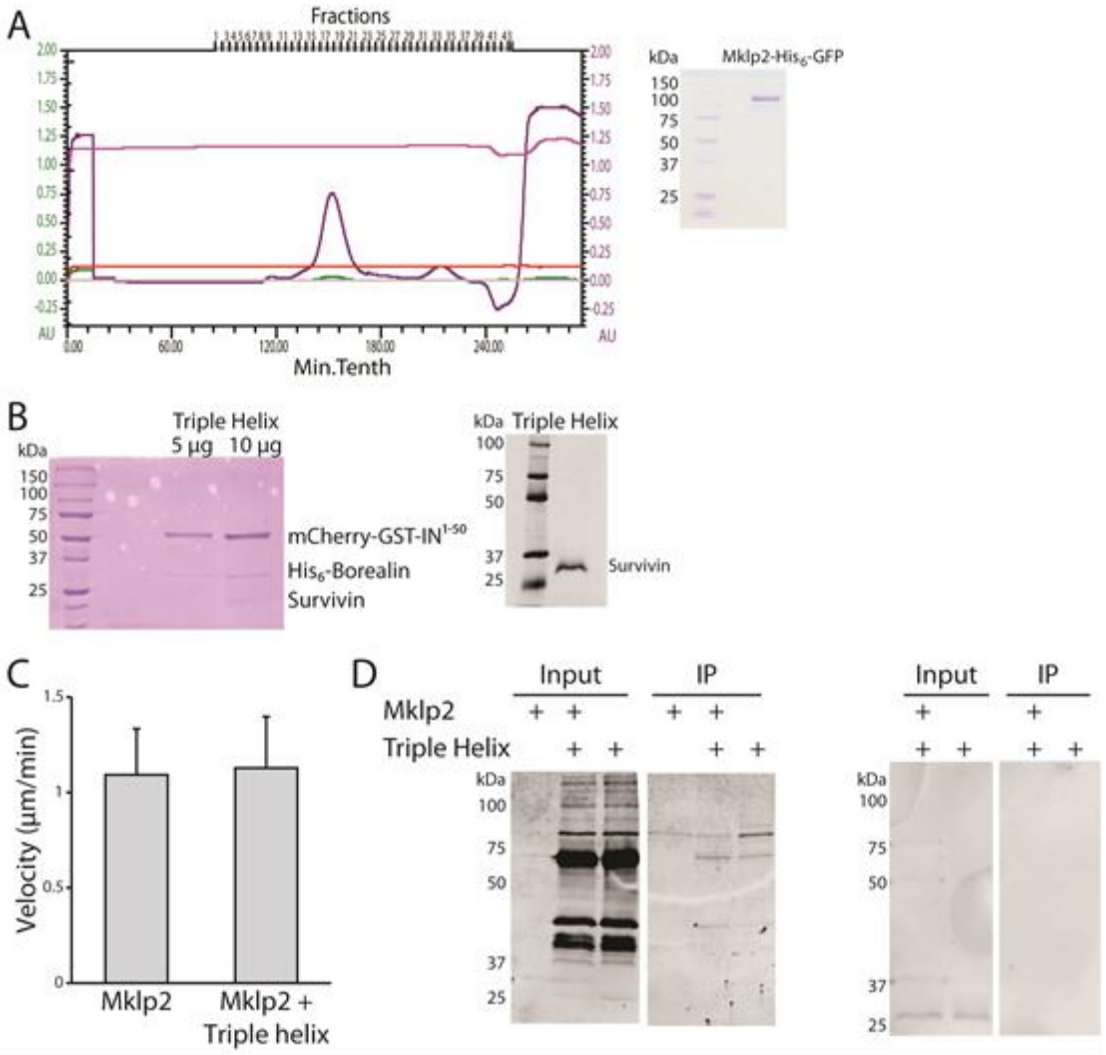

Figure A1.5 Purification and characterization of Mklp2-His$_6$-GFP and CPC triple helix. A) Left: Elution profile of Mklp2-His$_6$-GFP over an S200 gel filtration column. Peak fractions (17-19) were combined and frozen. Right: Coomassie-stained gel of Mklp2-His$_6$-GFP. Molecular weight standards are indicated in kDa. B) Left: Coomassie-stained gel of 5 µg or 10 µg of CPC triple helix. Right: Western Blot of CPC triple helix probed for survivin. Molecular weight standards are indicated in kDa. C) Quantification of MT gliding velocities for Mklp2-His$_6$-GFP with and without CPC triple helix. Data represents mean ± SE, n=48 events. D) Co-immunoprecipitation of Mklp2-His$_6$-GFP with CPC triple helix. Left blots probed with anti-mCherry to detect GST-mCherry-INCENP. Right blots probed with anti-Survivin. Molecular weight standards are indicated in kDa.

It is important to mention that Mklp2 does not tolerate the addition of sucrose, and therefore, we supplemented glycerol as a cryo-preservant. We first characterized the motility of Mklp2-His$_6$-GFP using *in vitro* MT gliding assays. Mklp2-His$_6$-GFP glides MTs at a rate of 1.1 ± 0.2 µm/min (data represents mean ± SE, n=27 events) which is slower than the velocity of Mklp2-GFP single

molecules in cell lysates (Figure A1.5 C). To test whether the CPC influences the activity of Mklp2, similar to centralspindlin (Tao et al., 2016), we also recombinantly expressed and purified the components of the CPC triple helix (GST- mCherry-INCENP$^{1-50}$, His$_6$-Borealin, and Survivin). The addition of triple helix to MT gliding assays did not significantly change the velocity of Mklp2 (1.1 ± 0.3 μm/min, n=21 events, Figure A1.5 C). We also attempted to analyze the single molecule behavior of Mklp2-His$_6$-GFP *in vitro*, however, we found the motor to be highly salt- and pH-sensitive, and were unable to replicate processive movement of the motor. Again, the addition of the CPC triple helix did not affect the behavior of the motor in single molecule experiments.

Our observation that the addition of triple helix did not affect the behavoir of Mklp2 led us to question whether recombinant triple helix was forming a complex with Mkp2 *in vitro*. To investigate whether our CPC construct could bind Mklp2-His$_6$-GFP we performed co-immunoprecipitation experiments. Using anti-GFP beads we sucessfully pulled down Mklp2-His$_6$-GFP, however, we were unable to co-immunoprecipitate GST-mCherry-INCENP or Survivin (Figure A1.5 D). This result suggests that the CPC triple helix complex and Mklp2 do not stably assoicate *in vitro*. One possible explanation is that our INCENP fragment is too short to promote complex formation. As INCENP contains a phospho-regulatory site (Thr 59) at its N-terminus that modulates Mklp2 association in cells, it is reasonalbe to think a longer fragment of INCENP would be more likely to bind Mklp2. Alternatively, the placement of the protein tags may interfere with Mklp2 binding, and we could test this by switching tag position.

CPC off-loading at the metaphase-to-anaphase transition

In cells depleted of Mklp2, the CPC remains associated with the chromosomes throughout mitotic exit (Gruneberg et al., 2004). This observation led us to hypothesize that off-loading from

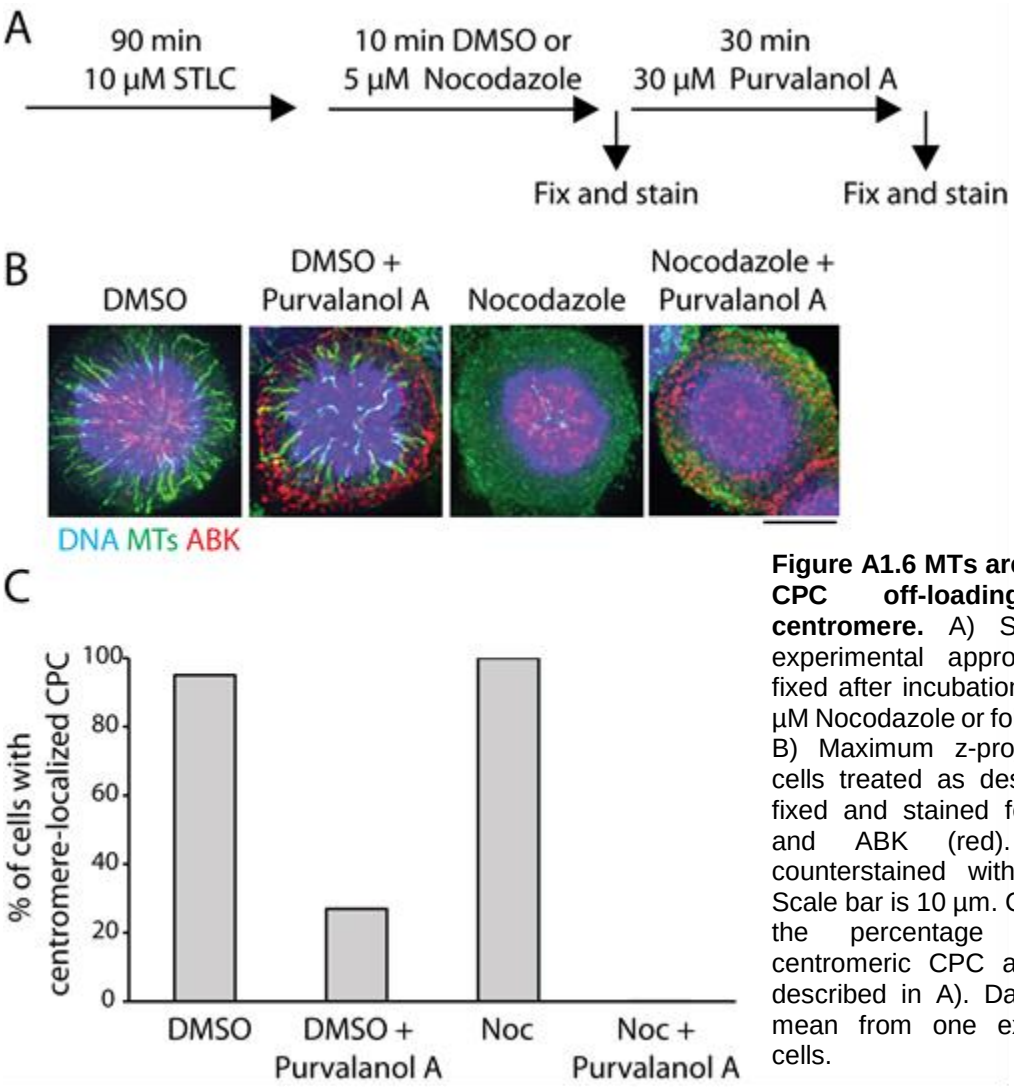

Figure A1.6 MTs are not required for CPC off-loading from the centromere. A) Schematic of the experimental approach. Cells were fixed after incubation with DMSO or 5 µM Nocodazole or following mitotic exit. B) Maximum z-projections of HeLa cells treated as described in A) and fixed and stained for tubulin (green) and ABK (red). DNA was counterstained with Hoescht (blue). Scale bar is 10 µm. C) Quantification of the percentage of cells with centromeric CPC after treatment as described in A). Data represents the mean from one experiment, n>400 cells.

the centeromere may require MTs. In support of this idea, we observed that Mklp2-depleted cells do not exhibit the characteristic "streaming" of GFP-INCENP in early C phase that we observe in unperturbed cells using live imaging. To examine the role of MTs during CPC off-loading we utilized monopolar cytokinesis as a model system (Hu et al., 2008). Cells were arrested as monopoles using the Eg5 inhibitor 10 µM STLC, and then exposed to DMSO or 5 µM nocadazole for 10 min to depolymerize MTs. Cells were then forced to exit mitosis using the Cdk1 inhibitor 30 µM purvalanol A (Hu et al., 2008) and fixed and stained to analyze the localization of the CPC

(antiboides to INCENP and ABK). As expected, 95% of cells (n=105) arrested with STLC showed prominenent CPC localization at the centromere. In control cells treated with DMSO before mitotic exit, the CPC was targeted to midzone MT plus ends and the polarized furrow and only 27% of cells (n=101, Figure A1.6 A and B) showed centromere-localized CPC. Nocodazole treatment before mitotic exit did not affect CPC centromere localization, 100% of cells counted showed CPC immunoflourescence at the centromere (n=100 cells). When cells were forced to exit mitosis after nocodazole, the majority of CPC was cytoplasmic (Figure A1.6 B). Only a fraction of cells had any centromeric CPC (2%, n=101 cells) suggesting that MTs are not required to promote CPC off-loading as cells transition to C phase. Given the finding that Mklp2 depletion abolishes off-loading, it is possible that Mklp2-dependent off-loading does not depend on MTs. If Mklp2 does function to pull the CPC from the centromere at the metaphase to anapahse transition, we would predict Mklp2-depleted cells treated with nocodazole, would show centromeric CPC localization during C phase. Furthermore, it would be usefult to identify mutations in INCENP or Mklp2 that abolish interactions *in vitro*, and test whether these mutants can promote centromeric off-loading of the CPC.

REFERENCES

Adams, R.R., Wheatley, S.P., Gouldsworthy, A.M., Kandels-Lewis, S.E., Carmena, M., Smythe, C., Gerloff, D.L., and Earnshaw, W.C. (2000). INCENP binds the Aurora-related kinase AIRK2 and is required to target it to chromosomes, the central spindle and cleavage furrow. Curr Biol *10*, 1075-1078.

Afonso, O., Matos, I., Pereira, A.J., Aguiar, P., Lampson, M.A., and Maiato, H. (2014). Feedback control of chromosome separation by a midzone Aurora B gradient. Science *345*, 332-336.

Aist, J.R., Bayles, C.J., Tao, W., and Berns, M.W. (1991). Direct experimental evidence for the existence, structural basis and function of astral forces during anaphase B in vivo. J Cell Sci *100 (Pt 2)*, 279-288.

Alberts, B., Johnson, A., Lewis, J., Raff, M., Roberts, K., and Walter, P. (2008). Molecular Biology of the Cell, Vol 5 (New York, NY: Garland Science).

Alushin, G.M., Lander, G.C., Kellogg, E.H., Zhang, R., Baker, D., and Nogales, E. (2014). High-resolution microtubule structures reveal the structural transitions in alphabeta-tubulin upon GTP hydrolysis. Cell *157*, 1117-1129.

Andersen, S.S. (2000). Spindle assembly and the art of regulating microtubule dynamics by MAPs and Stathmin/Op18. Trends Cell Biol *10*, 261-267.

Andrews, P.D., Ovechkina, Y., Morrice, N., Wagenbach, M., Duncan, K., Wordeman, L., and Swedlow, J.R. (2004). Aurora B regulates MCAK at the mitotic centromere. Dev Cell *6*, 253-268.

Asbury, C. (2017). Anaphase A: Disassembling Microtubules Move Chromosomes toward Spindle Poles. Biology *6*, 15.

Aubin, J.E., Osborn, M., and Weber, K. (1981). Inhibition of cytokinesis and altered contractile ring morphology induced by cytochalasins in synchronized PtK2 cells. Experimental cell research *136*, 63-79.

Avunie-Masala, R., Movshovich, N., Nissenkorn, Y., Gerson-Gurwitz, A., Fridman, V., Koivomagi, M., Loog, M., Hoyt, M.A., Zaritsky, A., and Gheber, L. (2011). Phospho-regulation of kinesin-5 during anaphase spindle elongation. J Cell Sci *124*, 873-878.

Ballestrem, C., Wehrle-Haller, B., Hinz, B., and Imhof, B.A. (2000). Actin-dependent Lamellipodia Formation and Microtubule-dependent Tail Retraction Control-directed Cell Migration.

Bancaud, A., Huet, S., Rabut, G., and Ellenburg, J. (2010). Fluorescence Perturbation Techniques to Study Mobility and Molecular Dynamics of Proteins in Live Cells: FRAP, Photoactivation, Photoconversion, and FLIP. Cold Spring Harb Protoc *12*.

Basant, A., Lekomtsev, S., Tse, Y.C., Zhang, D., Longhini, K.M., Petronczki, M., and Glotzer, M. (2015). Aurora B kinase promotes cytokinesis by inducing centralspindlin oligomers that associate with the plasma membrane. Dev Cell *33*, 204-215.

Beardmore, V.A., Ahonen, L.J., Gorbsky, G.J., and Kallio, M.J. (2004). Survivin dynamics increases at centromeres during G2/M phase transition and is regulated by microtubule-attachment and Aurora B kinase activity. J Cell Sci *117*, 4033-4042.

Belmont, L.D., Hyman, A.A., Sawin, K.E., and Mitchison, T.J. (1990). Real-time visualization of cell cycle-dependent changes in microtubule dynamics in cytoplasmic extracts. Cell *62*, 579-589.

Bement, W.M., Benink, H.A., and von Dassow, G. (2005). A microtubule-dependent zone of active RhoA during cleavage plane specification. The Journal of cell biology *170*, 91-101.

Benashski, S., Harrison, A., Patel-King, R.S., and King, S.M. (1997). Dimerization of the highly conserved light chain shared by dynein and myosin V. J Biol Chem *272*, 20929-20935.

Bieling, P., Telley, I.A., and Surrey, T. (2010). A minimal midzone protein module controls formation and length of antiparallel microtubule overlaps. Cell *142*, 420-432.

Bishop, J.D., and Schumacher, J.M. (2002). Phosphorylation of the carboxyl terminus of inner centromere protein (INCENP) by the Aurora B Kinase stimulates Aurora B kinase activity. J Biol Chem *277*, 27577-27580.

Bray, D., and White, J.G. (2017). Cortical flow in animal cells. Science *239*, 883-889.

Bringmann, H., and Hyman, A.A. (2005). A cytokinesis furrow is positioned by two consecutive signals. Nature *436*, 731-734.

Brinkley, B.R., and Cartwright, J., Jr. (1975). Cold-labile and cold-stable microtubules in the mitotic spindle of mammalian cells. Ann N Y Acad Sci *253*, 428-439.

Brouhard, G.J. (2015). Dynamic instability 30 years later: complexities in microtubule growth and catastrophe. Mol Biol Cell *26*, 1207-1210.

Brust-Mascher, I., Civelekoglu-Scholey, G., Kwon, M., Mogilner, A., and Scholey, J.M. (2004). Model for anaphase B: role of three mitotic motors in a switch from poleward flux to spindle elongation. Proc Natl Acad Sci U S A *101*, 15938-15943.

Campbell, N.A., Simon, E.J., and Reece, J.B. (2004). Essential Biology, Vol 2 (San Francisco, CA: Pearson Education).

Canman, J.C., Cameron, L.A., Maddox, P.S., Straight, A., Tirnauer, J.S., Mitchison, T.J., Fang, G., Kapoor, T.M., and Salmon, E.D. (2003). Determining the position of the cell division plane. Nature *424*, 1074-1078.

Canman, J.C., Hoffman, D.B., and Salmon, E.D. (2000). The role of pre- and post-anaphase microtubules in the cytokinesis phase of the cell cycle. Current biology : CB *10*, 611-614.

Capalbo, L., Mela, I., Abad, M.A., Jeyaprakash, A.A., Edwardson, J.M., and D'Avino, P.P. (2016). Coordinated regulation of the ESCRT-III component CHMP4C by the chromosomal passenger complex and centralspindlin during cytokinesis. Open Biol *6*.

Caplow, M., Ruhlen, R.L., and Shanks, J. (1994). The free energy for hydrolysis of a microtubule-bound nucleotide triphosphate is near zero: all of the free energy for hydrolysis is stored in the microtubule lattice. J Cell Biol *127*, 779-788.

Carmena, M., Ruchaud, S., and Earnshaw, W.C. (2009). Making the Auroras glow: regulation of Aurora A and B kinase function by interacting proteins. Curr Opin Cell Biol *21*, 796-805.

Carmena, M., Wheelock, M., Funabiki, H., and Earnshaw, W.C. (2012). The chromosomal passenger complex (CPC): from easy rider to the godfather of mitosis. Nat Rev Mol Cell Biol *13*, 789-803.

Cesario, J.M., Jang, J.K., Redding, B., Shah, N., Rahman, T., and McKim, K.S. (2006). Kinesin 6 family member Subito participates in mitotic spindle assembly and interacts with mitotic regulators. Journal of cell science *119*, 4770-4780.

Chen, Q., Lakshmikanth, G.S., Spudich, J.A., and De Lozanne, A. (2007). The localization of inner centromeric protein (INCENP) at the cleavage furrow is dependent on Kif12 and involves interactions of the N terminus of INCENP with the actin cytoskeleton. Molecular biology of the cell *18*, 3366-3374.

Cimini, D., Fioravanti, D., Tanzarella, C., and Degrassi, F. (1998). Simultaneous inhibition of contractile ring and central spindle formation in mammalian cells treated with cytochalasin B. Chromosoma *107*, 479-485.

Cole, D.G., Saxton, W.M., Sheehan, K.B., and Scholey, J.M. (1994). A "slow" homotetrameric kinesin-related motor protein purified from Drosophila embryos. J Biol Chem *269*, 22913-22916.

Collins, E., Mann, B.J., and Wadsworth, P. (2014). Eg5 restricts anaphase B spindle elongation in mammalian cells. Cytoskeleton (Hoboken) *71*, 136-144.

Cooke, C.A., Heck, M.M., and Earnshaw, W.C. (1987). The inner centromere protein (INCENP) antigens: movement from inner centromere to midbody during mitosis. J Cell Biol *105*, 2053-2067.

Cooper, G.M. (2000). The Cell: A molecular approach, Vol 2 (Sunderland, MA: Sinauer Associates).

Davies, T., Kodera, N., Kaminski Schierle, G.S., Rees, E., Erdelyi, M., Kaminski, C.F., Ando, T., and Mishima, M. (2015). CYK4 promotes antiparallel microtubule bundling by optimizing MKLP1 neck conformation. PLoS Biol *13*, e1002121.

De Los Santos, C., Chang, C.W., Mycek, M.A., and Cardullo, R.A. (2015). FRAP, FLIM, and FRET: Detection and analysis of cellular dynamics on a molecular scale using fluorescence microscopy. Mol Reprod Dev *82*, 587-604.

Dechant, R., and Glotzer, M. (2003). Centrosome Separation and Central Spindle Assembly Act in Redundant Pathways that Regulate Microtubule Density and Trigger Cleavage Furrow Formation. Developmental Cell *4*, 333-344.

DeLuca, J.G., Gall, W.E., Ciferri, C., Cimini, D., Musacchio, A., and Salmon, E.D. (2006). Kinetochore microtubule dynamics and attachment stability are regulated by Hec1. Cell *127*, 969-982.

Desai, A., Maddox, P.S., Mitchison, T.J., and Salmon, E.D. (1998). Anaphase A chromosome movement and poleward spindle microtubule flux occur At similar rates in Xenopus extract spindles. J Cell Biol *141*, 703-713.

Desai, A., Verma, S., Mitchison, T.J., and Walczak, C.E. (1999). Kin I kinesins are microtubule-destabilizing enzymes. Cell *96*, 69-78.

Ditchfield, C., Johnson, V.L., Tighe, A., Ellston, R., Haworth, C., Johnson, T., Mortlock, A., Keen, N., and Taylor, S.S. (2003). Aurora B couples chromosome alignment with anaphase by targeting BubR1, Mad2, and Cenp-E to kinetochores. The Journal of cell biology *161*, 267-280.

Douglas, M.E., Davies, T., Joseph, N., and Mishima, M. (2010). Aurora B and 14-3-3 coordinately regulate clustering of centralspindlin during cytokinesis. Curr Biol *20*, 927-933.

Earnshaw, W.C., and Cooke, C.A. (1991). Analysis of the distribution of the INCENPs throughout mitosis reveals the existence of a pathway of structural changes in the chromosomes during metaphase and early events in cleavage furrow formation. J Cell Sci *98 (Pt 4)*, 443-461.

Eggert, U.S., Mitchison, T.J., and Field, C.M. (2006). Animal Cytokinesis: From Parts List to Mechanisms. Annual Review of Biochemistry.

Emanuele, M.J., Lan, W., Jwa, M., Miller, S.A., Chan, C.S., and Stukenberg, P.T. (2008). Aurora B kinase and protein phosphatase 1 have opposing roles in modulating kinetochore assembly. J Cell Biol *181*, 241-254.

Fededa, J.P., and Gerlich, D.W. (2012). Molecular control of animal cell cytokinesis. Nat Cell Biol *14*, 440-447.

Finger, F.P., and White, J.G. (2002). Fusion and Fission: Membrane Trafficking in Animal Cytokinesis. Cell *108*, 727-730.

Fink, G., Schuchardt, I., Colombelli, J., Stelzer, E., and Steinberg, G. (2006). Dynein-mediated pulling forces drive rapid mitotic spindle elongation in Ustilago maydis. Embo J *25*, 4897-4908.

Flemming, W. (1965). Contributions to the knowledge of the cell and its vital processes. J Cell Biol *25*, 3-69.

Foe, V.E., and von Dassow, G. (2008). Stable and dynamic microtubules coordinately shape the myosin activation zone during cytokinetic furrow formation. The Journal of cell biology *183*, 457-470.

Fuller, B.G., Lampson, M.A., Foley, E.A., Rosasco-Nitcher, S., Le, K.V., Tobelmann, P., Brautigan, D.L., Stukenberg, P.T., and Kapoor, T.M. (2008). Midzone activation of aurora B in anaphase produces an intracellular phosphorylation gradient. Nature *453*, 1132-1136.

Fung, S.Y., Kitagawa, M., Liao, P.J., Wong, J., and Lee, S.H. (2017). Opposing Activities of Aurora B Kinase and B56-PP2A Phosphatase on MKlp2 Determine Abscission Timing. Curr Biol *27*, 78-86.

Ganem, N.J., Upton, K., and Compton, D.A. (2005). Efficient mitosis in human cells lacking poleward microtubule flux. Curr Biol *15*, 1827-1832.

Gayek, A.S., and Ohi, R. (2014). Kinetochore-microtubule stability governs the metaphase requirement for Eg5. Mol Biol Cell *25*, 2051-2060.

Giansanti, M.G., Bonaccorsi, S., Williams, B., Williams, E.V., Santolamazza, C., Goldberg, M.L., and Gatti, M. (1998). Cooperative interactions between the central spindle and the contractile ring during Drosophila cytokinesis. Genes Dev *12*, 396-410.

Gibson, D.G., Young, L., Chuang, R.Y., Venter, J.C., Hutchison, C.A., 3rd, and Smith, H.O. (2009). Enzymatic assembly of DNA molecules up to several hundred kilobases. Nat Methods *6*, 343-345.

Glotzer, M. (2009). The 3Ms of central spindle assembly: microtubules, motors and MAPs. Nature Reviews Molecular Cell Biology *10*, 9-20.

Goode, B., Drubin, D., and Barnes, G. (2000). Functional cooperation between the microtubule and actin cytoskeletons. Curr Opin Cell Biol *12*, 63-71.

Goryachev, A.B., Leda, M., Miller, A.L., von Dassow, G., and Bement, W.M. (2016). How to make a static cytokinetic furrow out of traveling excitable waves. Small GTPases *7*, 65-70.

Green, R.A., Paluch, E., and Oegema, K. (2012). Cytokinesis in animal cells. Annu Rev Cell Dev Biol *28*, 29-58.

Grill, S.W., and Hyman, A.A. (2005). Spindle positioning by cortical pulling forces. Dev Cell *8*, 461-465.

Gruneberg, U., Neef, R., Honda, R., Nigg, E.A., and Barr, F.A. (2004). Relocation of Aurora B from centromeres to the central spindle at the metaphase to anaphase transition requires MKlp2. The Journal of cell biology *166*, 167-172.

Gruneberg, U., Neef, R., Li, X., Chan, E.H., Chalamalasetty, R.B., Nigg, E.A., and Barr, F.A. (2006). KIF14 and citron kinase act together to promote efficient cytokinesis. J Cell Biol *172*, 363-372.

Guse, A., Mishima, M., and Glotzer, M. (2005). Phosphorylation of ZEN-4/MKLP1 by aurora B regulates completion of cytokinesis. Curr Biol *15*, 778-786.

Heald, R., and Khodjakov, A. (2015). Thirty years of search and capture: The complex simplicity of mitotic spindle assembly. J Cell Biol *211*, 1103-1111.

Helenius, J., Brouhard, G., Kalaidzidis, Y., Diez, S., and Howard, J. (2006). The depolymerizing kinesin MCAK uses lattice diffusion to rapidly target microtubule ends. Nature *441*, 115-119.

Hirokawa, N., and Takemura, R. (2004). Kinesin superfamily proteins and their various functions and dynamics. Exp Cell Res *301*, 50-59.

Hoeijmakers, J.H. (2009). DNA damage, aging, and cancer. N Engl J Med *361*, 1475-1485.

Hogan, C.J., Wein, H., Wordeman, L., Scholey, J.M., Sawin, K.E., and Cande, W.Z. (1993). Inhibition of anaphase spindle elongation in vitro by a peptide antibody that recognizes kinesin motor domain. Proc Natl Acad Sci U S A *90*, 6611-6615.

Holland, A.J., and Cleveland, D.W. (2012). Losing balance: the origin and impact of aneuploidy in cancer. EMBO Rep *13*, 501-514.

Hornick, J.E., Karanjeet, K., Collins, E.S., and Hinchcliffe, E.H. (2010). Kinesins to the core: The role of microtubule-based motor proteins in building the mitotic spindle midzone. Semin Cell Dev Biol *21*, 290-299.

Houdusse, A., and Sweeney, H.L. (2016). How Myosin Generates Force on Actin Filaments. Trends Biochem Sci *41*, 989-997.

Howard, J., and Hyman, A.A. (2003). Dynamics and mechanics of the microtubule plus end. Nature *422*, 753-758.

Hu, C.K., Coughlin, M., Field, C.M., and Mitchison, T.J. (2008). Cell polarization during monopolar cytokinesis. J Cell Biol *181*, 195-202.

Hu, C.K., Coughlin, M., Field, C.M., and Mitchison, T.J. (2011). KIF4 regulates midzone length during cytokinesis. Current biology : CB *21*, 815-824.

Hu, C.K., Ozlu, N., Coughlin, M., Steen, J.J., and Mitchison, T.J. (2012). Plk1 negatively regulates PRC1 to prevent premature midzone formation before cytokinesis. Mol Biol Cell *23*, 2702-2711.

Huang, J.-D., Brady, S.T., Richards, B.W., Stenoien, D., Resau, J.H., Copeland, N.G., and Jenkins, N.A. (1999). Direct interaction of microtubule- and actin-based transport motors. Nature *397*, 267-270.

Hummer, S., and Mayer, T.U. (2009). Cdk1 negatively regulates midzone localization of the mitotic kinesin Mklp2 and the chromosomal passenger complex. Current biology : CB *19*, 607-612.

Hwang, E., Kusch, J., Barral, Y., and Huffaker, T.C. (2003). Spindle orientation in Saccharomyces cerevisiae depends on the transport of microtubule ends along polarized actin cables.

Inoue, S., and Salmon, E.D. (1995). Force generation by microtubule assembly/disassembly in mitosis and related movements. Mol Biol Cell *6*, 1619-1640.

Jang, J.K., Rahman, T., and McKim, K.S. (2005). The kinesinlike protein Subito contributes to central spindle assembly and organization of the meiotic spindle in Drosophila oocytes. Molecular biology of the cell *16*, 4684-4694.

Jeyaprakash, A.A., Klein, U.R., Lindner, D., Ebert, J., Nigg, E.A., and Conti, E. (2007). Structure of a Survivin-Borealin-INCENP core complex reveals how chromosomal passengers travel together. Cell *131*, 271-285.

Joglekar, A., Bloom, K.S., and Salmon, E.D. (2010). Mechanisms of force generation by end-on kinetochore-microtubule attachments. Curr Opin Cell Biol *22*, 57-67.

Kaitna, S., Mendoza, M., Jantsch-Plunger, V., and Glotzer, M. (2000). Incenp and an aurora-like kinase form a complex essential for chromosome segregation and efficient completion of cytokinesis. Current biology : CB *10*, 1172-1181.

Kapoor, T.M. (2017). Metaphase Spindle Assembly. Biology *6*.

Kapoor, T.M., Mayer, T.U., Coughlin, M.L., and Mitchison, T.J. (2000). Probing spindle assembly mechanisms with monastrol, a small molecule inhibitor of the mitotic kinesin, Eg5. J Cell Biol *150*, 975-988.

Kasza, K.E., and Zallen, J.A. (2011). Dynamics and regulation of contractile actin-myosin networks in morphogenesis. Curr Opin Cell Biol *23*, 30-38.

Kellogg, E.H., Hejab, N.M., Howes, S., Northcote, P., Miller, J.H., Diaz, J.F., Downing, K.H., and Nogales, E. (2017). Insights into the Distinct Mechanisms of Action of Taxane and Non-Taxane Microtubule Stabilizers from Cryo-EM Structures. J Mol Biol *429*, 633-646.

Kellogg, E.H., Howes, S., Ti, S.C., Ramirez-Aportela, E., Kapoor, T.M., Chacon, P., and Nogales, E. (2016). Near-atomic cryo-EM structure of PRC1 bound to the microtubule. Proc Natl Acad Sci U S A *113*, 9430-9439.

Kelly, A.E., Sampath, S.C., Maniar, T.A., Woo, E.M., Chait, B.T., and Funabiki, H. (2007). Chromosomal enrichment and activation of the aurora B pathway are coupled to spatially regulate spindle assembly. Developmental cell *12*, 31-43.

Kepiro, M., Varkuti, B.H., Vegner, L., Voros, G., Hegyi, G., Varga, M., and Malnasi-Csizmadia, A. (2014). para-Nitroblebbistatin, the non-cytotoxic and photostable myosin II inhibitor. Angewandte Chemie *53*, 8211-8215.

Khandelia, P., Yap, K., and Makeyev, E.V. (2011). Streamlined platform for short hairpin RNA interference and transgenesis in cultured mammalian cells. Proc Natl Acad Sci U S A *108*, 12799-12804.

Kitagawa, M., Fung, S.Y., Hameed, U.F., Goto, H., Inagaki, M., and Lee, S.H. (2014). Cdk1 coordinates timely activation of MKlp2 kinesin with relocation of the chromosome passenger complex for cytokinesis. Cell Rep *7*, 166-179.

Kitagawa, M., Fung, S.Y., Onishi, N., Saya, H., and Lee, S.H. (2013). Targeting Aurora B to the equatorial cortex by MKlp2 is required for cytokinesis. PLoS One *8*, e64826.

Kristofferson, D., Mitchison, T., and Kirschner, M. (1986). Direct observation of steady-state microtubule dynamics. J Cell Biol *102*, 1007-1019.

Kurasawa, Y., Earnshaw, W.C., Mochizuki, Y., Dohmae, N., and Todokoro, K. (2004). Essential roles of KIF4 and its binding partner PRC1 in organized central spindle midzone formation. EMBO J *23*, 3237-3248.

Kwon, M., Bagonis, M., Danuser, G., and Pellman, D. (2015). Direct Microtubule-Binding by Myosin-10 Orients Centrosomes toward Retraction Fibers and Subcortical Actin Clouds.

Langford, G. (1995). Actin- and microtubule-dependent organelle motors: interrelationships between the two motility systems. Curr Opin Cell Biol *7*, 82-88.

Li, J., Wang, J., Jiao, H., Liao, J., and Xu, X. (2010). Cytokinesis and cancer: Polo loves ROCK'n' Rho(A). J Genet Genomics *37*, 159-172.

MacLean-Fletcher, S., and Pollard, T.D. (1980). Mechanism of action of cytochalasin B on actin. Cell *20*, 329-341.

Mali, P., Yang, L., Esvelt, K.M., Aach, J., Guell, M., DiCarlo, J.E., Norville, J.E., and Church, G.M. (2013). RNA-guided human genome engineering via Cas9. Science *339*, 823-826.

Malumbres, M., and Barbacid, M. (2009). Cell cycle, CDKs and cancer: a changing paradigm. Nat Rev Cancer *9*, 153-166.

Mandato, C.A., Benink, H.A., and Bement, W.M. (2000). Microtubule-actomyosin interactions in cortical flow and cytokinesis. Cytoskeleton *45*, 87-92.

Manders, E.M., Stap, J., Brakenhoff, G.J., van Driel, R., and Aten, J.A. (1992). Dynamics of three-dimensional replication patterns during the S-phase, analysed by double labelling of DNA and confocal microscopy. J Cell Sci *103 (Pt 3)*, 857-862.

Manning, A.L., Ganem, N.J., Bakhoum, S.F., Wagenbach, M., Wordeman, L., and Compton, D.A. (2007). The kinesin-13 proteins Kif2a, Kif2b, and Kif2c/MCAK have distinct roles during mitosis in human cells. Mol Biol Cell *18*, 2970-2979.

Mastronarde, D.N., McDonald, K.L., Ding, R., and McIntosh, J.R. (1993). Interpolar spindle microtubules in PTK cells.

Matsumura, F. (2005). Regulation of myosin II during cytokinesis in higher eukaryotes. Trends Cell Biol *15*, 371-377.

Mazia, D. (1961). Mitosis and the physiology of cell division. , Vol In The Cell: Biochemistry, Physiology, Morphology, Vol III (London, UK: Academic Press).

McIntosh, J.R., and Hays, T. (2016). A Brief History of Research on Mitotic Mechanisms. Biology (Basel) *5*.

McKinney, S.A., Murphy, C.S., Hazelwood, K.L., Davidson, M.W., and Looger, L.L. (2009). A bright and photostable photoconvertible fluorescent protein for fusion tags. Nat Methods *6*, 131-133.

McNeill, P.A., and Berns, M.W. (1981). Chromosome behavior after laser microirradiation of a single kinetochore in mitotic PtK2 cells. J Cell Biol *88*, 543-553.

Mikulich, A., Kavaliauskiene, S., and Juzenas, P. (2012). Blebbistatin, a myosin inhibitor, is phototoxic to human cancer cells under exposure to blue light. Biochimica et biophysica acta *1820*, 870-877.

Miller, A.L. (2011). The contractile ring. Curr Biol *21*, R976-978.

Mishima, M. (2016). Centralspindlin in Rappaport's cleavage signaling. Semin Cell Dev Biol *53*, 45-56.

Mishima, M., Kaitna, S., and Glotzer, M. (2002). Central Spindle Assembly and Cytokinesis Require a Kinesin-like Protein/RhoGAP Complex with Microtubule Bundling Activity. Developmental Cell *2*, 41-54.

Mitchison, T.J., Evans, L., Schulze, E., and Kirschner, M. (1986). Sites of microtubule assembly and disassembly in the mitotic spindle. Cell *45*, 515-527.

Mitchison, T.J., and Kirschner, M. (1984). Dynamic instability of microtubule growth. Nature *312*, 237-242.

Mitchison, T.J. (1992). Compare and contrast actin filaments and microtubules. Mol Biol Cell *3*, 1309-1315.

Murthy, K., and Wadsworth, P. (2005). Myosin-II-dependent localization and dynamics of F-actin during cytokinesis. Curr Biol *15*, 724-731.

Nahse, V., Christ, L., Stenmark, H., and Campsteijn, C. (2017). The Abscission Checkpoint: Making It to the Final Cut. Trends Cell Biol *27*, 1-11.

Neef, R., Klein, U.R., Kopajtich, R., and Barr, F.A. (2006). Cooperation between mitotic kinesins controls the late stages of cytokinesis. Curr Biol *16*, 301-307.

Neef, R., Preisinger, C., Sutcliffe, J., Kopajtich, R., Nigg, E.A., Mayer, T.U., and Barr, F.A. (2003). Phosphorylation of mitotic kinesin-like protein 2 by polo-like kinase 1 is required for cytokinesis. J Cell Biol *162*, 863-875.

Nguyen, P.A., Groen, A.C., Loose, M., Ishihara, K., Wuhr, M., Field, C.M., and Mitchison, T.J. (2014). Spatial organization of cytokinesis signaling reconstituted in a cell-free system. Science *346*, 244-247.

Nogales, E., Whittaker, M., Milligan, R.A., and Downing, K.H. (1999). High-resolution model of the microtubule. Cell *96*, 79-88.

Nojima, H. (1997). Cell cycle checkpoints, chromosome stability and the progression of cancer. Hum Cell *10*, 221-230.

Noujaim, M., Bechstedt, S., Wieczorek, M., and Brouhard, G.J. (2014). Microtubules accelerate the kinase activity of Aurora-B by a reduction in dimensionality. PLoS One *9*, e86786.

Nunes Bastos, R., Gandhi, S.R., Baron, R.D., Gruneberg, U., Nigg, E.A., and Barr, F.A. (2013). Aurora B suppresses microtubule dynamics and limits central spindle size by locally activating KIF4A. J Cell Biol *202*, 605-621.

Nurse, P. (2000). A long twentieth century of the cell cycle and beyond. Cell *100*, 71-78.

Ohi, R., Burbank, K., Liu, Q., and Mitchison, T.J. (2007). Nonredundant functions of Kinesin-13s during meiotic spindle assembly. Curr Biol *17*, 953-959.

Otegui, M.S., Verbrugghe, K.J., and Skop, A.R. (2005). Midbodies and phragmoplasts: analogous structures involved in cytokinesis. Trends Cell Biol *15*, 404-413.

Palmer, R.E., Sullivan, D.S., Huffaker, T., and Koshland, D. (1992). Role of astral microtubules and actin in spindle orientation and migration in the budding yeast, Saccharomyces cerevisiae.

Pavicic-Kaltenbrunner, V., Mishima, M., and Glotzer, M. (2007). Cooperative Assembly of CYK-4/MgcRacGAP and ZEN-4/MKLP1 to Form the Centralspindlin Complex. Molecular Biology of the Cell.

Pollard, T.D. (1976). The role of actin in the temperature-dependent gelation and contraction of extracts of Acanthamoeba. J Cell Biol *68*, 579-601.

Pollard, T.D. (2003). Ray rappaport chronology: Twenty-five years of seminal papers on cytokinesis in the journal of experimental zoology. Journal of Experimental Zoology Part A: Ecological Genetics and Physiology *301A*, 9-14.

Porter, A.C. (2008). Preventing DNA over-replication: a Cdk perspective. Cell Division *3*, 3.

Powers, A.F., Franck, A.D., Gestaut, D.R., Cooper, J., Gracyzk, B., Wei, R.R., Wordeman, L., Davis, T.N., and Asbury, C.L. (2009). The Ndc80 kinetochore complex forms load-bearing attachments to dynamic microtubule tips via biased diffusion. Cell *136*, 865-875.

Prokopenko, S.N., Brumby, A., O'Keefe, L., Prior, L., He, Y., Saint, R., and Bellen, H.J. (1999). A putative exchange factor for Rho1 GTPase is required for initiation of cytokinesis in Drosophila. Genes Dev *13*, 2301-2314.

Raich, W.B., Moran, A.N., Rothman, J.H., and Hardin, J. (1998). Cytokinesis and Midzone Microtubule Organization inCaenorhabditis elegans Require the Kinesin-like Protein ZEN-4. Molecular Biology of the Cell.

Rankin, K.E., and Wordeman, L. (2010). Long astral microtubules uncouple mitotic spindles from the cytokinetic furrow.

Rappaport, R. (1961). Experiments concerning the cleavage stimulus in sand dollar eggs. Journal of Experimental Zoology Part A: Ecological Genetics and Physiology *148*, 81-89.

Reed, S.I. (2003). Ratchets and clocks: the cell cycle, ubiquitylation and protein turnover. Nature Reviews Molecular Cell Biology *4*, 855-864.

Ridley, A.J., Schwartz, M.A., Burridge, K., Firtel, R.A., Ginsberg, M.H., Borisy, G., Parsons, J.T., and Horwitz, A.R. (2003). Cell Migration: Integrating Signals from Front to Back.

Rode, A., Maass, K.K., Willmund, K.V., Lichter, P., and Ernst, A. (2016). Chromothripsis in cancer cells: An update. Int J Cancer *138*, 2322-2333.

Rodriguez, O.C., Schaefer, A.W., Mandato, C.A., Forscher, P., Bement, W.M., and Waterman-Storer, C.M. (2003). Conserved microtubule-actin interactions in cell movement and morphogenesis. Nature Cell Biology *5*, 599-609.

Roostalu, J., Schiebel, E., and Khmelinskii, A. (2010). Cell cycle control of spindle elongation. Cell Cycle *9*, 1084-1090.

Rosasco-Nitcher, S.E., Lan, W., Khorasanizadeh, S., and Stukenberg, P.T. (2008). Centromeric Aurora-B activation requires TD-60, microtubules, and substrate priming phosphorylation. Science *319*, 469-472.

Rosenblatt, J., Cramer, L.P., Baum, B., and McGee, K.M. (2004). Myosin II-dependent cortical movement is required for centrosome separation and positioning during mitotic spindle assembly. Cell *117*, 361-372.

Rozelle, D.K., Hansen, S.D., and Kaplan, K.B. (2011). Chromosome passenger complexes control anaphase duration and spindle elongation via a kinesin-5 brake. J Cell Biol *193*, 285-294.

Sakamoto, T., Limouze, J., Combs, C.A., Straight, A.F., and Sellers, J.R. (2005). Blebbistatin, a myosin II inhibitor, is photoinactivated by blue light. Biochemistry *44*, 584-588.

Salmon, E.D., Goode, D., Maugel, T.K., and Bonar, D.B. (1976). Pressure-induced depolymerization of spindle microtubules. III. Differential stability in HeLa cells. J Cell Biol *69*, 443-454.

Samejima, K., Platani, M., Wolny, M., Ogawa, H., Vargiu, G., Knight, P.J., Peckham, M., and Earnshaw, W.C. (2015). The INCENP Coil is a Single Alpha Helical (SAH) Domain that Binds Directly to Microtubules and is Important for CPC Localization and Function in Mitosis. J Biol Chem.

Savoian, M.S., Earnshaw, W.C., Khodjakov, A., and Rieder, C.L. (1999). Cleavage furrows formed between centrosomes lacking an intervening spindle and chromosomes contain microtubule bundles, INCENP, and CHO1 but not CENP-E. Molecular biology of the cell *10*, 297-311.

Saxton, W.M., and McIntosh, J.R. (1987). Interzone microtubule behavior in late anaphase and telophase spindles. J Cell Biol *105*, 875-886.

Schaefer, A.W., Kabir, N., and Forscher, P. (2002). Filopodia and actin arcs guide the assembly and transport of two populations of microtubules with unique dynamic parameters in neuronal growth cones.

Schmucker, S., and Sumara, I. (2014). Molecular dynamics of PLK1 during mitosis. Mol Cell Oncol *1*, e954507.

Scholey, J., Civelekoglu-Scholey, G., and Brust-Mascher, I. (2017). Anaphase B. Biology *5*, 51.

Schroeder, T. (1972). The contractile ring. II. Determining its brief existence, volumetric changes, and vital role in cleaving Arbacia eggs. J Cell Biol *53*, 419-434.

Sessa, F., Mapelli, M., Ciferri, C., Tarricone, C., Areces, L.B., Schneider, T.R., Stukenberg, P.T., and Musacchio, A. (2005). Mechanism of Aurora B activation by INCENP and inhibition by hesperadin. Mol Cell *18*, 379-391.

Shannon, K.B., Canman, J.C., Ben Moree, C., Tirnauer, J.S., and Salmon, E.D. (2005). Taxol-stabilized microtubules can position the cytokinetic furrow in mammalian cells. Molecular biology of the cell *16*, 4423-4436.

Shirasu, M., Yonetani, A., and Walczak, C.E. (1999). Microtubule dynamics in Xenopus egg extracts. Microsc Res Tech *44*, 435-445.

Shrestha, S., Wilmeth, L.J., Eyer, J., and Shuster, C.B. (2012). PRC1 controls spindle polarization and recruitment of cytokinetic factors during monopolar cytokinesis. Mol Biol Cell *23*, 1196-1207.

Skau, C.T., and Waterman, C.M. (2015). Specification of Architecture and Function of Actin Structures by Actin Nucleation Factors. Annu Rev Biophys *44*, 285-310.

Steigemann, P., Wurzenberger, C., Schmitz, M.H., Held, M., Guizetti, J., Maar, S., and Gerlich, D.W. (2009). Aurora B-mediated abscission checkpoint protects against tetraploidization. Cell *136*, 473-484.

Straight, A.F., Cheung, A., Limouze, J., Chen, I., Westwood, N.J., Sellers, J.R., and Mitchison, T.J. (2003). Dissecting temporal and spatial control of cytokinesis with a myosin II Inhibitor. Science *299*, 1743-1747.

Straight, A.F., and Field, C.M. (2000). Microtubules, membranes and cytokinesis. Curr Biol *10*, R760-770.

Sturgill, E.G., Norris, S.R., Guo, Y., and Ohi, R. (2016). Kinesin-5 inhibitor resistance is driven by kinesin-12. In J Cell Biol, pp. 213-227.

Sturgill, E.G., and Ohi, R. (2013). Kinesin-12 differentially affects spindle assembly depending on its microtubule substrate. Curr Biol *23*, 1280-1290.

Su, K.C., Takaki, T., and Petronczki, M. (2011). Targeting of the RhoGEF Ect2 to the equatorial membrane controls cleavage furrow formation during cytokinesis. Dev Cell *21*, 1104-1115.

Subramanian, R., Ti, S.C., Tan, L., Darst, S.A., and Kapoor, T.M. (2013). Marking and measuring single microtubules by PRC1 and kinesin-4. Cell *154*, 377-390.

Subramanian, R., Wilson-Kubalek, E.M., Arthur, C.P., Bick, M.J., Campbell, E.A., Darst, S.A., Milligan, R.A., and Kapoor, T.M. (2010). Insights into antiparallel microtubule crosslinking by PRC1, a conserved nonmotor microtubule binding protein. Cell *142*, 433-443.

Taneja, N., Fenix, A.M., Rathbun, L., Millis, B.A., Tyska, M.J., Hehnly, H., and Burnette, D.T. (2016). Focal adhesions control cleavage furrow shape and spindle tilt during mitosis. Sci Rep *6*, 29846.

Tao, L., Fasulo, B., Warecki, B., and Sullivan, W. (2016). Tum/RacGAP functions as a switch activating the Pav/kinesin-6 motor. Nat Commun *7*, 11182.

Tarantino, N., Tinevez, J.-Y., Crowell, E.F., Boisson, B., Henriques, R., Mhlanga, M., Agou, F., Israël, A., and Laplantine, E. (2014a). TNF and IL-1 exhibit distinct ubiquitin requirements for inducing NEMO–IKK supramolecular structures.

Tarantino, N., Tinevez, J.Y., Crowell, E.F., Boisson, B., Henriques, R., Mhlanga, M., Agou, F., Israel, A., and Laplantine, E. (2014b). TNF and IL-1 exhibit distinct ubiquitin requirements for inducing NEMO-IKK supramolecular structures. J Cell Biol *204*, 231-245.

Tinevez, J.Y., Perry, N., Schindelin, J., Hoopes, G.M., Reynolds, G.D., Laplantine, E., Bednarek, S.Y., Shorte, S.L., and Eliceiri, K.W. (2016). TrackMate: An open and extensible platform for single-particle tracking. Methods.

Tsukahara, T., Tanno, Y., and Watanabe, Y. (2010). Phosphorylation of the CPC by Cdk1 promotes chromosome bi-orientation. Nature *467*, 719-723.

Tyson, J.J., and Novak, B. (2008). Temporal organization of the cell cycle. Curr Biol *18*, R759-r768.

Uehara, R., Tsukada, Y., Kamasaki, T., Poser, I., Yoda, K., Gerlich, D.W., and Goshima, G. (2013). Aurora B and Kif2A control microtubule length for assembly of a functional central spindle during anaphase. J Cell Biol *202*, 623-636.

van der Horst, A., Vromans, M.J., Bouwman, K., van der Waal, M.S., Hadders, M.A., and Lens, S.M. (2015). Inter-domain Cooperation in INCENP Promotes Aurora B Relocation from Centromeres to Microtubules. Cell Rep *12*, 380-387.

Verbrugghe, K.J.C., and White, J.G. (2004). SPD-1 Is Required for the Formation of the Spindle Midzone but Is Not Essential for the Completion of Cytokinesis in C. elegans Embryos. Current Biology *14*, 1755-1760.

Wagner, E., and Glotzer, M. (2016). Local RhoA activation induces cytokinetic furrows independent of spindle position and cell cycle stage. J Cell Biol *213*, 641-649.

Walczak, C.E. (2003). The Kin I kinesins are microtubule end-stimulated ATPases. Mol Cell *11*, 286-288.

Walczak, C.E., Gayek, S., and Ohi, R. (2013). Microtubule-depolymerizing kinesins. Annu Rev Cell Dev Biol *29*, 417-441.

Wang, E., Ballister, E.R., and Lampson, M.A. (2011). Aurora B dynamics at centromeres create a diffusion-based phosphorylation gradient. J Cell Biol *194*, 539-549.

Wang, H., Brust-Mascher, I., Civelekoglu-Scholey, G., and Scholey, J.M. (2013). Patronin mediates a switch from kinesin-13-dependent poleward flux to anaphase B spindle elongation. J Cell Biol *203*, 35-46.

Wang, Y.L. (1985). Exchange of actin subunits at the leading edge of living fibroblasts: possible role of treadmilling. J Cell Biol *101*, 597-602.

Waters, J.C., Mitchison, T.J., Rieder, C.L., and Salmon, E.D. (1996). The kinetochore microtubule minus-end disassembly associated with poleward flux produces a force that can do work. Mol Biol Cell *7*, 1547-1558.

Wheatley, S.P. (1999). Updates on the mechanics and regulation of cytokinesis in animal cells. Cell Biol Int *23*, 797-803.

Wheatley, S.P., Carvalho, A., Vagnarelli, P., and Earnshaw, W.C. (2001a). INCENP is required for proper targeting of Survivin to the centromeres and the anaphase spindle during mitosis. Curr Biol *11*, 886-890.

Wheatley, S.P., Kandels-Lewis, S.E., Adams, R.R., Ainsztein, A.M., and Earnshaw, W.C. (2001b). INCENP binds directly to tubulin and requires dynamic microtubules to target to the cleavage furrow. Exp Cell Res *262*, 122-127.

Wheatley, S.P., and Wang, Y. (1996). Midzone microtubule bundles are continuously required for cytokinesis in cultured epithelial cells. The Journal of cell biology *135*, 981-989.

Wittmann, T., Hyman, A., and Desai, A. (2001). The spindle: a dynamic assembly of microtubules and motors. Nat Cell Biol *3*, E28-34.

Yang, F., Camp, D.G., 2nd, Gritsenko, M.A., Luo, Q., Kelly, R.T., Clauss, T.R., Brinkley, W.R., Smith, R.D., and Stenoien, D.L. (2007). Identification of a novel mitotic phosphorylation motif associated with protein localization to the mitotic apparatus. J Cell Sci *120*, 4060-4070.

Zaytsev, A.V., Mick, J.E., Maslennikov, E., Nikashin, B., DeLuca, J.G., and Grishchuk, E.L. (2015). Multisite phosphorylation of the NDC80 complex gradually tunes its microtubule-binding affinity. Mol Biol Cell *26*, 1829-1844.

Zhou, F.-Q., Waterman-Storer, C.M., and Cohan, C.S. (2002). Focal loss of actin bundles causes microtubule redistribution and growth cone turning.

Zhu, C., Bossy-Wetzel, E., and Jiang, W. (2005a). Recruitment of MKLP1 to the spindle midzone/midbody by INCENP is essential for midbody formation and completion of cytokinesis in human cells. Biochem J *389*, 373-381.

Zhu, C., Zhao, J., Bibikova, M., Leverson, J.D., Bossy-Wetzel, E., Fan, J.B., Abraham, R.T., and Jiang, W. (2005b). Functional analysis of human microtubule-based motor proteins, the kinesins and dyneins, in mitosis/cytokinesis using RNA interference. Mol Biol Cell *16*, 3187-3199.